AD-A109 687 ANALYTICAL METHODS INC REDMOND WA F/G 20/4
A SURFACE SINGULARITY METHOD FOR ROTORS IN HOVER OR CLIMB.(U)
DEC 81 J M SUMMA, B MASKEW DAAJ02-76-C-0069
UNCLASSIFIED AMI-8103 USAAVRADCOM-TR-81-D-23 NL

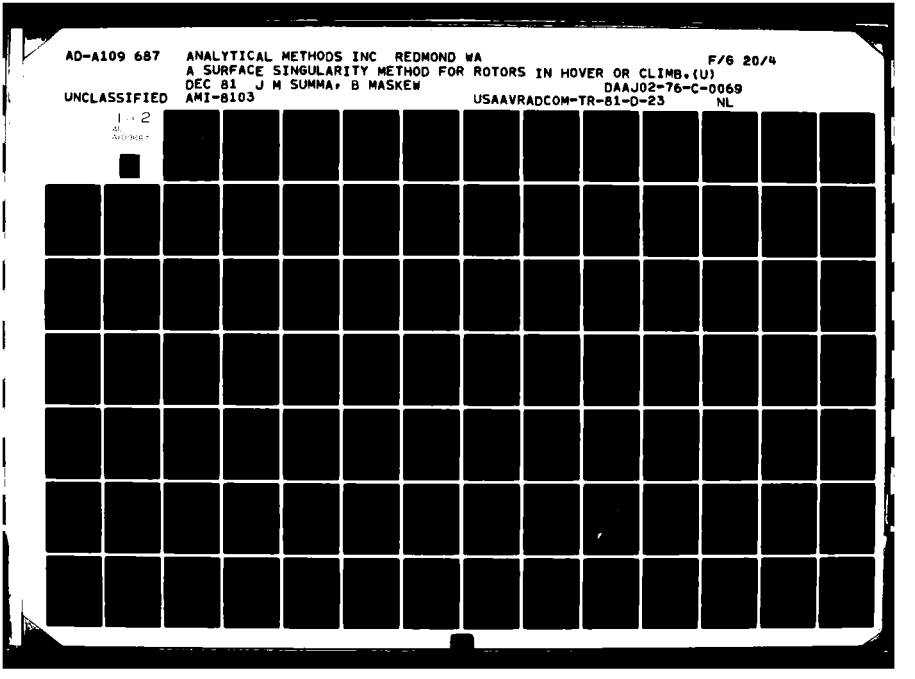

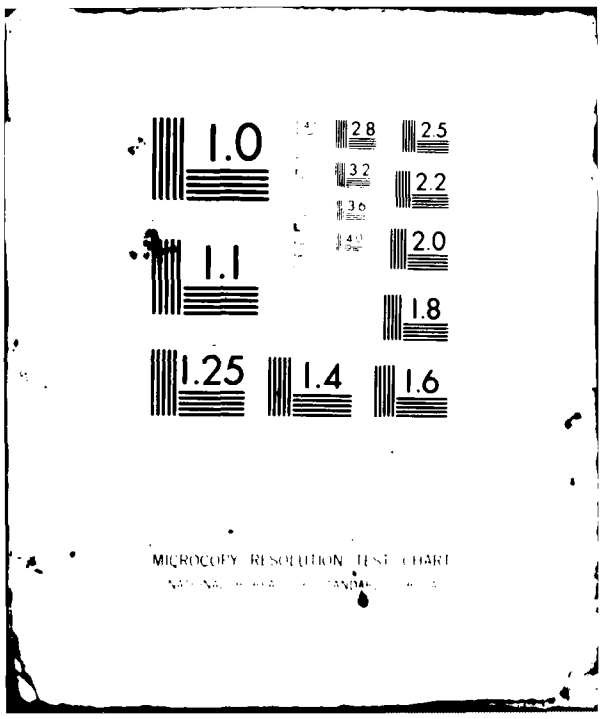
1.0
2.8
2.5
3.2
2.2
3.6
4.0
2.0
1.1
1.8
1.25
1.4
1.6
MICROCOPY RESOLUTION TEST CHART

USAAVRADCOM-TR-81-D-23

(12) LEVEL II

AD A109687

# A SURFACE SINGULARITY METHOD FOR ROTORS IN HOVER OR CLIMB

J. Michael Summa and Brian Maskew
Analytical Methods, Inc.
2047 — 152nd Avenue N.E.
Redmond, Wash. 98052



December 1981

Final Report for Period 29 March 1979 - 30 September 1981



Approved for public release;
distribution unlimited.

Prepared for

APPLIED TECHNOLOGY LABORATORY
U. S. ARMY RESEARCH AND TECHNOLOGY LABORATORIES (AVRADCOM)
Fort Eustis, Va. 23604

(8)

## APPLIED TECHNOLOGY LABORATORY POSITION STATEMENT

This report documents an engineering analysis and the resulting computer code which is considered to be technically sound for the prediction of rotorcraft hover and vertical climb performance. The computed results from the program should be used for design purposes only after correlation of the program with test data for rotor systems of similar configuration.

The computer code resulting from this contract will be provided to qualified users, upon request, for use in the design and analysis of rotary-wing aircraft.

The Project Engineer for this contract was Mr. W. D. Vann, Aeromechanics Technical Area, Aeronautical Technology Division.

Unclassified

SECURITY CLASSIFICATION OF THIS PAGE (When Data Entered)

| REPORT DOCUMENTATION PAGE | READ INSTRUCTIONS BEFORE COMPLETING FORM |
|---|---|
| 1. REPORT NUMBER: USAAVRADCOM TR 81-D-23 | 2. GOVT ACCESSION NO.: AD-A109 087 |
| | 3. RECIPIENT'S CATALOG NUMBER: |
| 4. TITLE (and Subtitle): A SURFACE SINGULARITY METHOD FOR ROTORS IN HOVER OR CLIMB | 5. TYPE OF REPORT & PERIOD COVERED: Final Report 3/29/79 - 9/30/81 |
| | 6. PERFORMING ORG. REPORT NUMBER: AMI Report 8103 |
| 7. AUTHOR(s): J. MICHAEL SUMMA and BRIAN MASKEW | 8. CONTRACT OR GRANT NUMBER(s): DAAJ02-76-C-0069 |
| 9. PERFORMING ORGANIZATION NAME AND ADDRESS: Analytical Methods, Inc. 2047 - 152nd Avenue N.E. Redmond, Washington 98052 | 10. PROGRAM ELEMENT, PROJECT, TASK AREA & WORK UNIT NUMBERS: 62209A 1F262209AH76 00 176 EK |
| 11. CONTROLLING OFFICE NAME AND ADDRESS: Applied Technology Laboratory, U.S. Army Research and Technology Laboratories (AVRADCOM), Fort Eustis, Virginia 23604 | 12. REPORT DATE: December 1981 |
| | 13. NUMBER OF PAGES: 142 |
| 14. MONITORING AGENCY NAME & ADDRESS(if different from Controlling Office) | 15. SECURITY CLASS. (of this report): Unclassified |
| | 15a. DECLASSIFICATION/DOWNGRADING SCHEDULE |

16. DISTRIBUTION STATEMENT (of this Report)

Approved for public release; distribution unlimited.

17. DISTRIBUTION STATEMENT (of the abstract entered in Block 20, if different from Report)

18. SUPPLEMENTARY NOTES

19. KEY WORDS (Continue on reverse side if necessary and identify by block number)

Helicopter Rotors
Helicopter Rotor Hover Performance
Helicopter Rotor Wake
Wake Geometry
Vortices
Hovering
Helicopter Rotor Aerodynamics
Helicopter Rotor Airloads
Surface Singularity Method

20. ABSTRACT (Continue on reverse side if necessary and identify by block number)

A surface singularity potential flow code, ROTAIR, has been assembled for the calculation of detailed surface pressures on rotors in hover or climb. This method is basically a marriage of two codes: the fixed-wing surface singularity doublet code and the rotor lifting-surface code. The program includes a tip vortex separation model. Also, the rotor tip surface is panelled so that pressures are calculated right around the tip-edge surface.

DD FORM 1 JAN 73 1473 EDITION OF 1 NOV 65 IS OBSOLETE

Unclassified

SECURITY CLASSIFICATION OF THIS PAGE (When Data Entered)

20. Continued.

Preliminary calculations have verified the capabilities of the program for computing blade surface properties in the presence of a close-vortex passage. Additionally, calculated pressure distributions compare favorably with experimental data for a low aspect ratio two-bladed rotor, and the calculated circulation distribution is consistent with that computed earlier with the lifting-surface code. Finally, the newly developed far-wake doublet model promises to keep computing efforts practical.

1
B

## PREFACE

This program was sponsored by the Applied Technology Laboratory, U.S. Army Research and Technology Laboratories (AVRADCOM), Fort Eustis, Virginia, and was carried out under Contract DAAJ02-76-C-0069. The contract monitor was Mr. W.D. Vann, and the authors would like to take this opportunity to acknowledge his helpful comments and constructive criticism during the course of the study.

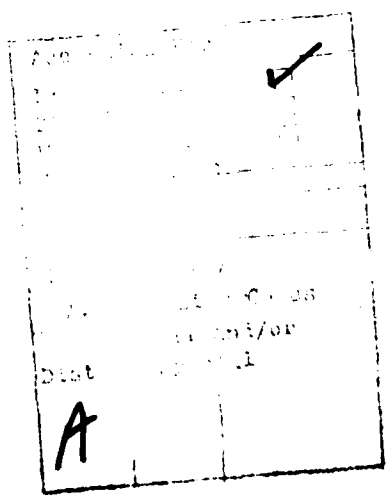

TABLE OF CONTENTS

TABLE OF CONTENTS (Continued)

## LIST OF ILLUSTRATIONS

## LIST OF ILLUSTRATIONS (Continued)

## LIST OF ILLUSTRATIONS (Continued)



2
F

## 1.0 INTRODUCTION

In the last 25 years, a great deal of progress has been made in the design of the helicopter. Rotary wing aircraft are now faster, more efficient, quieter and carry more payload than ever before. For example, in just one generation hover efficiency (figure of merit) has been increased by about 15%, which translates into approximately double the payload capability. These advances are a direct result of improved understanding of helicopter aerodynamics that has come with the development of better analytical methods and experimental techniques. The theoretical methods available today are certainly much more advanced than those available in the 1950's.

However, it must be surprising for those of us who have been involved in the development of methods for the prediction of rotary wing airloads to realize that it was approximately 25 years ago that Gray[1,2] first characterized the hovering rotor wake as composed of strong, rolled up helical tip vortices and separate inboard sheets of weak vorticity. Since that time, research and development efforts have concentrated on the prescribed wake method. Still, it was almost 15 years before Landgrebe[3] had parameterized the prescribed wake constants in terms of blade geometric properties and rotor thrust coefficient based on a series of model rotor tests and a lifting-line representation of the rotor blades. During the 1970's, additional model rotor tests have led to continued refinements to the prescribed wake constants, and maximum blade circulation has replaced

---

[1]Gray, R.B., "On the Motion of the Helical Vortex Shed from a Single-Bladed Hovering Helicopter Rotor and its Application to the Calculation of the Spanwise Aerodynamic Loading", Princeton University Aero. Engr. Dept., Report No. 313, September 1955.

[2]Gray, R.B., "An Aerodynamic Analysis of a Single-Bladed Rotor in Hovering and Low-Speed Forward Flight as Determined from Smoke Studies of the Vorticity Distribution in the Wake", Princeton University Aero. Engr. Dept., Report No. 356, September 1956.

[3]Landgrebe, A.J., "An Analytical and Experimental Investigation of Helicopter Rotor Hover Performance and Wake Geometry Characteristics", USAAMRDL Tech. Rept. 71-24, Eustis Directorate, U.S. Army Air Mobility Research and Development Laboratory, Fort Eustis, Virginia, June 1971, AD 728835.

rotor thrust in the empirical prescription.[4,5] That these analytical methods demonstrate good correlation for integrated loads for a large number of conventional rotors should be expected since the prescribed wake constants are intimately related to the theoretical methods themselves. However, these methods are less successful when compared with known collective settings,[6] which implies that although integrated performance is predicted correctly, local sectional loads are probably not properly calculated. Certainly, if the wake itself deviates from the experimental data base for the prescribed wake constants, performance predictions could be significantly in error. In fact, detailed performance predictions for the new technology rotor blade tips that exist today still remain uncertain.

The lifting-surface method reported in Reference 7 should help in analyzing the new planforms, providing the linearized lifting-surface assumptions are met and the prescribed contraction boundaries are acceptable. The resulting computer program, HOVER, is described in detail in Reference 8.

---

[4]Landgrebe, A.J., Moffit, R.C., and Clark, D.R., "Aerodynamic Technology for Advanced Rotorcraft--Part I", J. Am. Hel. Soc., Vol. 22, No. 2, April 1977.

[5]Kocurek, J.D., "Hover Performance Methodology at Bell Helicopter Textron", 36th Annual Forum of the American Helicopter Society, Preprint No. 80-3, May 1980.

[6]Caradonna, F.X., and Tung, C., "Experimental and Analytical Studies of a Model Helicopter Rotor in Hover", Sixth European Rotorcraft and Powered Lift Aircraft Forum, Paper No. 25, Bristol, England, September 1980.

[7]Summa, J.M., and Clark, D.R., "A Lifting-Surface Method for Hover/Climb Airloads", 35th Annual National Forum of the American Helicopter Society, Preprint No. 79-3, May 1979.

[8]Summa, J.M., "Evaluation of Blade Tip Planform Effects on Hover Performance", Contract DAAJ02-76-C-0069, Applied Technology Laboratory, U.S. Army Research and Technology Laboratories (AVRADCOM), Fort Eustis, Virginia, to be published.

With this program, the axial displacements of the tip vortices are relaxed to force-free locations while the contraction boundary is prescribed as in the earlier methods.[3,5] Convergence of the relaxed wake and rotor loading with the program have been demonstrated for a small number of rotors, but, unfortunately, extensive correlation efforts and calculations for newer blade geometries have not been undertaken. It is anticipated that such calculation will be completed within the next year.

Meanwhile, Green's function surface singularity method, described in this report, has been developed to examine the detailed pressure distributions on rotor blades of arbitrary shape, and to include the thick blade surface vorticity effects at first blade passage. Of course, this new method is also the first step toward the eventual goal of the elimination of the two-dimensional constraints in the profile power predictions.

The basic methodology for the surface singularity code was developed for fixed-wing applications involving unsteady oscillations and has been described in References 9 and 10. Rotary wing wake technology has been added to the basic method along with the necessary methods to calculate rotorcraft airloads. The resulting computer code, named ROTAIR, is, therefore, based on technologies developed in HOVER and the fixed-wing computer programs.

This report describes briefly the basic fundamentals of the surface potential method as applied to the rotor in hover or climb. Further details of the fundamentals can be found in References 9 and 10. The complete description of the blade surface geometric description in ROTAIR is described in Section 3.0, while the wake modelling and geometry are presented in Section 4.0. Rather than repeating technology developments already reported in great detail in Reference 8, wake modifications made to the methods for incorporation into ROTAIR are emphasized. Finally, the method of rotor airloads computation and data calculations are discussed in Sections 5.0 and 6.0, respectively.

---

[9]Maskew, B., "Unsteady Potential Flow Analysis of Rotor Blade Tip Shapes", Interim Report and Program User Guide, Contract NAS1-15472, NASA Langley Research Center, April 1980.

[10]Maskew, B., "Influence of Rotor Blade Tip Shape on Tip Vortex Shedding--An Unsteady, Inviscid Analysis", Presented at the 36th Annual Forum of the American Helicopter Society, Preprint No. 80-6, May 1980.

## 2.0 SURFACE SINGULARITY METHOD FOR ROTORS

The complete mathematical formulation for the general motion of multiple bodies through an ideal fluid was rigorously developed in Appendix A of Reference 8. In that formulation, the boundary condition of zero flow penetration at the blade surface was used to obtain solutions for the blade surface doublet distribution. Consequently, the Neumann velocity boundary condition of no flow across the boundary was enforced on the external (outside of the body) flow field, and a doublet only distribution was utilized. However, for the motion of closed bodies, the internal Dirichlet boundary condition of zero potential inside the body can be used equally as well. In fact, there are numerical advantages to solving for the velocity potential directly, since it is one order less singular than the velocity induced by a potential doublet distribution. For example, in Reference 11 it was demonstrated that for comparable density of control points where the boundary conditions are satisfied, the low-order method gives comparable accuracy to the higher-order solutions. It was also shown that problems associated with some earlier low-order panel methods, e.g., leakage in internal flows and junctions and also poor trailing-edge solutions, do not appear for the velocity potential method. Consequently, the surface singularity method for the rotor problem uses the Dirichlet boundary condition for the velocity potential. For completeness, the mathematical formulation given in Reference 9 is repeated here with only slight modifications for the rotor problem of concern here. Also, the formulation for a single blade only is explicitly developed in the following sections since the influences of secondary blades and wakes are obtained by simple rotations for the case of hover or climb. The reader is referred to Reference 7 for details of the multiple-blade problem.

---

[11]Maskew, B., "Prediction of Subsonic Aerodynamic Characteristics--A Case for Low-Order Panel Methods", AIAA 19th Aerospace Sciences Meeting, AIAA-81-0252, January 1981.

## 2.1 BASIC FORMULATION

Consider the whole of space divided into two regions by the surface of the blade and assume the existence of Laplacian velocity potential distributions in the two regions, i.e., $\Phi$ in the flow field and $\Phi_i$ in the blade interior. If we now apply Green's third identity to the two regions, then the total potential at a point, P, on the inside surface of the blade can be written:

$$4\pi\Phi_P = \iint_{S-P} \left(\Phi - \Phi_i\right) \underline{n} \cdot \nabla\left(\frac{1}{r}\right) dS - 2\pi\left(\Phi - \Phi_i\right)_P$$

$$+ \iint_W \left(\Phi_U - \Phi_L\right) \underline{n} \cdot \nabla\left(\frac{1}{r}\right) dW$$

$$- \iint_S \frac{1}{r} \underline{n} \cdot \left(\nabla\Phi - \nabla\Phi_i\right) dS + 4\pi\Phi_{\infty_P} \qquad (1)$$

Here, r is the length of the vector from the surface element to the point, P, and S-P signifies that the point, P, is excluded from the surface integration. Equation (1) includes the contribution from the wake surface, W.

The Dirichlet boundary condition is now applied in the interior region to render a unique distribution. Two forms have been considered in the present work: (1) $\Phi_i = 0$ and (2) $\Phi_i = \Phi_\infty$. The first form gives a simpler and more cost-effective method for the general case, but the second form, which is used for the present calculations, has proven to be more reliable in practice. For the second form, Eq (1) becomes

$$0 = \iint_{S-P} \phi\, \underline{n} \cdot \nabla\left(\frac{1}{r}\right) dS - 2\pi\phi_P + \iint_{W} \left(\phi_U - \phi_L\right) \underline{n} \cdot \nabla\left(\frac{1}{r}\right) dW$$

$$- \iint_{S} \frac{1}{r}\, \underline{n} \cdot \nabla\phi\, dS \qquad (2)$$

where $\phi$, the perturbation potential in the flow field, has been substituted for $\phi - \phi_\infty$.

The first two terms in Eq (2) give the perturbation potential due to a distribution of normal doublets of strength, $\phi$, on the blade surface. Similarly, the third term represents a doublet distribution of strength, $\phi_U - \phi_L$, on the wake and the fourth term represents a source distribution of strength, $\underline{n} \cdot \nabla\phi$, on the blade surface.

Equation (2) is basically the same as the formulation given by Morino,[12] who used a direct application of Green's theorem in the flow field. The present approach to the problem is a special case of a multi-domain formulation which has led to a more general three-dimensional method in which large regions of separated flow are modelled in a similar way to that in the CLMAX program.[13]

The source term in Eq (2) can be evaluated directly from the condition of no flow penetration at the surface. The flow velocity relative to the blade-fixed frame is

$$\underline{V} = \underline{v} - \underline{V}_\infty - \underline{\omega} \times \underline{R}, \qquad (3)$$

---

[12] Morino, L., Chen, L.T., and Socio, E.O., "Steady and Oscillatory Subsonic and Supersonic Aerodynamics Around Complex Configurations", AIAA J., Vol. 13, No. 3, March 1975, pp. 368-374.

[13] Maskew, B., and Dvorak, F.A., "The Prediction of $C_{LMAX}$ Using a Separated Flow Model", J. Amer. Hel. Soc., April 1978.

where the perturbation velocity, $\underline{v} = -\nabla\phi$.

For zero penetration, $\underline{V} \cdot \underline{n} = 0$. Hence,

$$\underline{n} \cdot \nabla\phi = -\underline{n} \cdot \underline{V}_\infty - \underline{n} \cdot \underline{\omega} \times \underline{R},$$

and Eq (2) becomes

$$0 = \iint_{S-P} \phi\, \underline{n} \cdot \nabla\left(\frac{1}{r}\right) dS - 2\pi\phi_P + \int_W \left(\phi_U - \phi_L\right) \underline{n} \cdot \nabla\left(\frac{1}{r}\right) dW$$

$$+ \iint_S \frac{1}{r} \left(\underline{n} \cdot \underline{V}_\infty + \underline{n} \cdot \underline{\omega} \times \underline{R}\right) dS \qquad (4)$$

This is the basic equation of the method. It is solved for the unknown surface perturbation potential, $\phi$, or surface doublet distribution for a given wake geometry. The doublet distribution, $\phi_U - \phi_L$, on the wake is equal to the surface doublet jump at the blade trailing edge, as specified by the Kutta condition. The wake geometry is either prescribed or relaxed to a force-free location by the methods described in Reference 8. Once the surface potential distribution is known, the surface velocities are obtained by differentiation, and the blade surface pressures are calculated in the usual manner.

## 2.2 NUMERICAL PROCEDURE

The general arrangement of the configuration is shown in Figure 1. The x,y,z coordinate system with unit vectors, $\underline{i}$, $\underline{j}$,$\underline{k}$, is fixed relative to the blade. For the present applications, the blade rotates about the z-axis at a rate, $\Omega$, and climbs at a speed, $W_C$, along the z-axis.

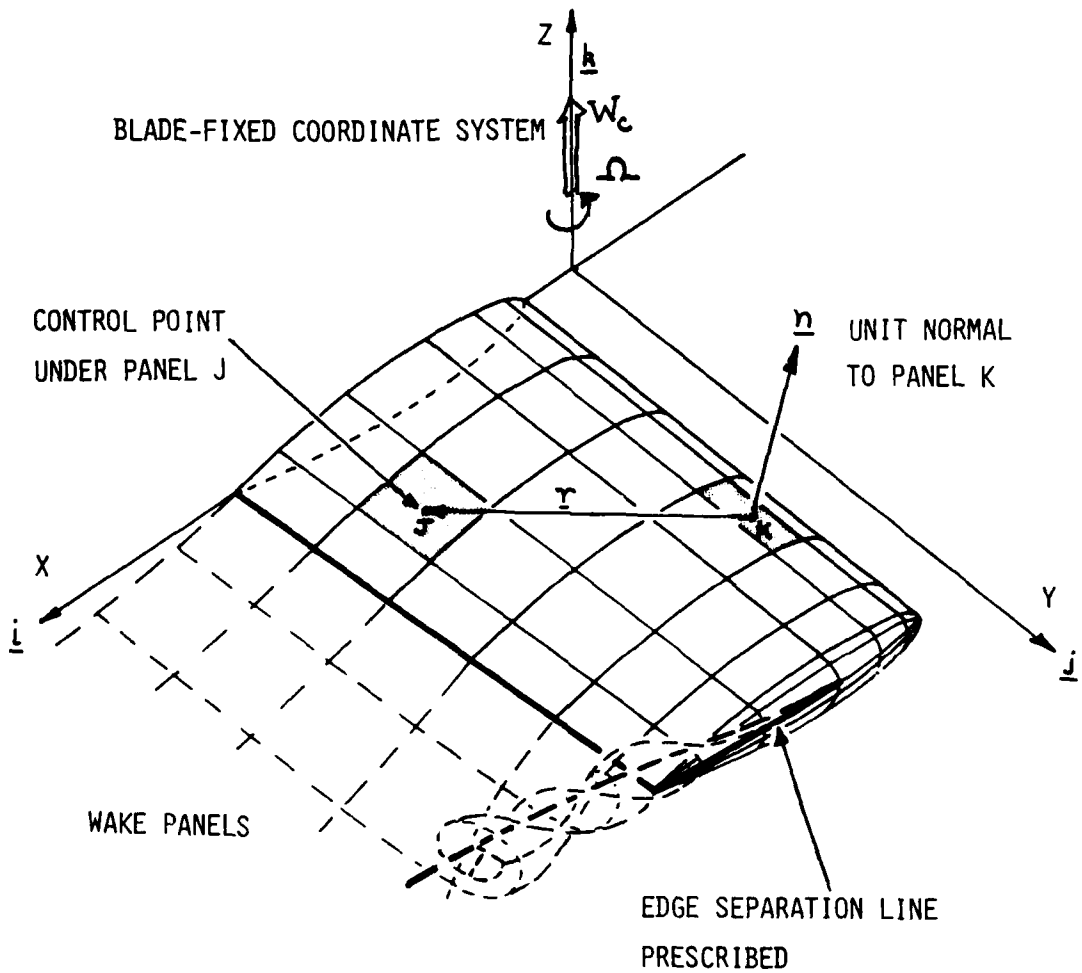


Figure 1. General Arrangement of the Configuration.

The numerical procedure has options for both a prescribed and relaxed wake calculation scheme. The flow chart for the procedure is shown in Figure 2. The input data is assembled in three main parts: basic data, surface patch geometry description, and basic wake geometry description. Details of the input parameters and the program output are given in Appendixes B and C as well as a more detailed flow diagram showing the connections between subroutines in the code.

The surface of the blade is represented by planar quadrilateral panels over each of which the doublet and source distributions are assumed constant. Special features are included in the present code to extend the panelling around the tip edge and to allow the user to extend the wake along the tip edge (Figure 1). Automatic panelling routines are installed to simplify user input. The geometry description is given in detail in Section 3.0.

Equation (4) is satisfied simultaneously at a point at the center of each panel. If there are N panels representing the blade surface, Eq (4) becomes

$$\sum_{\substack{k=1 \\ K\neq J}}^{N} \left| \mu_K \, C_{JK} \right| - 2\pi\mu_J + E_J = 0; \qquad J=1,N \tag{5}$$

where $\mu_K$ is the unknown doublet value on panel K. (Note: $\mu_K = \sigma_K/4\pi$.)

$$E_J = \sum_{K=1}^{N_W} \left| \mu_{W_K} \, C_{JK} \right| + \pi R_J + \underline{V}_\infty \cdot \underline{n}_J$$

where $N_W$ is the number of panels in the wake, and $\underline{V}_\infty = W_C\underline{k}$.

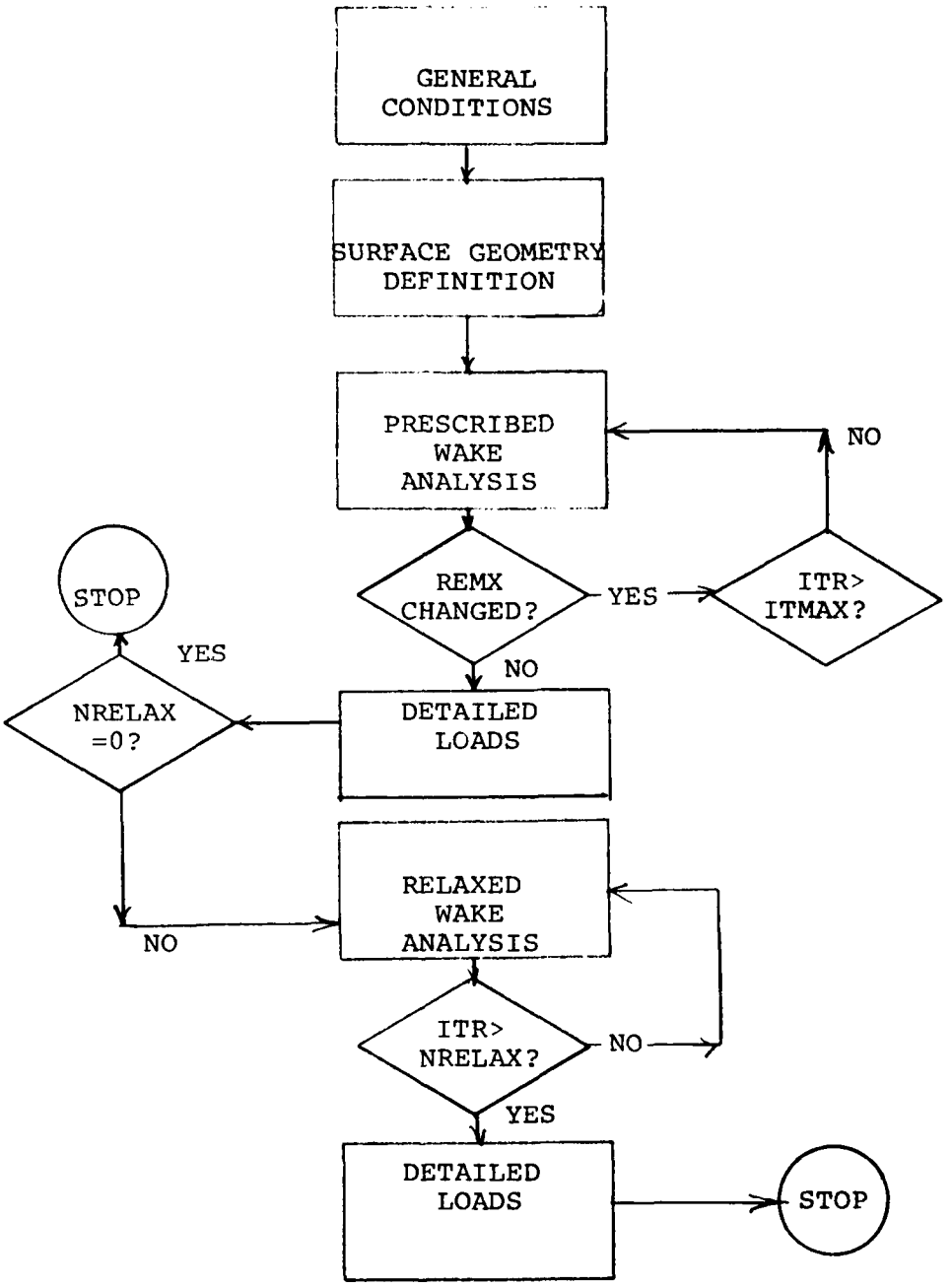


Figure 2. Flow Diagram for the Method.

$$\sigma_{R_J} = \left\{ \sum_{K=1}^{N} \underline{k} \times \underline{R}_K \cdot \underline{n}_K \, B_{JK} \right\} /4\pi$$

is the source distribution due to blade rotation about the pitch axis, and

$$\underline{\sigma}_{M_J} = \left\{ \sum_{K=1}^{N} \underline{n}_K \, B_{JK} \right\} /4\pi$$

are the components of a three-part source distribution due to the relative translation of the blade and the onset flow. (Note: In the present case, only the z-component is nonzero for the climb condition.)

The quantities $B_{JK}$ and $C_{JK}$ are the velocity potential influence coefficients for the constant source and doublet distributions, respectively, on panel K acting on the control point on panel J. These include contributions from the respective secondary blade panels. Expressions for these influence coefficients have been given by Morino in Reference 12 based on hyperbolic paraboloidal panels. Slightly different expressions are installed in the present code based on planar panels.

Equation (5) is solved by a direct method for $N \leq 320$ and by an iterative method for $N > 320$.

The surface gradient of $\mu$ is evaluated on each panel by differentiating a two-way parabolic fit through the doublet values on the panel and its four immediate neighbors. At the separation lines a simple differencing is applied for the gradients approaching the separation line. The surface pressure distribution and resultant airloads are calculated as described in Section 5.0.

The prescribed wake iteration loop requires that the user input the empirical wake constants for the desired rotor thrust coefficient and an approximate radial position of the maximum circulation. The iteration continues until the maximum circulation position is unchanged. Once the collective iteration loop is added to the program, the blade collective, $\theta_{75}$, would then be updated until the calculated thrust equals the requested thrust. If requested, a relaxed wake iteration loop similar to that described in Reference 8 is then calculated for a fixed-blade collective.

## 3.0 BLADE GEOMETRY DEFINITION

This section describes the way the geometry routines process user input to generate the discrete panel representation of the rotor blade. Details are included to emphasize the versatility of the routines. With the exception of the method of providing for coning angle rotation, $\beta$, and collective pitch rotation, $\theta_{75}$, the geometry description is carried over from Reference 9.

### 3.1 BLADE SURFACE ORIENTATION

When defining the surface geometry of a rotor, the primary blade is described in its own local coordinate system for convenience. The blade surface is then relocated to the appropriate position with respect to the rotor hub.

The blade specification starts with the appropriate transformation information which converts from the blade definition system, or "blade coordinate system" (B.C.S.) to the hub coordinate system (H.C.S.). This information includes the flapping hinge radial position, YFLAP, the blade coning angle, $\beta$, and the blade collective setting, $\theta_{75}$. As illustrated in Figure 3, the origin of the B.C.S. is positioned at YFLAP distance from the axis-of-rotation on the $Y_{H.C.S.}$ axis, the blade (or B.C.S.) is then coned $\beta$ degrees about the $X_{H.C.S.}$ axis, and finally rotated to the requested $\theta_{75}$ degrees about the $Y_{B.C.S.}$ axis. Since the rotor radius is used for nondimensionalization, care must be exercised to ensure that the final blade radius includes YFLAP. A test is made at the geometry stage in ROTAIR, and if in error, the program is halted with a message for the user to check the radius defining stations. Finally, the blade surface is described within the B.C.S. in patches of panels.

### 3.2 PATCHES

#### 3.2.1 Convention

Panels representing the surface of the configuration may be assembled in a number of PATCHES. Each patch has a regular array of panels arranged in rows and columns (Figure 4). A patch is basically a four-sided shape when "opened out". It must always be regarded as such, even if one of the sides or two opposite sides are made zero, or if some of the sides have kinks. In the following discussions, patches will often be regarded as rectangular; this is purely a convenience for discussing relationships and is not a shape restriction. Our view of the patch will always be from the outside; i.e., looking onto the surface from a point in the flow field.

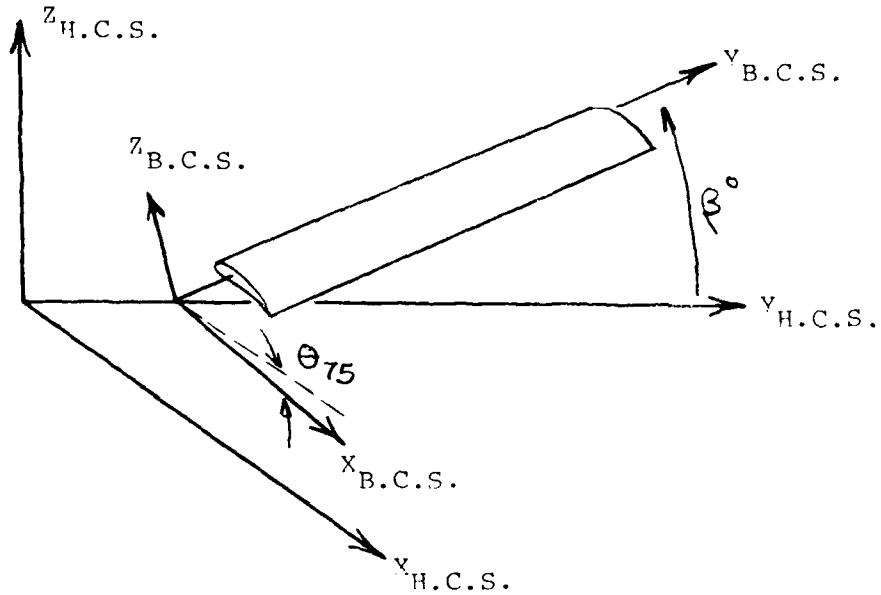


Figure 3. Rotor Blade Orientation (H.C.S. and B.C.S. Descriptions).

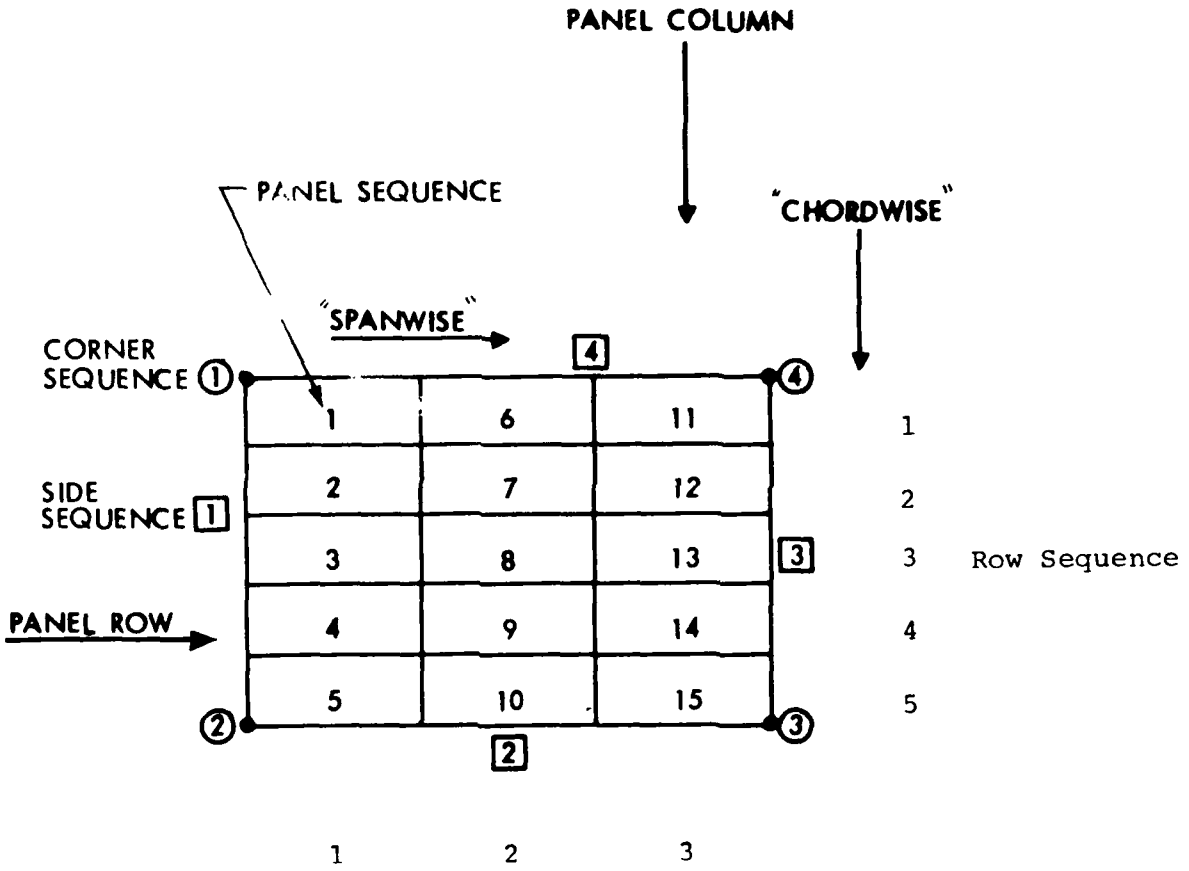


Figure 4. Patch Conventions.

For convenience the terms "chordwise" and "spanwise" are used to describe the directions of the panel columns and rows, respectively (Figure 4). These directions are analogous to the conventional wing layout, but in the patch context these directions are not restricted to the x and y directions, respectively. For example, on a patch representing the wing tip it is convenient to have the columns of panels vertical and the rows of panels to be parallel to the wing chord; therefore, in this case the "chordwise" direction on the patch is actually vertical while its "spanwise" direction is along the wing chord (see Figure 10).

Patch geometry is defined using chordwise lines called SECTIONS. (These are described later in 3.2.2.) A set of sections distributed spanwise across a patch defines the patch surface. The convention adopted here is that points defining a section shape proceed from top to bottom (Figure 5). (In the case where a patch represents the main surface of a rotor blade, this convention causes the points defining each section to proceed from the trailing-edge lower surface and finish at the trailing-edge upper surface.) In our view of the patch, the order of the sections proceeds in the positive, spanwise direction (Figure 5).

For the purpose of automatically connecting panels from one patch to another, it is important to identify patch sides. The convention adopted here is that the first and last sections defining a patch correspond to sides 1 and 3, respectively. With this convention, the order of the sides is anticlockwise (Figure 4). The order of the corner points follows the same sequence as the sides, starting with 1 at the top of side 1. All the panels within a patch take the same side and corner point convention as for the patch. For convenience, the panels are referred to in ROWS, which run spanwise, and COLUMNS, which run chordwise (Figure 4). Panel arrangements within a patch are referred to by ROWS x COLUMNS.

### 3.2.2 Sections

Each section of a patch may be defined in its own local coordinate system, referred to as the section coordinate system, or S.C.S. The user provides the necessary information to transform the S.C.S. into the B.C.S. at the beginning of each section. This transformation is performed immediately after a section's geometric description is complete. This transformation is separate from that described earlier in 3.1 in which the complete blade geometry is converted into the H.C.S. (at which stage the S.C.S. geometry is discarded). This double transformation (both levels of which are optional) offers useful flexibility when preparing the input data. One particular advantage is that the geometric relationships, especially the rotations, are kept reasonably simple without sacrificing generality.

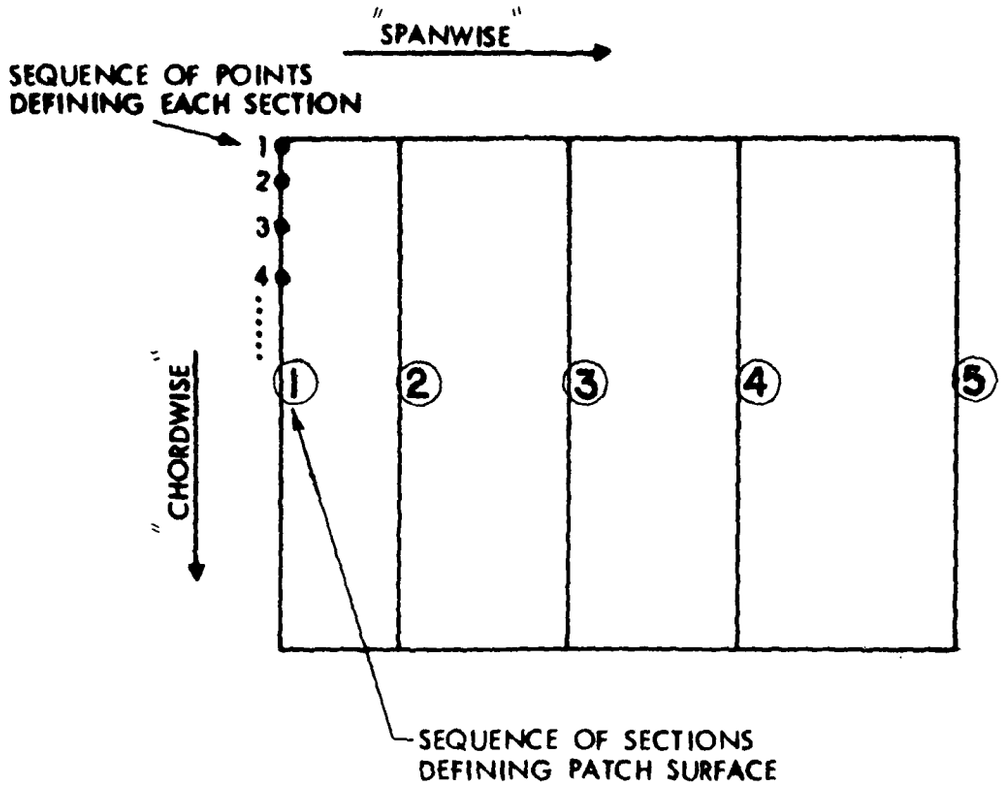


Figure 5. Sections Defining Patch Surface.

The information required to transform from the S.C.S. into the B.C.S. (see Figure 6) consists of : (1) the translation vector (STX, STY, STZ), which is the position vector of the S.C.S. origin expressed in the B.C.S. coordinates; (2) a scaling factor (default 1.0), which is applied in the S.C.S.; (3) the rotation angle ($\alpha$, degrees) about the y-axis of the S.C.S.; and (4) the angle ($\theta$, degrees) in the B.C.S. x-y plane, between the projection of the S.C.S. x-axis and the B.C.S. x-axis. For most rotor blades, the $\theta$ rotation will be zero and the section twist angle, in this case $\alpha$, will be used to specify aribtrary radial twist distributions (Figure 7). It is not necessary for the resultant blade twist angle at the 3/4 radius to be zero. The geometry package computes the basic twist of the defined blade surface at the 3/4 radius station and rotates the blade to the specified $\theta_{75}$. However, because of the rotation procedures described in 3.1 for the final blade position, the translation vector (STX, STY, STZ) of the blade root section must be set so that the $Y_{B.C.S.}$ axis passes through the root section quarter chord point.

The contour line of each section is defined by a set of BASIC POINTS (BX, BZ). These points may be used as panel corner points; i.e., MANUAL PANELLING, in which case the user must take care over the number of input points. Alternatively, an AUTOMATIC PANELLING ROUTINE, referred to as the A.P.R., may be activated, which interpolates through the basic points to form a new set of points corresponding to panel corner points. (This is just a temporary set, as the user may opt to use the A.P.R. in the spanwise direction as well, in which case the section points do not necessarily line up with panel edges.)

Several options which provide great flexibility when preparing the input have been provided for defining the basic points. The options may be exercised at the section level so the input form may be changed from section to section. The options available at this time are described below and are controlled by the value of INMODE. INMODE values of 1 through 4 are illustrated in Figure 8.

INMODE values of 1, 2 and 3 are used when a section lies in one of the reference planes of the chosen S.C.S.; in these cases we have a constant coordinate, x, y, or z, respectively. With one coordinate fixed we need input only two coordinates for each basic point, e.g., y and z when INMODE = 1. Provision is made to specify a third quantity to give a local adjustment to the "constant" coordinate, e.g., when using INPUT = 2 we may specify x, z and $\delta$y. Usually the $\delta$ quantity is left blank (i.e., 0); however, nonzero $\delta$ values allow the user to "bend" the input section about the specified "constant" coordinate. The basic value for the constant coordinate is zero until the section points

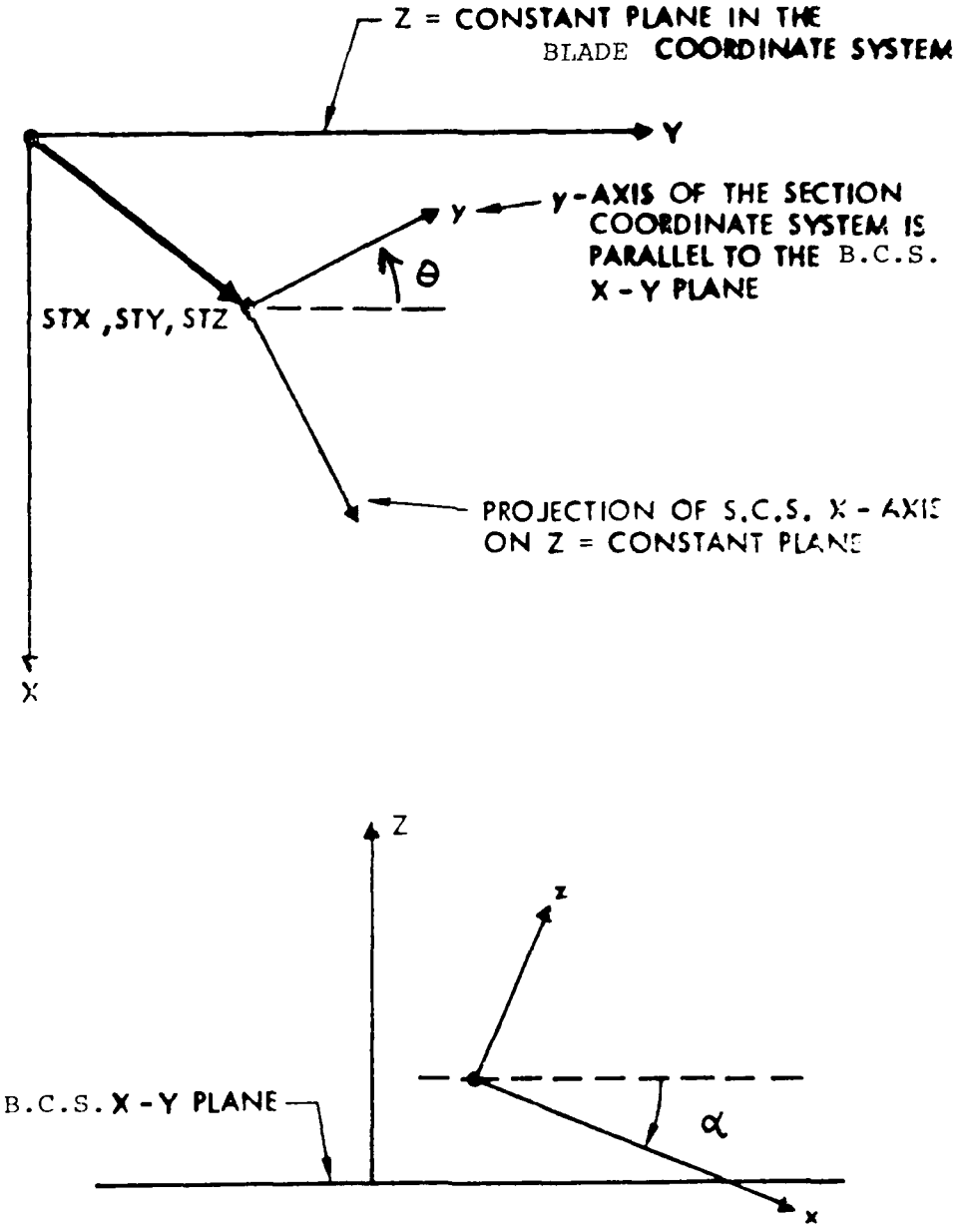


Figure 6. Section Transformation Into B.C.S.

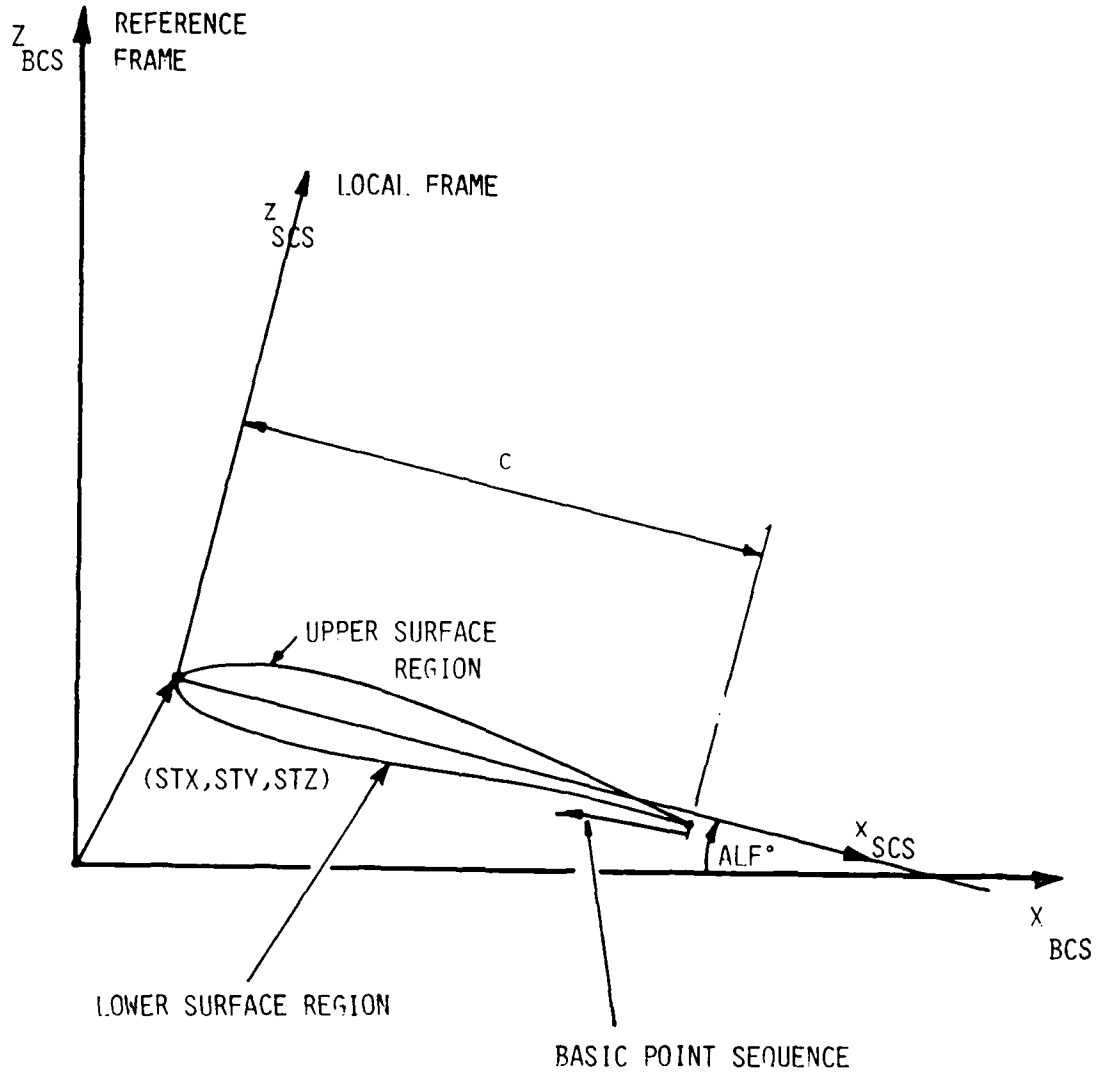


Figure 7. Section Coordinate System.

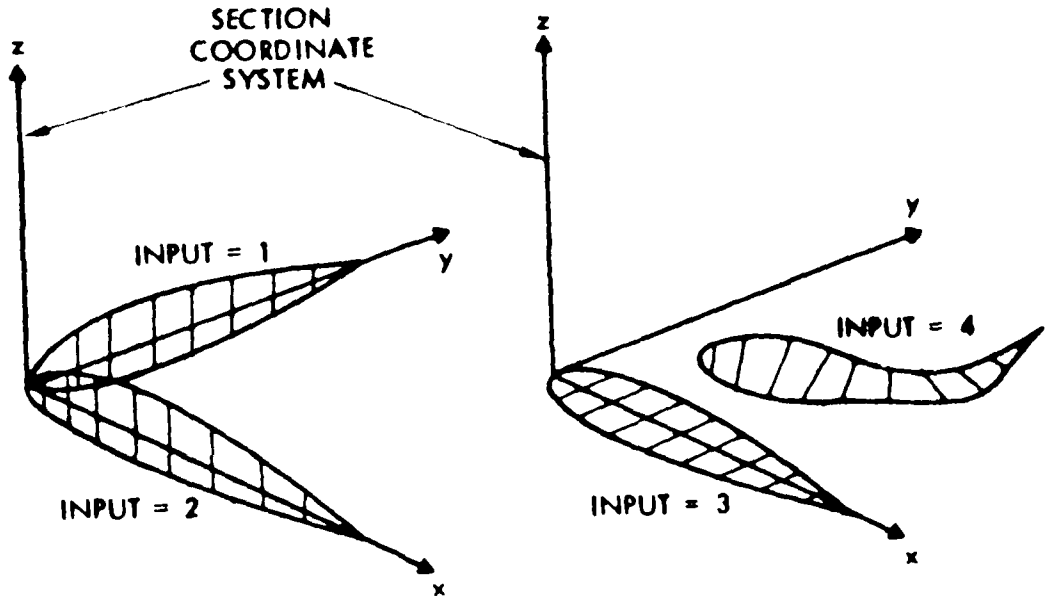


Figure 8. Basic Point Input Options 1 through 4.

are transformed into the B.C.S., so the value of that coordinate in the B.C.S. must be provided in the transformation information. INMODE value of 4, which requires all three components of each basic points position vector, is used when defining a completely arbitrary section shape. Finally, if the section shape has a NACA 4-digit form, then the INMODE parameter can be set to 5 and the code generates the panelling directly. The trailing-edge thickness has been made zero by modifying the coefficient in $x^4$ in the 4-digit equation, and the coordinates are generated in the INMODE = 2 format, i.e., x, z with y = 0.

Zero or negative values allow the present section's basic points to be copied over completely from any previously defined section. The section number is (-INMODE) except when INMODE = 0; the latter copies over the points from the section just completed. The section number specified is the absolute number from the beginning of the input and includes other copied sections as well as sections which may have been generated automatically. If the section counting becomes complicated, alternative ways of copying are available as described later in 3.2.5. The basic points are copied from the S.C.S. set (i.e., as originally specified) and are then transformed to the present B.C.S. according to the new section's transformation information.

### 3.2.3 Chordwise Regions

The basic points defining a section may be assembled in a number of CHORDWISE REGIONS for the purpose of controlling the panel density and distribution on that section. In addition, the option on manual or automatic panelling is selected at the chordwise region level, allowing the user to switch from one to another within each section wherever he chooses. Chordwise regions are used only as an input convenience and are discarded in the programs as soon as the surface panelling is complete.

A chordwise region must end on a basic point called a NODE POINT(Figure 9). A NODE CARD, containing the chordwise region panelling information (see below), inserted after a basic point in the input deck identifies that point as the end of a chordwise region. Node points are usually placed at "problem" areas where large velocity gradients are expected to occur, e.g., flap hinge line, leading edge, close-interference regions, but the user can place them wherever he wishes to change from one panel scheme to another. Four types of node points are provided at this time and are described below.

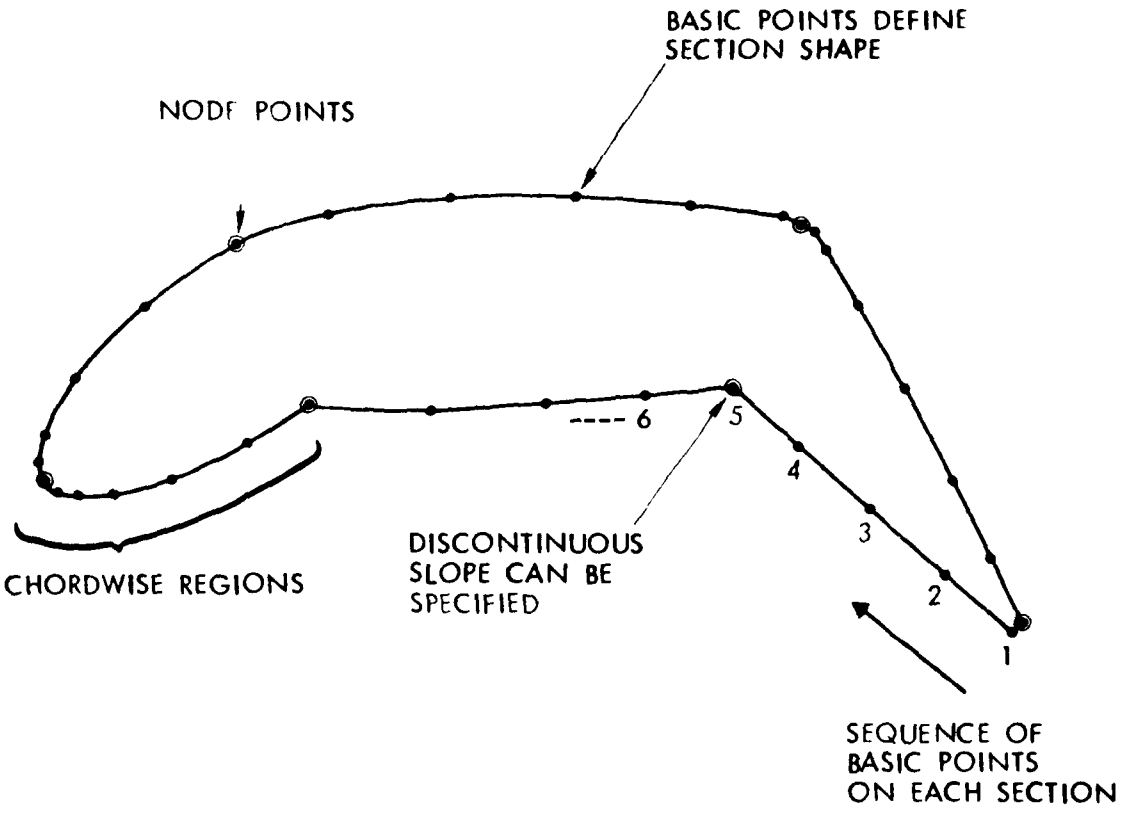


Figure 9. Chordwise Regions on a Section.

The information on a NODE CARD consists of just three integers:

(i) NODEC identifies the node point and its type.

(ii) NPC is the number of panels to be generated by the A.P.R. in the chordwise region just completed--a zero value gives manual panelling.

(iii) INTC controls the form of the distribution in the automatic panelling mode and is inactive in the manual panelling mode.

(The C on the end of each quantity distinguishes the chordwise from the corresponding spanwise quantities, which end in S; see Section 3.2.4)

NODEC values of 1 or 2 specify the end of a chordwise region with, respectively, continuous or discontinuous surface slope onto the next chordwise region. These values are therefore used only on regions ending in the interior of a section. The last point on a section is specified by NODEC = 3 and is the only node point that must always be specified even if manual panelling has been selected. Negative NODEC values are also permitted and initiate a special copying routine described in 3.2.5.

Four panel spacing options are provided in the A.P.R. The action of INTC values of 0, 1 and 2 is illustrated in Figure 10 and is based on the cosine distribution giving increased panel density towards, respectively, the beginning and end, the beginning only, or the end only, of the region. Equal spacing throughout the region is provided by ISPAC = 3. Coupled with the flexibility offered by the choice of chordwise region location, these spacing options have proven adequate so far; however, other options could easily be added should the need arise later, e.g., one based on increments in integrated surface curvature, or on increments in doublet value from a preliminary two-dimensional solution for the section.

Clearly, node cards provide the user with an extremely versatile panelling tool. With one card deck of basic points defining the configuration geometry, he can, from run to run, change the form of the panelling simply by changing two integer values on each node card. Not only that, he can also move node cards within the deck (but not the node cards at section ends) or remove some or add new ones from run to run. This allows the user to concentrate his panelling in the areas of interest, leaving other areas more sparsely panelled. It thereby provides a very effective use of the limited number of panels available, yet, on a subsequent run a few small changes to the node cards allow the emphasis to be switched to another area without having to punch a new basic geometry card deck.

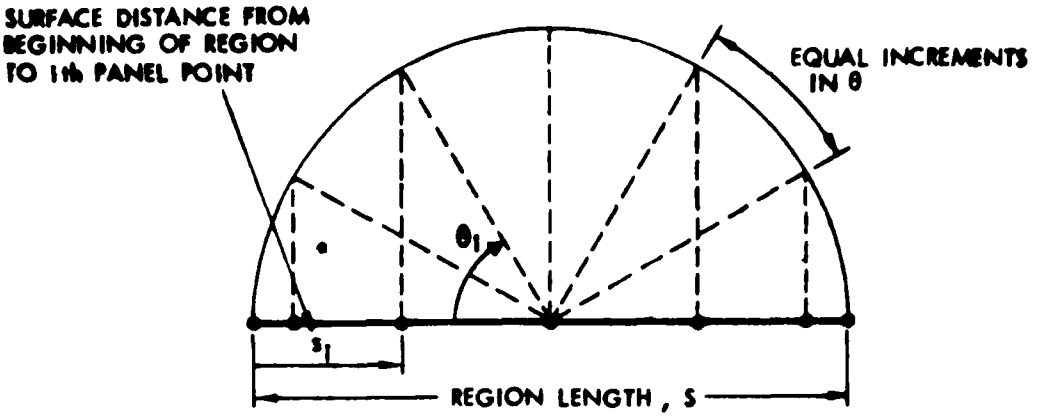


$s_1 = S(1 - COS(\theta_1))/2$

WHERE $\theta_1 = (I - 1)\pi/N$ AND N IS THE NUMBER OF INTERVALS REQUIRED

(a) INTC = 0

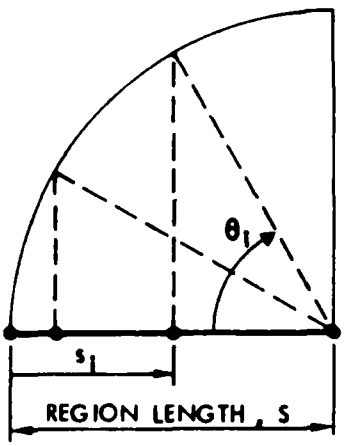


$s_1 = S(1 - COS(\theta_1))$

WHERE $\theta_1 = (I - 1)\pi/2N$

(b) INTC = 1

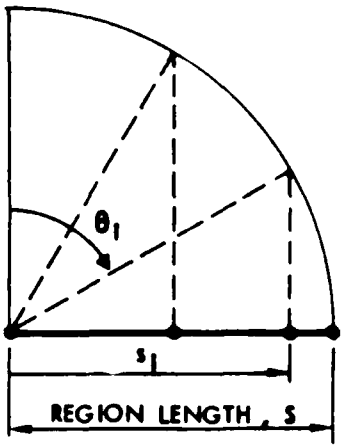


$s_1 = S\ SIN(\theta_1)$

WHERE $\theta_1 = (I - 1)\pi/2N$

(c) INTC = 2

Figure 10. Spacing Options 0, 1 and 2 in the A.P.R.

In most of our applications, the section basic points are assembled in two chordwise regions. The regions correspond to the section's lower and upper surfaces, respectively (Figure 7). The leading-edge point separates the two regions and is identified by a node card just after it with NODEC = 1 and JNTC = 2. The last basic point on a section is followed by a node card with NODEC = 3 and INTC = 1.

There is just one important ground rule for the use of node cards: the total number of panels (automatic and/or manual) on each section of a patch must be the same. The total is, in fact, the number of panel rows, NROW, for that patch. The program monitors the number of panels on each section and the calculations are terminated with an error message should the user make a mistake. Provided this ground rule is satisfied, it is not necessary for the panel distribution to be the same from section to section--in other words, the number of chordwise regions and their node information can vary from section to section.

### 3.2.4 Spanwise Regions

Sections defined within each patch may be assembled in a number of SPANWISE REGIONS for the purpose of controlling panel density and spacing in the spanwise direction. In forming spanwise regions, sections defined by the user take on a similar role to that of basic points in the chordwise regions. Although the options available for the spanwise regions are essentially the same as described for the chordwise regions in 3.2.3, the two are applied completely independently; for example, the user may request automatic panelling in the chordwise direction and manual in the spanwise direction. As in the case of chordwise regions, spanwise regions are used only as an input convenience and are discarded once the panelling is complete. 5 B

Spanwise regions must end at user-defined sections, called NODE SECTIONS (Figure 11). These usually coincide with kinks in the spanwise direction on the patch planform, but the user can place one whenever he wishes to change the form of the panelling or to change between manual and automatic panelling in the spanwise direction. For convenience, the spanwise node information is included on the section card together with the section transformation information (3.2.2). The function of the spanwise region node quantities, NODS, NPS, INTS--distinguished from the corresponding chordwise quantities by ending in S--follows closely the description in 3.2.3. NODS, however, must be set to zero (blank) on the first section of a patch and on all intermediate

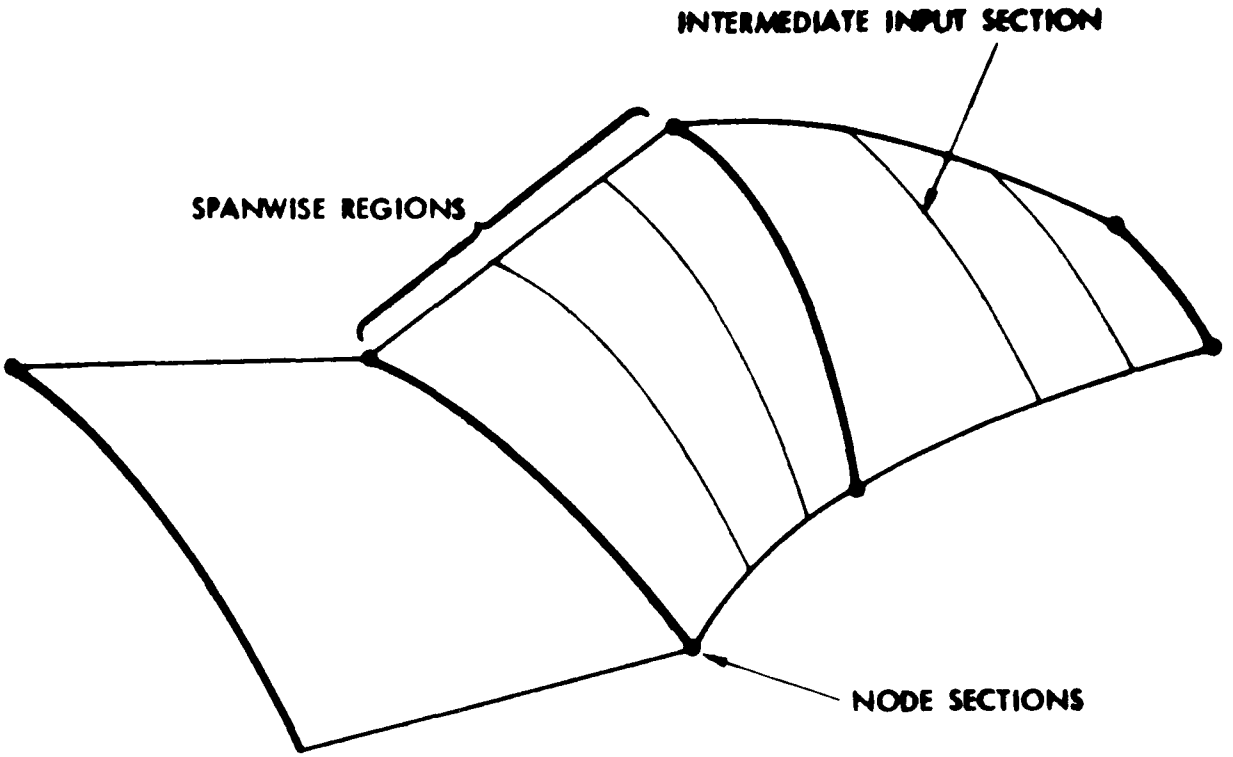


Figure 11. Spanwise Regions on a Patch.

input sections that are not node sections. (NPS and INTS are then inactive.) The last section on a patch is identified by a NODS value of 3 or 5; 5 is used if the patch is the last one on the configuration, in which case the present section completes the basic description of surface geometry.

The total number of panels defined (manually or automatically) across each patch in the spanwise direction is monitored by the program and becomes the number of panel columns, NCOL, for that patch. In view of the ease of generating panels, the code also monitors the running total of panels, and if a limit is exceeded, the calculation terminates with an appropriate error message. The limit is set internally by the storage capacity, but the user is given the opportunity to override that value with his own estimate (NPMAX on CARD 3) of the total he intends to use for that case. In the event of an input error, this will avoid the inadvertent and expensive use of, say, 1,000 panels when the user intended using only 100.

In the earlier hover work,[8] it was noted that errors in the surface doublet distribution can develop if a vortex passes within one panel width of the blade surface. With the present panelling options in the spanwise direction, problems of this nature can be minimized by requesting a patch break, edge, near the first vortex passage and selecting appropriate panel numbers in adjacent patches. For this purpose, it is sometimes convenient to know the panel number needed for a given spacing option to obtain a required minimum panel width, say $\Delta S_{MIN}$. The required number of panels, $NPS_{REQ}$, for the spacing options are as follows.

INTS = 0:

$$NPS_{REQ} = \frac{\pi}{\cos^{-1}\left(1 - \frac{2\Delta S_{MIN}}{S}\right)} \tag{6a}$$

INTS = 1:

$$NPS_{REQ} = \frac{\pi/2}{\cos^{-1}\left(1 - \frac{2\Delta S_{MIN}}{S}\right)} \tag{6b}$$

INTS = 2:

$$NPS_{REQ} = \frac{-F}{1 - F} \tag{6c}$$

where

$$F = \frac{\pi/2}{\sin^{-1}(1 - \frac{\Delta S_{MIN}}{S})}$$

INTS = 3:

$$NPS_{REQ} = \frac{S}{\Delta S_{MIN}} \tag{6d}$$

## 3.3 SPECIAL ROUTINES

The geometry routines described above may be applied for the complete configuration; however, special routines have been provided to reduce user input and, in particular, to avoid duplicating information already supplied. These routines, which are described below, are optional.

### 3.3.1 Copying Routine

We have already seen (3.2.2) a copying facility accessible at the section input level. This copies over a complete section, including the chordwise region information, and has, therefore, a rather limited application. More general copying routines are provided and are activated at the basic point level to copy STRINGS OF BASIC POINTS, rather than complete sections. This capability allows a new section to be assembled from parts of previously defined sections. Several strings of basic points may be assembled from a number of previously defined sections and the points selected need not follow the same direction as originally specified. Furthermore, the copied strings of points may be intermixed with strings of manually input basic points to complete the new section.

For this copying mode, the value of INMODE on the section card (3.2.2) must be in the range 1 to 4. The copying is activated by inserting a NODE CARD having a NEGATIVE sign on NODEC. This is regarded as a DUMMY node card because it does not necessarily terminate a chordwise region (see below). The negative value for NODEC determines the action at the end of the copied string of basic points. If NODEC = -1 or -2, then the last copied point becomes the end of a chordwise region on the new section and signifies, respectively, continuous or discontinuous slope onto the next chordwise region. We then continue to specify further basic points or, by inputting another negative node card, we can copy another string of basic points, and so on. If NODEC = -3, then the last copied point in the string completes the new section.

If the user does not require a chordwise region to end at the last point in a copied string, then he sets NODEC = -4 when he initiates the copy. When the string has been copied over, the program then expects to receive further basic points to complete the chordwise region or another negative node card can be used to copy another string of points, and so on. Clearly, if NODEC = -4, then the NPC and INTC values on the NODE CARD are inactive and may be left blank.

Whenever a negative node card is inserted, it must always be followed by a COPY CARD containing the following information (four integers) defining the location of the required string of points, IPCH, ISEC, IB, LB.

IPCH is the patch number containing the required points.

ISEC is the section number relative to the start of that patch.

IB, LB are, respectively, the first and last basic point numbers (inclusive) defining the string. The numbering is relative to the start of the section ISEC.

Thus, even in a complicated configuration, it is relatively easy to specify a string of basic points.

This option offers not only an alternative to the earlier copying routine, but also a more general capability because the copying is initiated at the basic point input level, rather than at the section input level. For example, the complete copied section need form only a part of the new section, it being possible to have other basic points, both before and after the copied string. In addition to this, the ability to break the copying into strings of points allows a new distribution of chordwise regions to be selected.

One restriction must be considered when using this copy routine--the new section's value for INMODE must coincide with the INMODE values on section from which strings of points are to be copied. This restriction has not posed a problem so far, but if it does, it would not be too difficult to remove.

### 3.3.2 Automatic Patch Generator

The patch covering the tip edge can be input by the user as an ordinary patch, but this can get tedious. Optional automatic procedures have been installed which simplify this input by generating a complete patch within the code. This AUTOMATIC PATCH GENERATOR (A.P.G.) is initiated at the patch input level by inserting a nonzero value for parameter, MAKE, on the patch data card. The value of MAKE identifies the patch number on the edge of which a closing patch is to be generated. The sign of MAKE determines whether the new patch is on side 3 (positive) or side 1 (negative) of the basic patch.

Consider Figure 12. Here we have already defined the patch representing the main surface. The end section of that patch provides the BASE SECTION from which the A.P.G. creates the new patch according to user instructions. When the A.P.G. has been activated, the next card must contain the following:

NPC, INTC, KURV, NODS, NPS, INTS.

The generated patch has one "chordwise" region with NPC panels spaced according to the value of INTC. The values for NPS and INTS determine the "spanwise" panelling on the patch. It is recommended that the same values be used for these as were used, respectively, for NPC, INTC on the lower surface of the base section; in particular, NPS = 0 should only be used if the value for NPC on the base section was also zero. The value of NODS must be 5 as this patch completes the patch input.

The function of KURV is described next. Sections defining the new patch are created automatically from the base section coordinates. The contour of each section generated may be either a straight line ("square-cut" tip) or a semicircle, depending on the value of the quantity, KURV, supplied by the user. If KURV is 0, sets of basic points are generated on straight lines joining upper and lower points on the base section. The same number of points is created even if the interval across the base section is zero, e.g., at the leading and trailing edges (Figure 12).

If KURV is 1, the basic points are created on semicircles having a diameter equal to the local "thickness" of the base section.

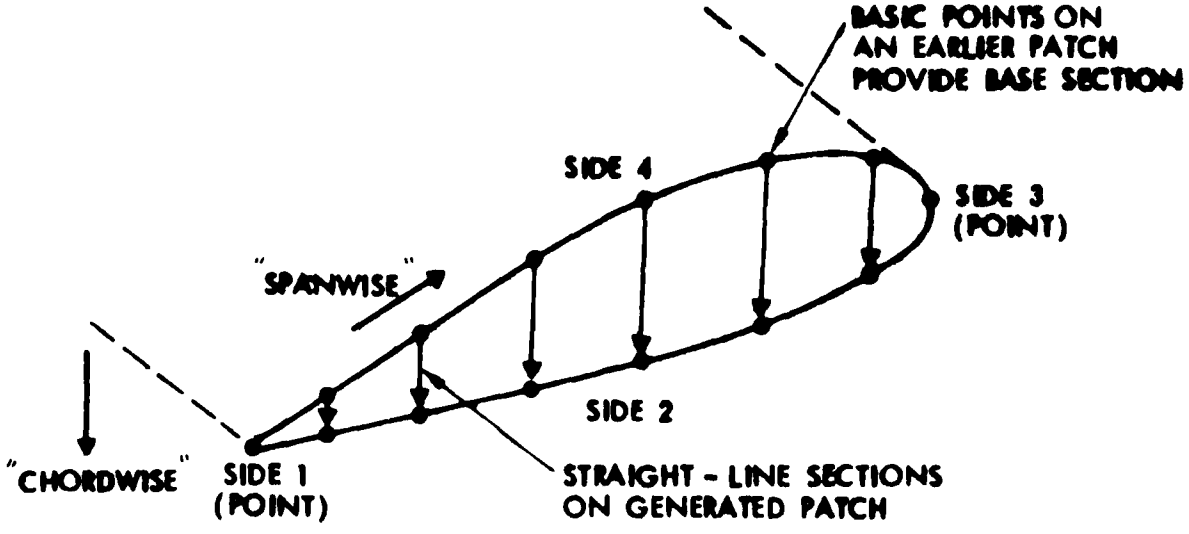


(a) FLAT EDGE PATCH (KURV = 0)

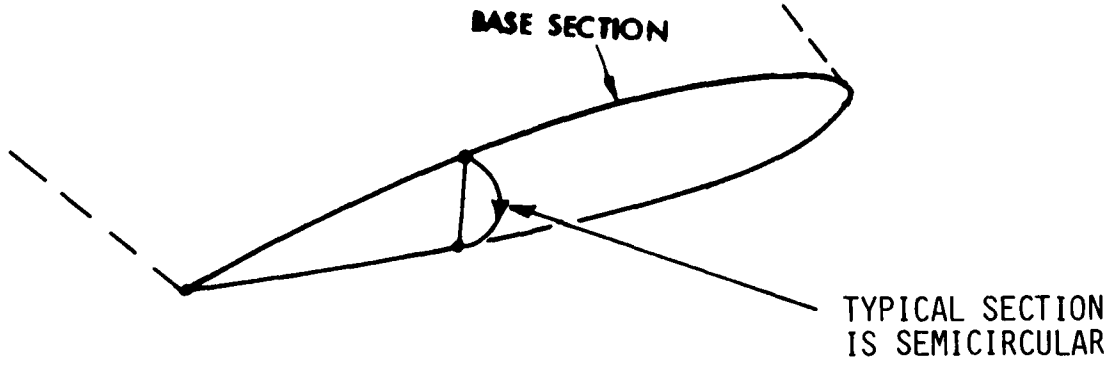


(b) PATCH WITH SEMICIRCULAR SECTIONS (KURV = 1)

Figure 12. Automatic Patch Generator.

## 4.0 WAKE ROUTINES

In general, the prescribed wake methods and the relaxed wake techniques developed for the HOVER code have been carried over for ROTAIR. Basic changes that were required for the surface potential method involved the attachment of the wake to the actual blade surface at its coned and twisted position, the structural change for the wake from individual filaments to wake columns for the velocity potential calculation, the description of the rotor wake in patches of panels, the modelling of the initial tip-edge wake geometry that separates from the thick-blade surface, and a velocity potential model of the far-wake influences.

### 4.1 WAKE PATCHING

Within ROTAIR, the rotor wake structure is now actually composed of three wakes as illustrated in Figure 13. WAKE 1 consists of all the wake columns that make up the inner sheet, i.e., the shed wake up to the maximum circulation location. WAKE 2 is composed of the wake columns comprising the outer tip sheet to the trailing edge of the tip section; therefore, the first wake column of WAKE 2 is the potential representation of the merged tip vortex. WAKE 3 includes the columns of wake panels that are shed from the tip-edge separation line. The extent of the separation across the blade tip is controlled by the user and is described later in this section. Regardless, WAKE 1 and WAKE 2 are always present while WAKE 3 can be eliminated if no tip-edge separation is required.

As shown schematically in Figure 13, the attachment of the wake patches to blade edges is independent of the patches of panels representing the blade surface. For example, the attachment line of WAKE 1 can terminate in the middle of a blade surface patch. Also, the actual streamwise lengths of each wake are controlled independently in the manner set up in the HOVER code. Of course, the length of WAKE 3, if it exists, is set by the user-specified merger azimuthal angle, PSIMRG.

In order to simplify user input, the actual patching of the wakes and the stitching of the wakes to the blade surface are automatically computed in ROTAIR. In this way, user input of a rotor wake for ROTAIR is almost identical to that required for HOVER.

### 4.2 INITIAL WAKE GEOMETRY

The global wake structure is still represented by the near-, intermediate- and far-wake regions originally developed for the HOVER code. However, the new far-wake model described later

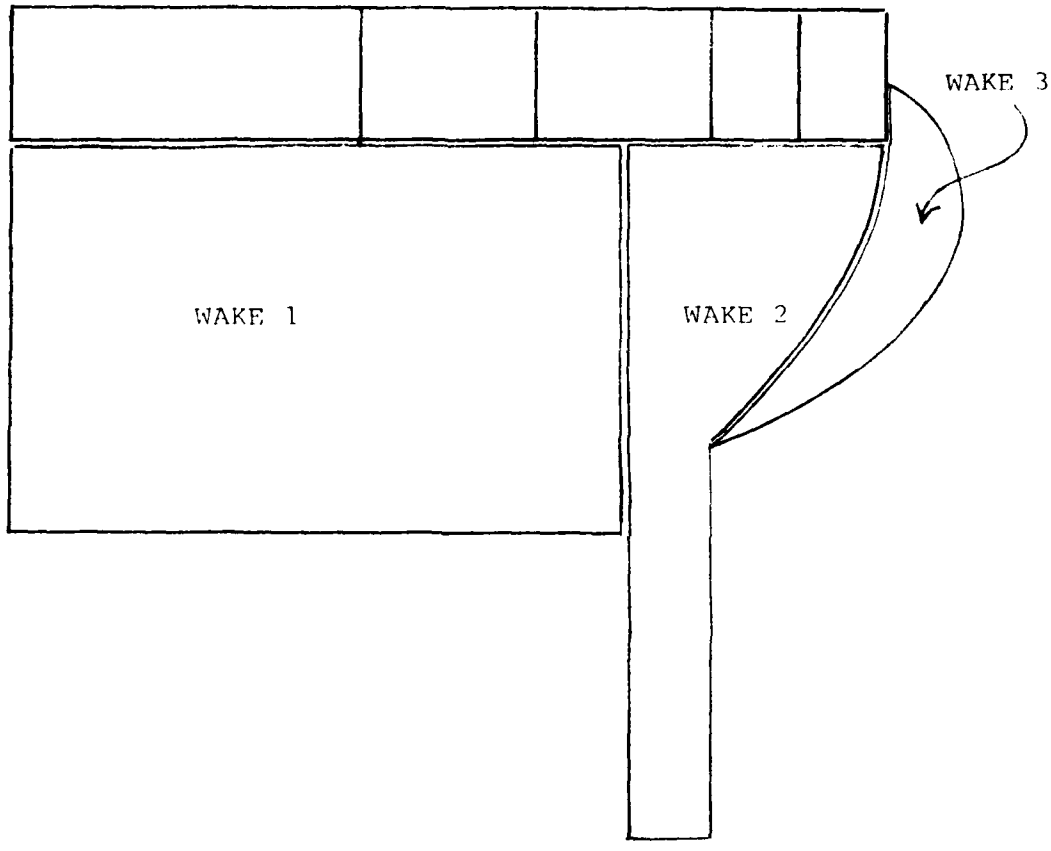


Figure 13. Wake Patching.

is now keyed to a PSIF2 specification so that the far-wake boundary is closer to the blade for inner sheet filaments (Figure 14). This change has resulted in significant savings of computer time; however, the old model may be required for wake relaxation calculations.

The near wake normally includes a few vortex passes below a blade, and the general wake equations (3) describing the filaments in this region are summarized below (see Figure 15).

(1) Tip Vortex Axial Coordinates: $\psi_b = \frac{2\pi}{b}$

$$\bar{z}_t = \begin{cases} k_1 \psi_w & 0 \leq \psi_w \leq \psi_b \\ (\bar{z}_t)_{\psi_b} + k_2 (\psi_w - \psi_b) & \psi_w \geq \psi_b \end{cases} \tag{7a}$$

(2) Tip Vortex Radial Coordinates:

$$\bar{r} = A + (1 - A)\, e^{-\lambda \psi_w} \tag{7b}$$

(3) Vortex Sheet Axial Coordinates: (usually, $\psi_o = \frac{\pi}{2}$)

$$(\bar{z}_t)_{\bar{r}=1} = \begin{cases} k_{1_{\bar{r}=1}} \psi_w & 0 \leq \psi_w \leq \psi_b \\ k_{1_{\bar{r}=1}} \psi_b + k_{2_{\bar{r}=1}} (\psi_w - \psi_b) & \psi_w \geq \psi_b \end{cases} \tag{7c}$$

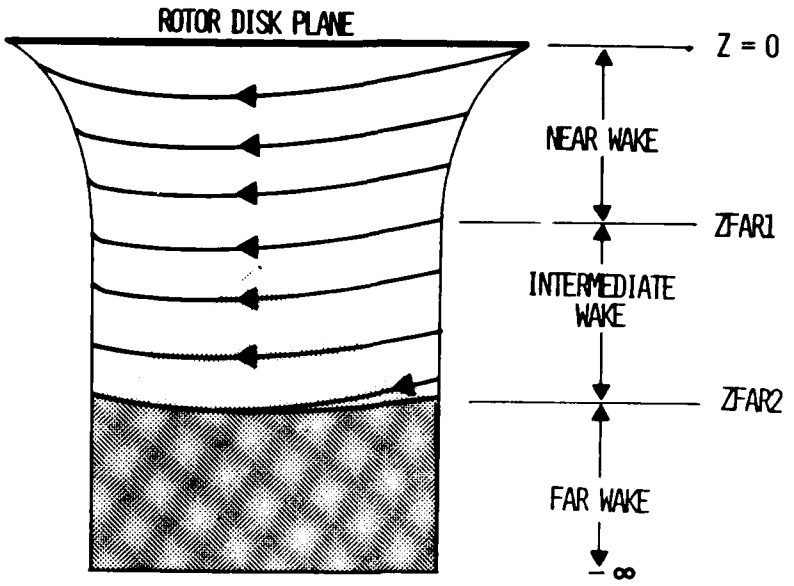


Figure 14. Global Wake Model.

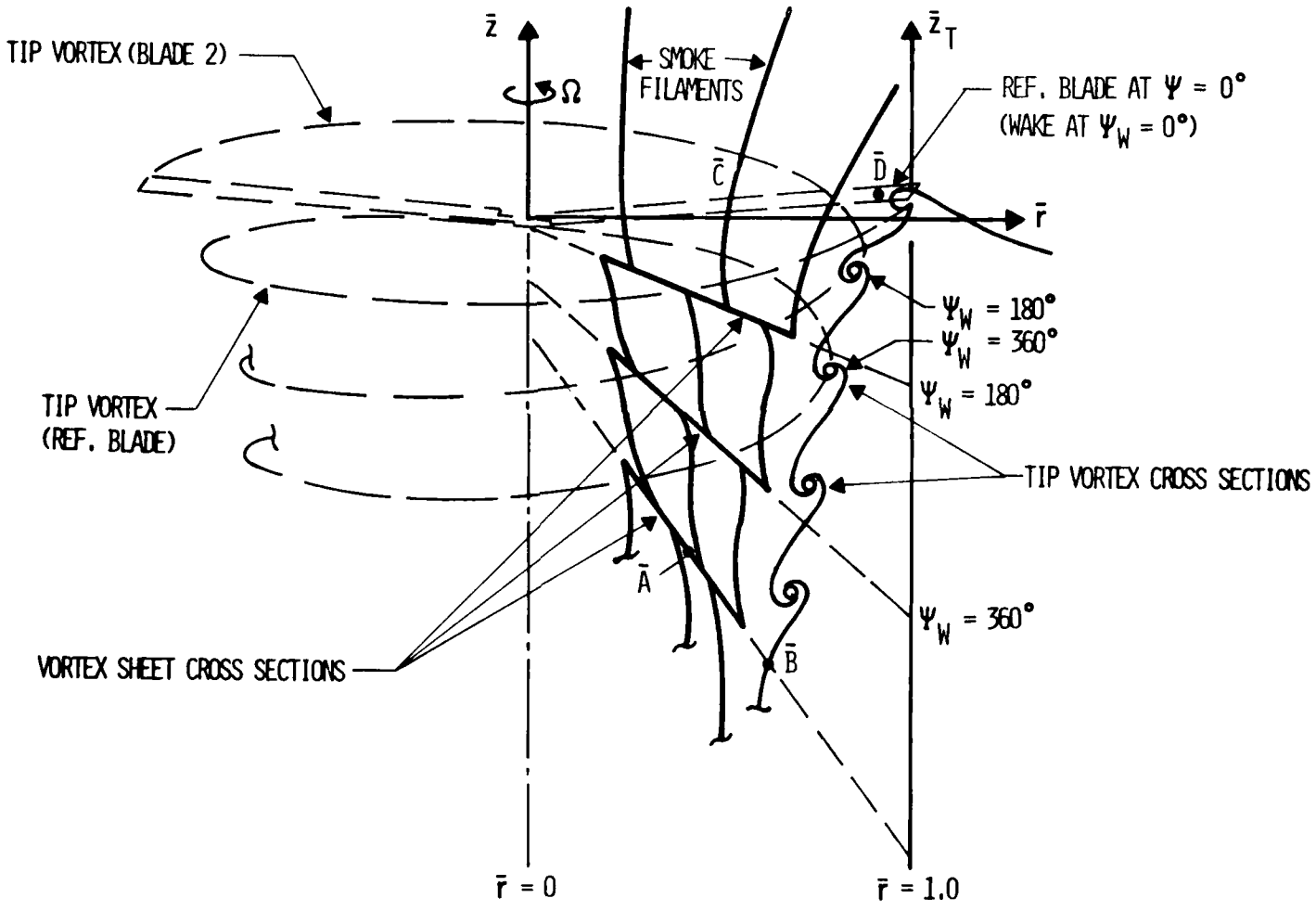


Figure 15. Schematic of Wake Cross-Section Showing Wake Coordinate System.

$$(\bar{z})_{\bar{r}=0} = \begin{cases} k_{1_{\bar{r}=0}} \psi_w & 0 \leq \psi_b \leq \psi_o \\ k_{1_{\bar{r}=0}} \psi_o + k_{2_{\bar{r}=0}} (\psi_w - \psi_o) & \psi_w \geq \psi_o \end{cases} \tag{7d}$$

(4) Vortex Sheet Radial Coordinates:

$$\bar{r}_{\bar{A}} = \left( \frac{\bar{r}_{\bar{c}}}{\bar{r}_{\bar{D}}} \right) \bar{r}_{\bar{B}} \tag{7e}$$

As shown in Figure 15, $\bar{z}_t$ are the axial coordinates with respect to the tip path plane. However, the wake actually leaves from the blade trailing-edge position. Consequently, an effective $k_1$ is calculated in ROTAIR to carry the tip wake filament from the trailing edge to the axial position at first blade passage. The equation for the tip vortex with respect to the tip path plane system is then

$$\bar{z}_t = \bar{z}_{TE} + K_{eff} (\psi - \psi_{TE}) \qquad \psi_{TE} \leq \psi \leq \psi_b$$

with

$$K_{eff} = \frac{\bar{z}_{\psi_b} - \bar{z}_{TE}}{\psi_b - \psi_{TE}}$$

The $(\bar{z}_t)_{\bar{r}=1}$ equation is similarly modified.

These wake coordinates must be transformed to the H.C.S. for use with the blade surface panelling. In general, the blade cone angle, $\beta$, requires a vertical displacement and a small inboard shift of the tip coordinates as shown in Figure 16.

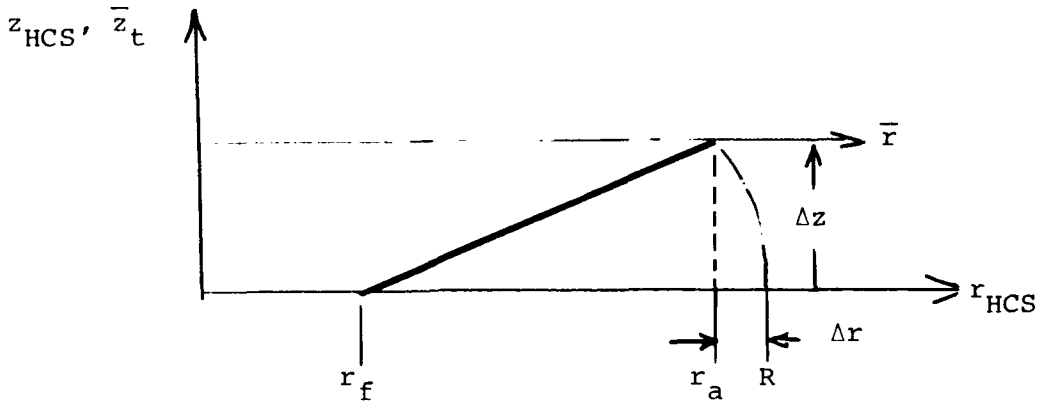


Figure 16. Effect of Blade Coning on Wake Coordinates.

Now, $\Delta z = (R - r_f) + \sin \beta$

and $\Delta r = R - \left[(R - r_f) \quad \cos \beta + r_f\right]$

Hence,

$$r_a = R - \Delta r = (R - r_f) \quad \cos \beta + r_f \ .$$

Consequently, the tip path plane tip vortex coordinates (Eq (7a), (7b) and (7c)) are modified to obtain the H.C.S. coordinates as follows:

$$z_{HCS} = \bar{z}_t + \Delta z \qquad (8a)$$

$$r_{HCS} = \bar{r}\ r_a \qquad (8b)$$

The detailed near wake segmentation is modelled in the manner of the HOVER code (Figures 17 and 18). The azimuthal step angle, $\Delta\psi_w$, of the wake sheet and the tip region can be specified independently, i.e., $\Delta\psi_{w_s}$ and $\Delta\psi_{w_t}$. Further, these step sizes in the wake (or, equivalently, the vortex segment lengths) can be changed to new values after the first blade passage. This flexibility allows very efficient computation without sacrificing accuracy in loads prediction.

The tip separation wake, WAKE 3, is modelled as illustrated in Figure 19. The user specifies the number of surface panels from the trailing edge that participate in the wake separation, NSEP; the height above the trailing edge that the tip vortex attains, DELZ; and the inboard shift of the tip vortex across the blade surface at the trailing edge, DELR. As a first approximation, DELZ and DELR can be set to a distance corresponding to the tip vortex leaving the blade surface at 1/2 the tip section geometric angle of attack. As experience is gained with the tip shedding, this procedure will be automated within the code. For this model, the feeding sheet filament effects are included, and the actual wake panelling of WAKE 3 is automatically generated.

The intermediate-wake region is composed of fixed-pitch, constant radius helices. The pitch and radius of each filament is determined by the final pitch and radius of the filament in the near wake.

Finally, recall that in the HOVER code the far-wake region represents a semi-infinite continuation of this vorticity model. That is, the downwash velocity components due to each helical vortex filament trailing behind the rotor is approximated by the velocity due to a cylinder of uniform vorticity in the far wake (Figure 20).

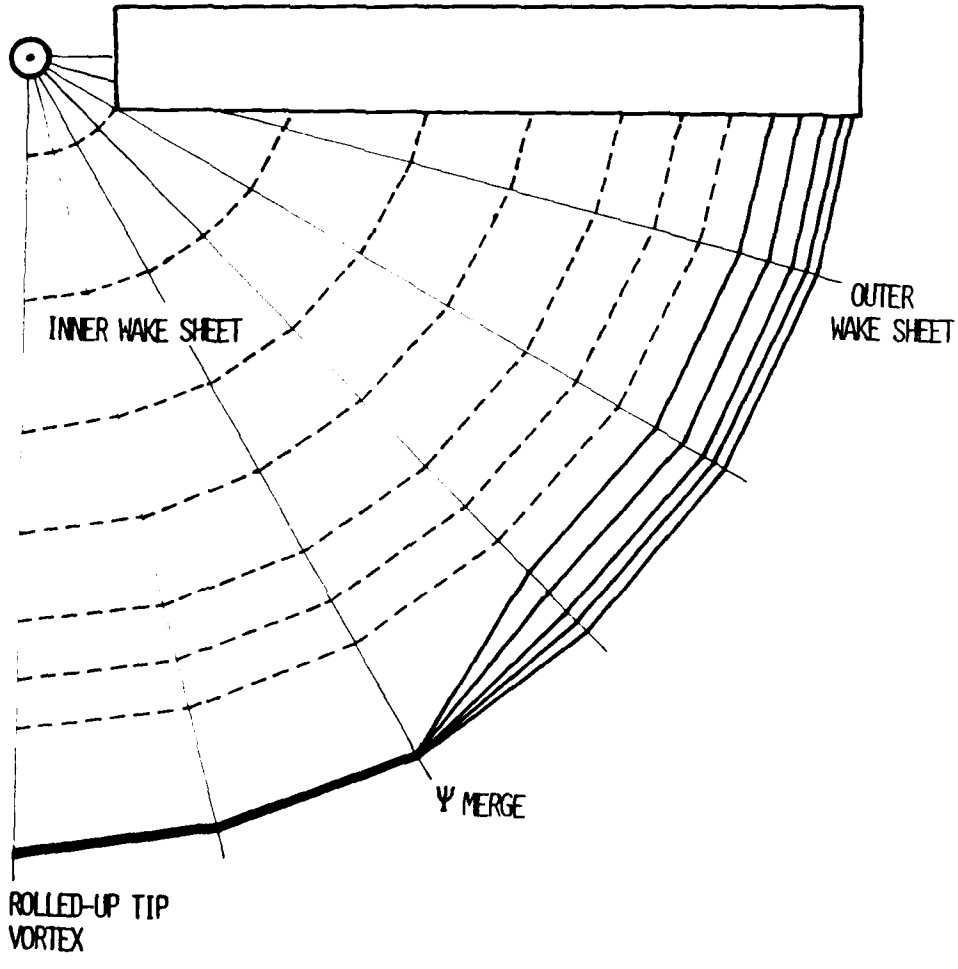


Figure 17. Rotor Wake Geometry (Top View).

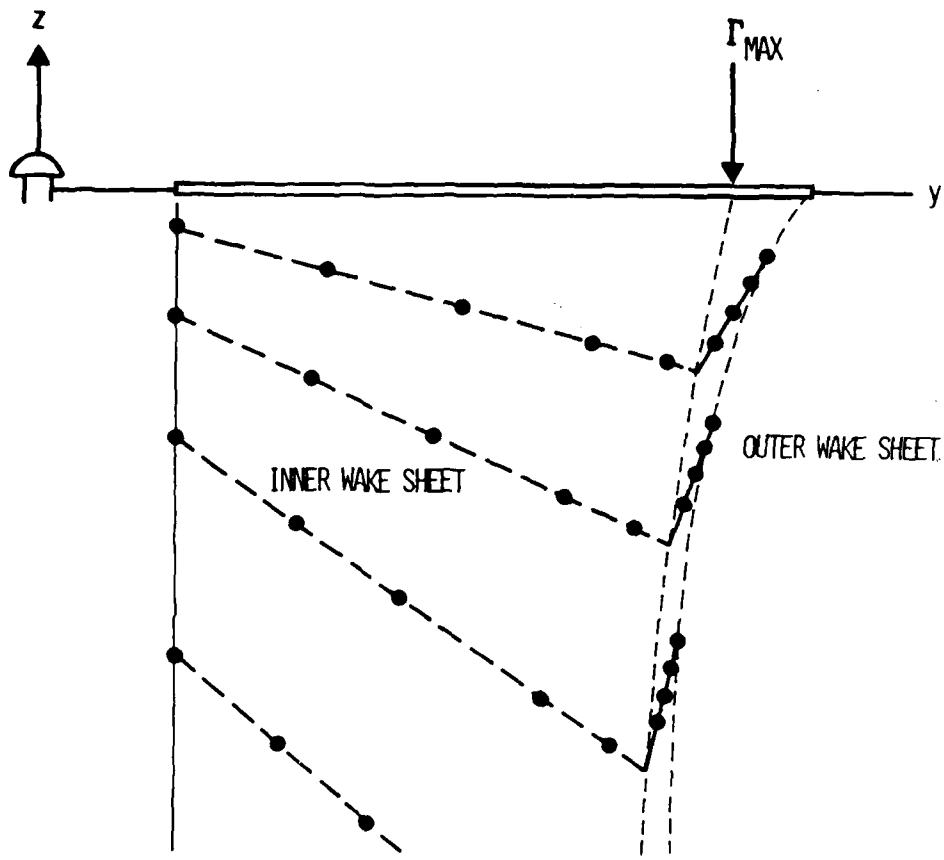


Figure 18. Rotor Wake Geometry (Azimuthal Section).

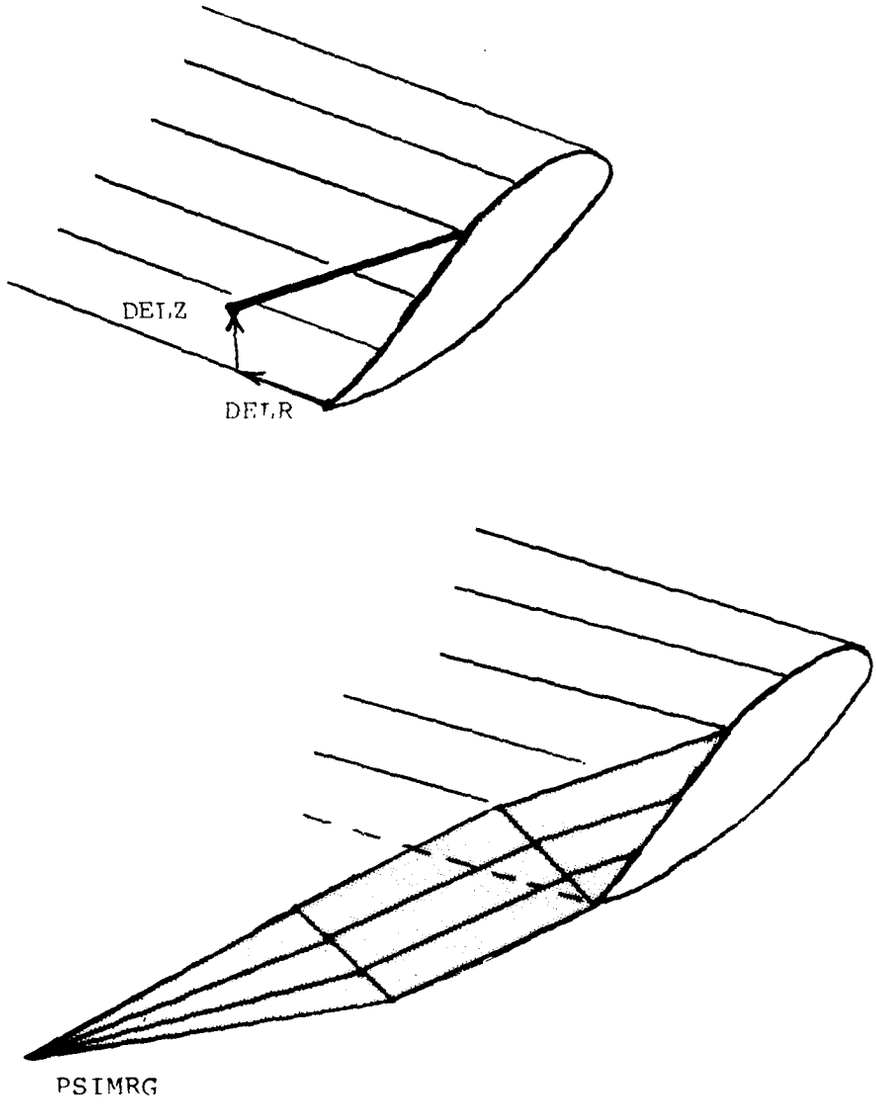


Figure 19. Rotor Tip Wake Separation.

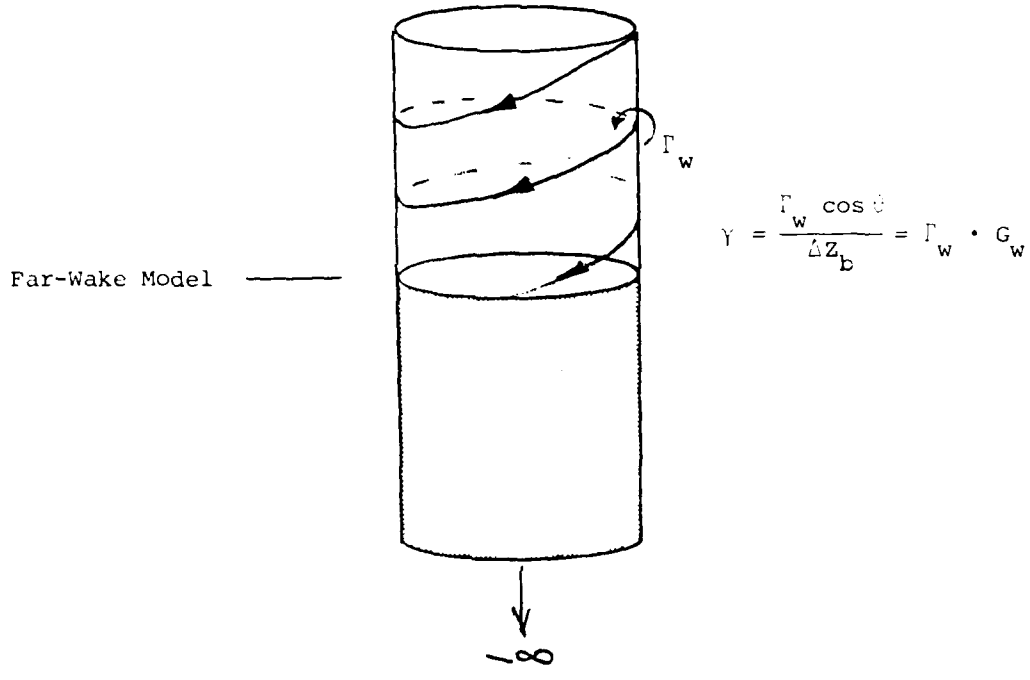


Figure 20. Far-Wake Vorticity Model.

Further, the velocity due to a semi-infinite cylinder of uniform vorticity is identical to that induced by a sink sheet on the capping surface of uniform strength equal to the vorticity (Figure 21).

In ROTAIR, this same model is used for velocity calculations with the modification that the starting axial location of the far-wake influence is individually determined for each vortex helix.

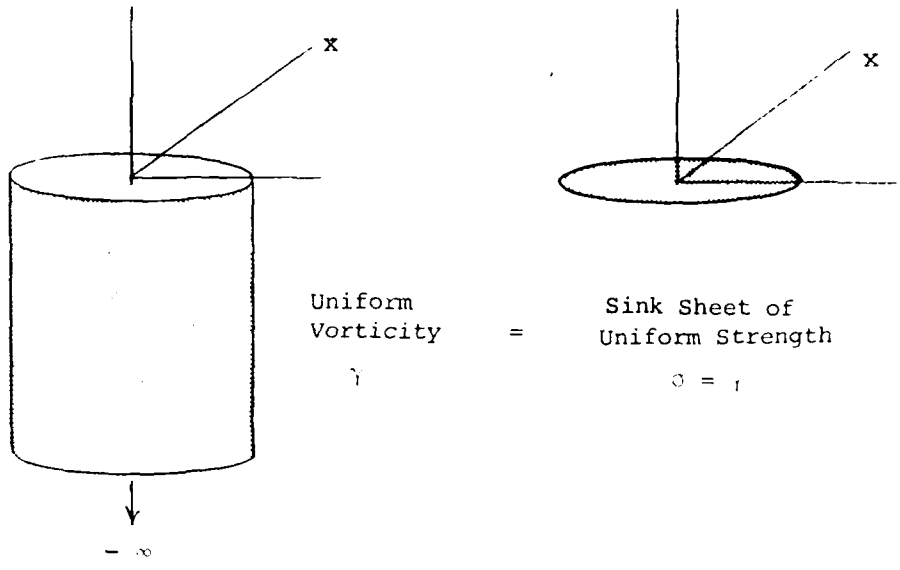


Figure 21. Equivalency of a Cylinder of Uniform Vorticity and a Sink Sheet of Uniform Strength.

While this sink sheet method works well for velocities, such a simplification for the velocity potential influence is not possible. Instead, the velocity potential induced by the far-wake is that due to the superposition of cylindrical potential sheaths of linearly increasing doublet distribution. The velocity and potential equivalence is schematically shown in the figure below.

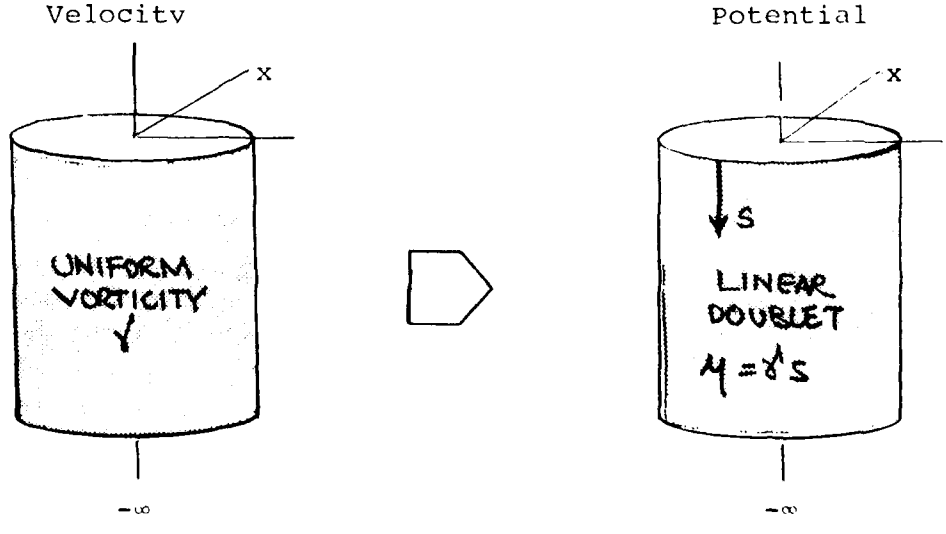


Figure 22. Illustration of the Velocity Potential Produced by a Cylinder of Uniform Vorticity.

This far-wake potential model has been added to ROTAIR for the aerodynamic matrix calculation. The accuracy of the model is demonstrated in Section 6.0.

## 4.3 PRESCRIBED WAKE ITERATION

The prescribed wake constants are determined by the empirical equations due to Landgrebe[3] or Kocurek.[14] These equations are also described in detail in the HOVER document.[8] Regardless of which equations are used, the wake constants are related to thrust coefficient (more recently, the constants have been related to maximum blade circulation, and not to blade collective). Therefore, the prescribed wake iteration should be properly carried out within a collective iteration. Consequently, for this intermediate time until the collective loop is available in ROTAIR, the user is required to read in the appropriate wake constants explicitly. Several computer runs will then be required to obtain the collective setting for a calculated thrust coefficient equal to the requested thrust coefficient used to position the wake. The prescribed wake iteration loop in ROTAIR continues until the blade maximum circulation location is unchanged.

## 4.4 RELAXED WAKE

If requested, the merged tip vortex position is then relaxed to a force-free location for the resultant fixed collective. The relaxation technologies developed for HOVER are incorporated here. These were all described in great detail in Reference 8, and the reader is referred to that document.

---

[14] Kocurek, J.D., and Tangler, J.L., "Prescribed Wake Lifting Surface Hover Performance Analysis", Presented at the 32nd Annual National VSTOL Forum of the American Helicopter Society, Washington, D.C., May 1976.

## 5.0 ROTOR PERFORMANCE CALCULATIONS

Since ROTAIR is a surface singularity method, the local surface velocities are calculated at all blade surface panel center points. With this information, the local panel surface pressure coefficients are obtained and rotor loading can then be calculated by surface pressure integration. Usually, the pressure coefficient is defined by reference to the local sectional onset flow velocity, say $\underline{V}_O$. For the rotor problem, this quantity varies linearly with the blade radius station. For the hover problem considered here, the characteristic velocity for normalization is the rotor tip rotation speed, $V_{TIP} = \Omega R$. Consequently, it is convenient to define two pressure coefficients--a conventional one based on the local sectional onset velocity for comparison with experimental data, and another based on the tip rotation velocity to observe the actual blade surface pressure distribution and also to facilitate the direct calculation of the integrated rotor performance. As indicated in Figure 23, the sectional characteristic onset flow velocity at section i is $\underline{V}_{O_i}$, so that

$$V_{O_i} = \sqrt{W^2_{CLIMB} + \Omega^2 Y_i^2}$$

Consequently, the conventional pressure coefficient at panel j of section i in variables normalized by rotor radius, R, is

$$C_{p_{ij}} = \frac{p - p_\infty}{\frac{1}{2}\rho V^2_{O_i}} = \frac{w_c^2 + r_{w_{ij}}^2 - v_{s_{ij}}^2}{w_c^2 + y_i^2} \qquad (9)$$

On the other hand, the pressure coefficient at panel i based on rotation tip speed is

$$C^*_{p_{ij}} = \frac{p - p_\infty}{\frac{1}{2}\rho(\Omega R)^2} = w_c^2 + r_{ij}^2 - v^2_{s_{ij}} \qquad (10)$$

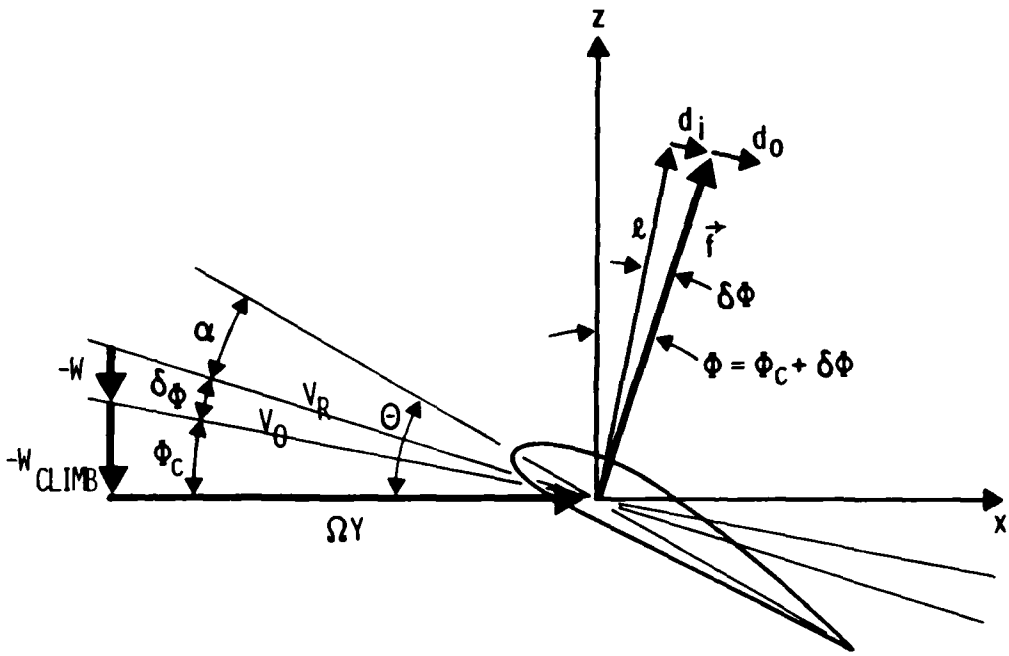


Figure 23. Sectional Aerodynamic Forces.

In both equations, $r_{ij}$ is the normalized radius to panel j, and $v_{s_{ij}}$ is the normalized surface velocity at panel j.

## 5.1 INVISCID ROTOR AERODYNAMIC PROPERTIES

The sectional properties can be found by integration of the pressure distribution around the airfoil surface. For our purposes here, the sectional loads are calculated for a given column of panels. The orientation of the column may or may not be streamwise, depending on the user input surface panelling requests. The following figure will be useful in the derivation of the sectional loading (see also Figure 23).

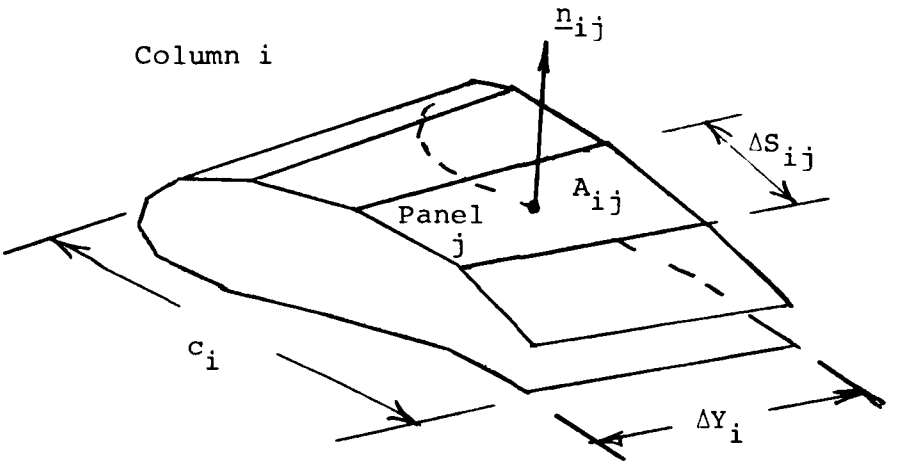


Figure 24. Illustration of the Pressure Loading on Panel j of Column i.

By definition

$$\underline{C}_{f_i} = \frac{\underline{f}_i}{\rho(\Omega R)^2 \pi R}$$

Consequently,

$$\underline{C}_{f_i} = \frac{1}{2\pi} \sum_j - C^*_{p_{ij}} \underline{n}_{ij} \Delta s_{ij}$$

However,

$$\Delta s_{ij} \approx \frac{A_{ij}}{\Delta y_{ij}}$$

and

$$\Delta y_{ij} \approx \Delta y_i \approx \frac{\frac{1}{2} \sum_j A_{ij}}{c_i}$$

Hence,

$$\underline{C}_{f_i} = \frac{c_i}{\pi} \frac{\sum_j -C^*_{p_{ij}} A_{ij} \underline{n}_{ij}}{\sum_j A_{ij}} \qquad (11)$$

Of course, the corresponding sectional moment coefficient about the H.C.S. origin is just

$$\underline{C}_{m_i} = \frac{\underline{m}_i}{\rho(\Omega R)^2 \pi R^2} = \frac{c_i}{\pi} \frac{\sum_j -C^*_{p_{ij}} A_{ij} \underline{r}_{ij} \hat{} \underline{n}_{ij}}{\sum_j A_{ij}} \qquad (12)$$

The corresponding integrated rotor aerodynamic coefficients are, respectively (b is the blade number),

$$\underline{C}_F = \frac{\underline{F}}{\rho(\Omega R)^2 \pi R^2} = b \sum_i \Delta y_i \, \underline{C}_{f_i}$$

or

$$\underline{C}_F = \frac{b}{2\pi} \sum_i \sum_j -C^*_{P_{ij}} A_{ij} \, \underline{n}_{ij} \tag{13}$$

and

$$\underline{C}_M = \frac{\underline{M}}{\rho(\Omega R)^2 \pi R^3} = b \sum_i \Delta y_i \, \underline{C}_{m_i}$$

or

$$\underline{C}_M = \frac{b}{2\pi} \sum_i \sum_j -C^*_{P_{IJ}} A_{ij} \, \underline{r}_{ij} \times \underline{n}_{ij} \tag{14}$$

The usual rotor performance coefficients are then obtained by taking appropriate components of Eq (11) through (14). The coefficients of interest computed by pressure integration are:

Sectional Thrust Coefficient: $C_{t_i} = \underline{C}_{f_i} \cdot \underline{k}$

Integrated Thrust Coefficient: $C_T = \underline{C}_F \cdot \underline{k}$

Sectional Induced Torque Coefficient: $C_{q_{I_i}} = -\underline{C}_{m_i} \cdot \underline{k}$

Integrated Induced Torque Coefficient: $C_{Q_I} = -\underline{C}_M \cdot \underline{k}$

The sectional force and moment components along the other H.C.S. axis are also computed in the program. Further, the sectional lift and induced drag coefficients are obtained from Eq (11) in the manner described in Reference 8. That is (see Figure 23),

$$C_{\ell_i} = \frac{\ell_i}{\frac{1}{2}\rho V_{o_i}^2 \bar{c}_i} = \frac{2\pi}{(w_c^2 + y_i^2)c_i} C_{f_i} \cos \delta\phi_i \qquad (15)$$

and

$$C_{d_i} = \frac{d_i}{\frac{1}{2}\rho V_{o_i}^2 \bar{c}_i} = \frac{2\pi}{(w_c^2 + y_i^2)c_i} C_{f_i} \sin \delta\phi_i \qquad (16)$$

Finally, if the mean velocity at a section is approximated by the section onset flow only, then the sectional lift, thrust, and integrated thrust coefficients can be obtained from the sectional circulation value, $\Gamma_{TE}$, as was done in Reference 8; i.e.,

$$C_{t_i} \approx \frac{1}{\pi} y_i \Gamma_{TE_i}$$

$$C_{\ell_i} \approx \frac{2\pi}{(w_c^2 + y_i^2)c_i} C_{t_i}$$

and

$$C_T = b \sum_i \Delta y_i C_{t_i}$$

These expressions are useful in that normal loads calculated by circulation converge faster, i.e., with fewer surface panels than those calculated by pressure integration.

## 5.2 VISCOUS AERODYNAMIC CONTRIBUTIONS

ROTAIR includes the capability of calculating the profile losses in the same manner as the HOVER code. However, in ROTAIR the defining stations for two-dimensional aerodynamic tables are independent of the stations used to describe the blade geometry. This greatly simplifies the user input of the aerodynamic tables for complex rotors. The profile drag coefficients are obtained by table interpolation at the calculated section lift coefficients and the resultant profile torque and thrust losses are computed. The reader is referred to Reference 8 for details. Eventually, this two-dimensional empirical calculation of profile losses should be replaced with a proper boundary layer calculation since the actual surface pressure distributions are now available.

## 6.0 PRELIMINARY RESULTS

The basic doublet code (VSAERO) for fixed-wing analysis[9] has been checked for many different wing configurations including the detailed flow around wing tips. Still, this code is constantly being improved and validated. In addition, the rotor version of the code, ROTAIR, described in this report, has been only recently developed and has been used for only a few conventional rotor configurations. Consequently, the results presented here are preliminary. Example calculations presented below serve to validate the programming and to illustrate the capabilities and limitations of ROTAIR.

### 6.1 FIXED-WING TIP FLOWS

Fixed-wing calculations have demonstrated the potential of the code for the detailed analysis of flows around rotor tips.[9] For example, steady pressure distributions calculated on a rectangular wing and plotted spanwise against surface distance in a number of cross-flow planes show a steady growth of the peak suction associated with attached flow (Figure 25). The wing has a rounded tip surface. The suction peak, which dominates the distributions downstream of the half-chord location, arises from growing velocity components in the cross-flow planes. Favorable pressure gradients exist in cross-flow planes near the leading edge, but adverse gradients develop once the suction peak becomes established, and these eventually reach unrealistic values under the attached flow constraints.

Prescribing separation along the tip does lead to more realistic tip pressure distributions. However, comparisons with experimental measurements have indicated the need to establish the extent of the edge separation in a more consistent manner. For example, calculated pressures on a swept wing are shown in Figure 26 plotted normal to the surface in a cut through the tip at .72 x/c. Incidence is 13° and the wing is twisted 4° nose down at the tip about the half-chord line. The extent of edge separation was set at about 30% of the tip chord in this case. The calculations for three wake iteration cycles are compared with experimental measurements taken by the N.L.R.[15] The experimental values have been interpolated at the calculation station. The general agreement appears good, but the upper surface suction is underpredicted by the calculation. Although the spanwise velocity component on the upper surface has reversed in the calculation, its level is clearly too low. Also the tip lower surface pressure is low compared with the

---

[15] Labrujere, Th.E., and De Vries, O., "Evaluation of a Potential Theoretical Model for the Wake Behind a Wing via Comparison of Measurements and Calculations", NLR, TR-74036 U, July 1974.

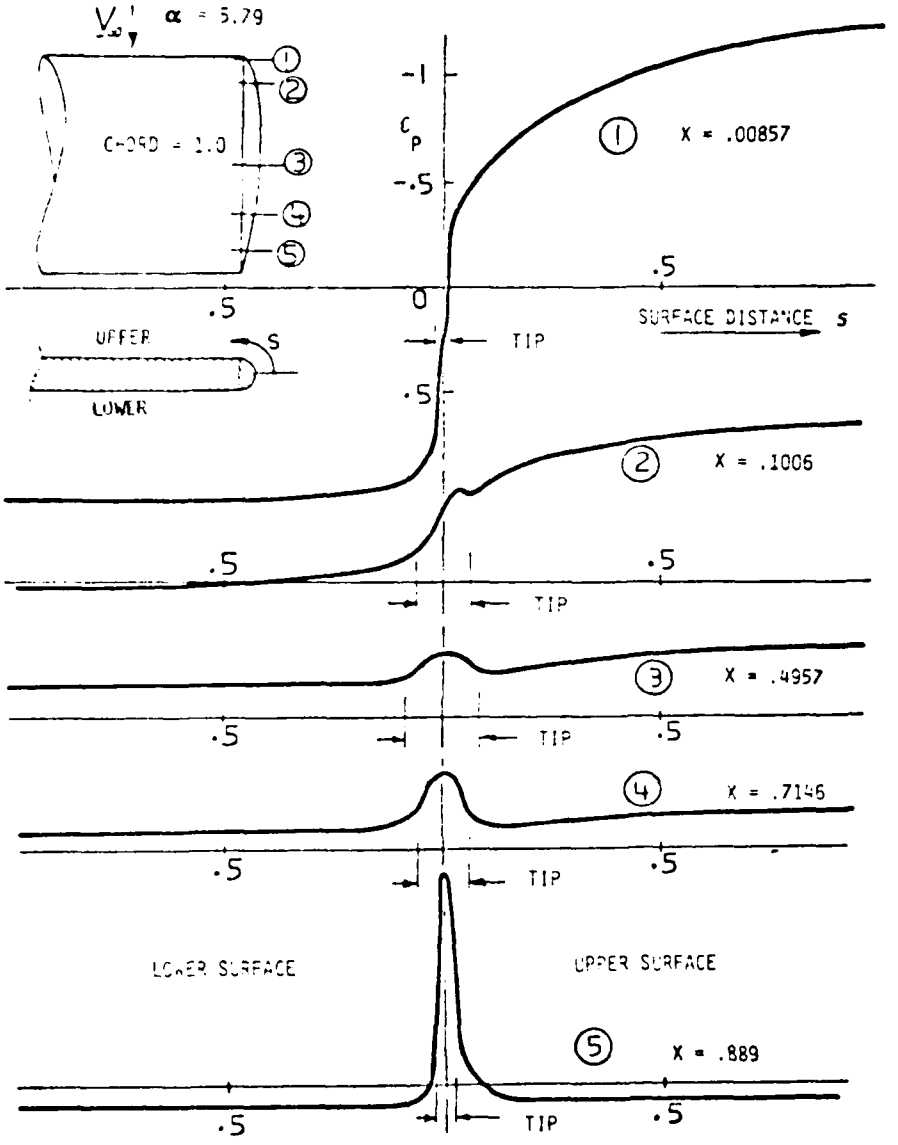


Figure 25. Spanwise Pressure Distributions Near the Tip of a Rectangular Wing in Steady Flow.

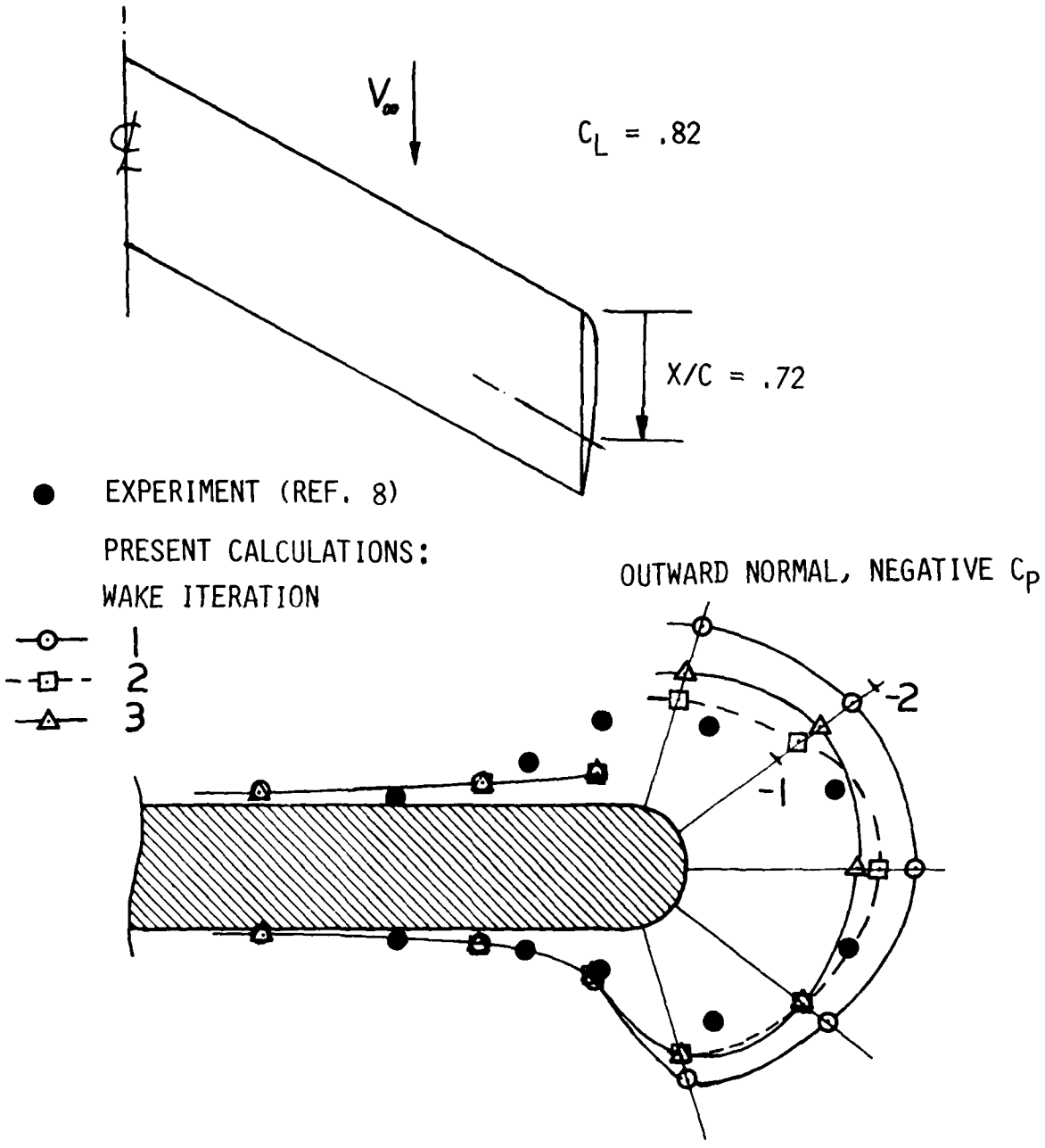


Figure 26. Spanwise Pressure Distribution Calculated Near the Tip of a Swept Wing with Prescribed Edge Separation.

experimental value, indicating that the cross-flow velocities there are too high in the calculation. Referring to the cross-flow analogy, it would appear that these discrepancies are consistent with too early a time; i.e., the calculation needs a larger extent of separation in this case.

Further work is planned at AMI to investigate ways of establishing the extent of separation along the tip edge. The coupling of a boundary layer calculation will be considered. Meanwhile, the present method provides a tool for the investigation of the tip flow and vortex formation.

## 6.2 ROTOR THICKNESS EFFECTS

A sample single-bladed rotor case was used to investigate the effects of blade thickness. In order to eliminate the effects of a returning wake, the wake was truncated at 180° (½ revolution) and the far-wake influence was set to zero. The blade was an aspect ratio 16, untwisted rectangular rotor. Compressibility was eliminated and the rotor was set to 1° of collective in order to maximize the thickness percentage changes. The results are illustrated in Figure 27. As can be seen on this expanded scale, the 2% thick airfoil results compare very well with the zero thickness vortex-lattice results. Increasing the thickness to 12% results in a loss of circulation. This trend is just the opposite of what occurs in the two-dimensional case. An empirical equation that is commonly used for wing design is

$$\left(\frac{dC_L}{d\alpha}\right)_{THICK} = \left(1 + f\,\frac{t}{c}\right)\left(\frac{dC_L}{d\alpha}\right)_{THIN},$$

where f ≈ 0.8. A two-dimensional version of the surface singularity code and VSAERO[9] were used to examine the thickness effects for fixed wings. The following results were obtained.

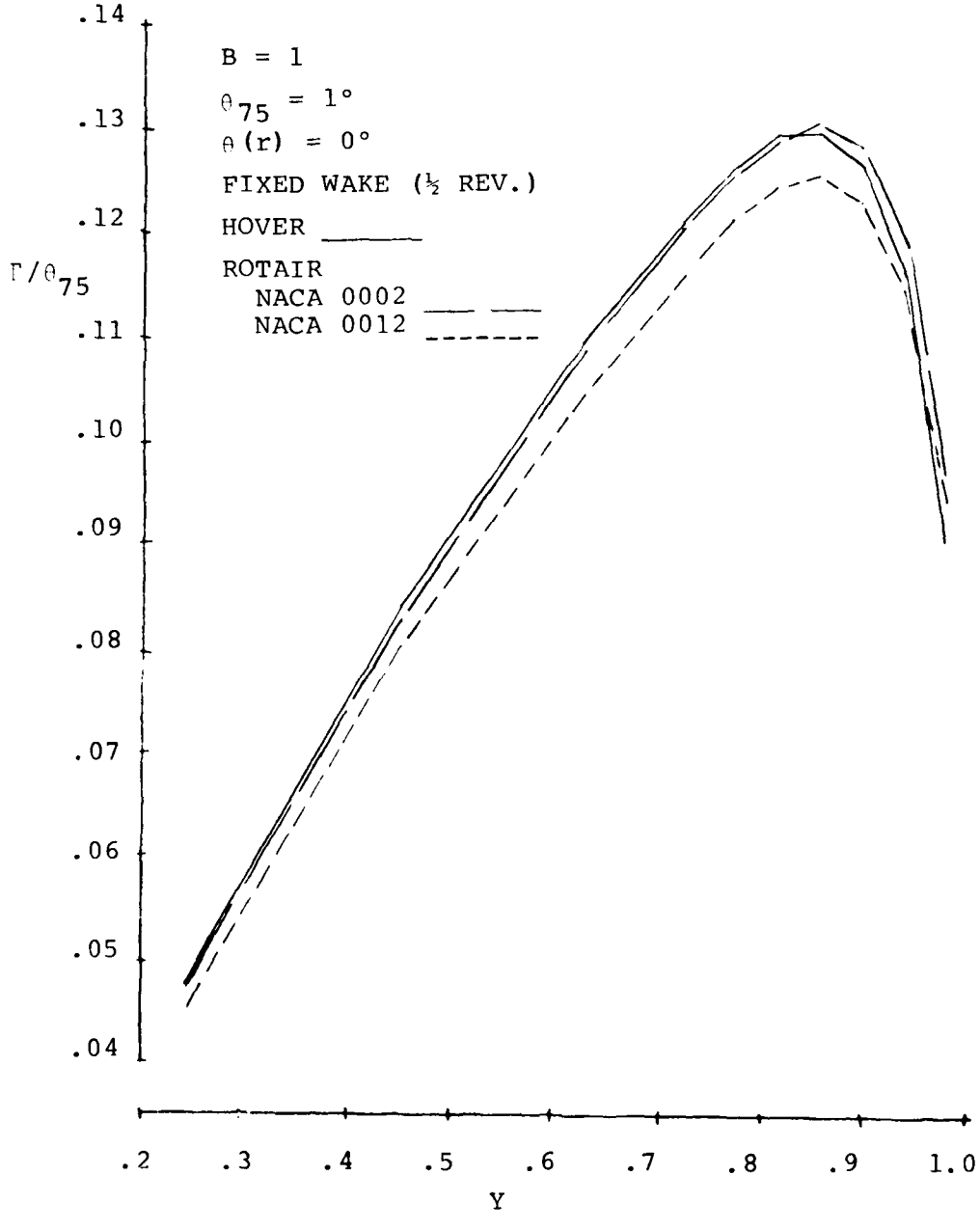


Figure 27. Effect of Thickness on Circulation for a Single-Bladed Rotor with No Wake Passage.

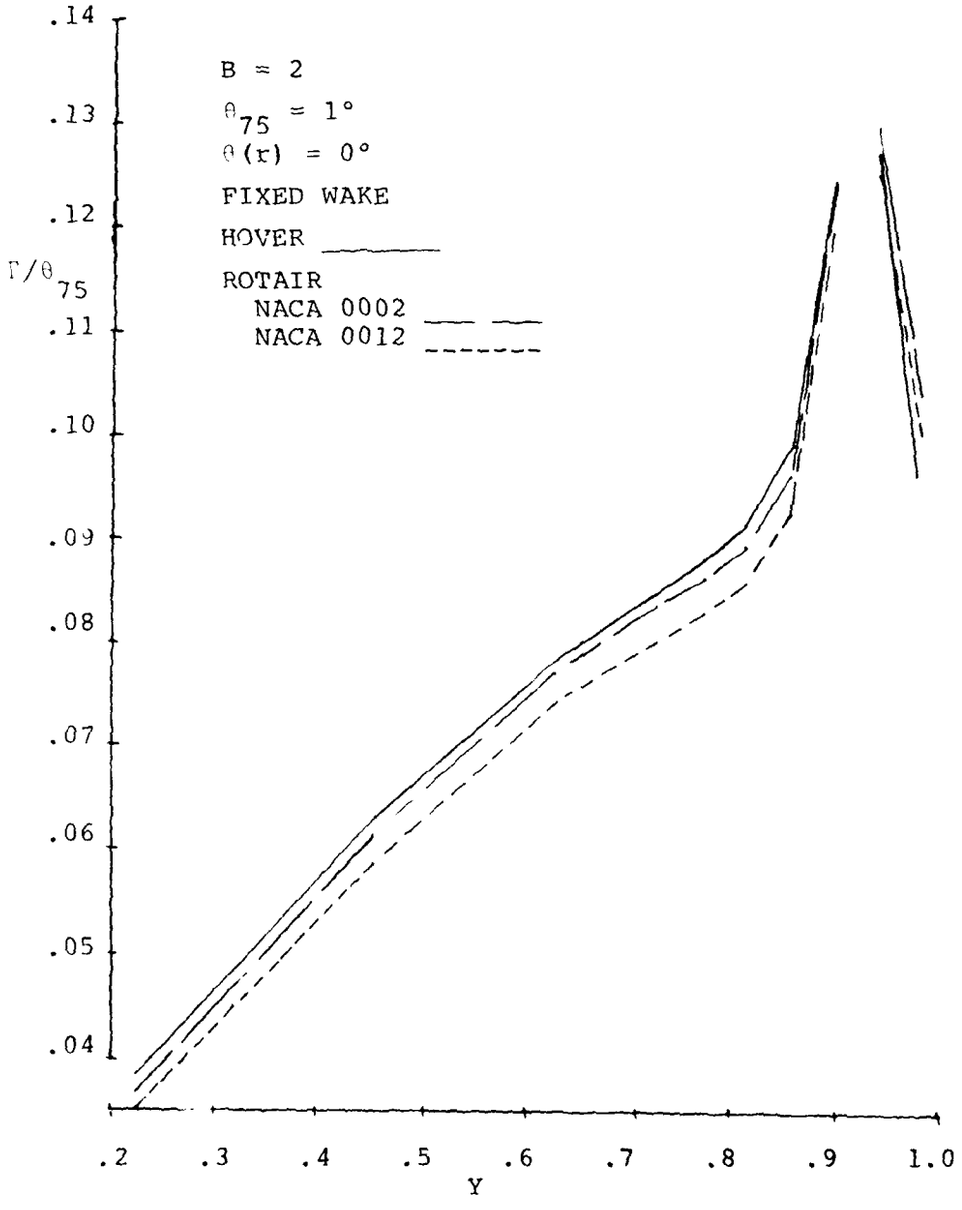


Figure 28. Effect of Thickness on Circulation for a Two-Bladed Rotor.

| | 2-D | VSAERO - RECTANGULAR WINGS | | |
|---|---|---|---|---|
| AR | ∞ | 200 | 2 | 6* |
| f | 0.75 | 0.18 | 0.007 | ~0 |

The two-dimensional results were for a Joukowski airfoil. The VSAERO runs were for t/c = 0.12 and t/c = 0.02. The results for the aspect ratio six wing included increased tip loading to simulate rotor loading by linearly twisting the wing tip upward 8°. Evidently, thickness effects are reversed, or, at least greatly reduced in the presence of highly three-dimenisonal flows. This behavior should be more thoroughly investigated in the future.

Similar comparison calculations were made for a two-bladed rotor at 1° collective with fixed-wake geometry. These are shown in Figure 28. Once more, thickness reduces the blade loading for the two-bladed case.

## 6.3 A CLOSE VORTEX PASSAGE CASE

Figures 29 through 31 illustrate various calculated performance characteristics for a single-bladed, untwisted rotor with an NACA 0012 airfoil section. As this was a preliminary calculation, the tip vortex shedding was not modelled (vortex wake shedding only from the trailing edge). Also, only ten panels were used around the airfoil section and ten columns of panels along the blade radius. While this is too few panels for obtaining all of the performance details in the neighborhood of the vortex, it is enough to verify the calculation capabilities of the code.

Two different calculations were made for comparison. The basic tip vortex wake constants for the two cases were

| | Case a | Case b |
|---|---|---|
| $K_1$ = | -.006 | -.02 |
| $K_2$ = | -.024 | -.08 |
| $\lambda$ = | .13365 | .13365 |

The radial position of the tip vortex for both cases was $R_{\psi_b}$ = 0.875. However, the first blade passage axial distance for case "a" was $z_{\psi_b}$ = -0.0377, while that for case "b" was $z_{\psi_b}$ = -0.126. The blade trailing edge was at $z_{TE}$ =-0.0125. For these calculations the wakes were arbitrarily truncated at $\psi_w$ = 480°.

In all of the figures, the "dashed" lines are values along the blade lower surface and "solid" lines are values along the blade upper surface. Also, the blade surface geometries at the requested data cuts are overlaid on the figures. Figures "a" illustrate results for the close vortex passage, while "b" show results for the distant vortex passage.

The radial distribution of doublet strength is shown in Figure 29. By comparing (a) and (b), the buildup and the spreading of the vorticity near the vortex and across the blade chord may be seen.

The strong, direct vortex action is almost wholly confined to the blade lower surface, while the upper surface values are the secondary result of the vortex induced doublet distribution on the blade surface. This represents a "classic" vortex surface interaction effect on the doublet distribution near the trailing edge of the thick blade (recall that vorticity is the gradient of the doublet distribution).

Figure 30 compares the spanwise velocity component variation near the blade leading edge. The strong deceleration caused by the free vortex to the usual acceleration of the flow on the lower surface around the tip is seen by comparing the results in figures "a" and "b". Finally, Figure 31 illustrates the radial distribution of minus $C_p$ for this same location near the blade leading edge.

The chordwise pressure plots (not shown here) display the expected reduction in the suction pressure peak inboard of the vortex and augmentation of the suction peak outboard.

## 6.4 OH-58A ROTOR CALCULATIONS

The OH-58A helicopter rotor is a two-bladed high aspect ratio rotor with -10.6 degrees of linear twist. Extensive performance prediction comparisons for the OH-58A by the

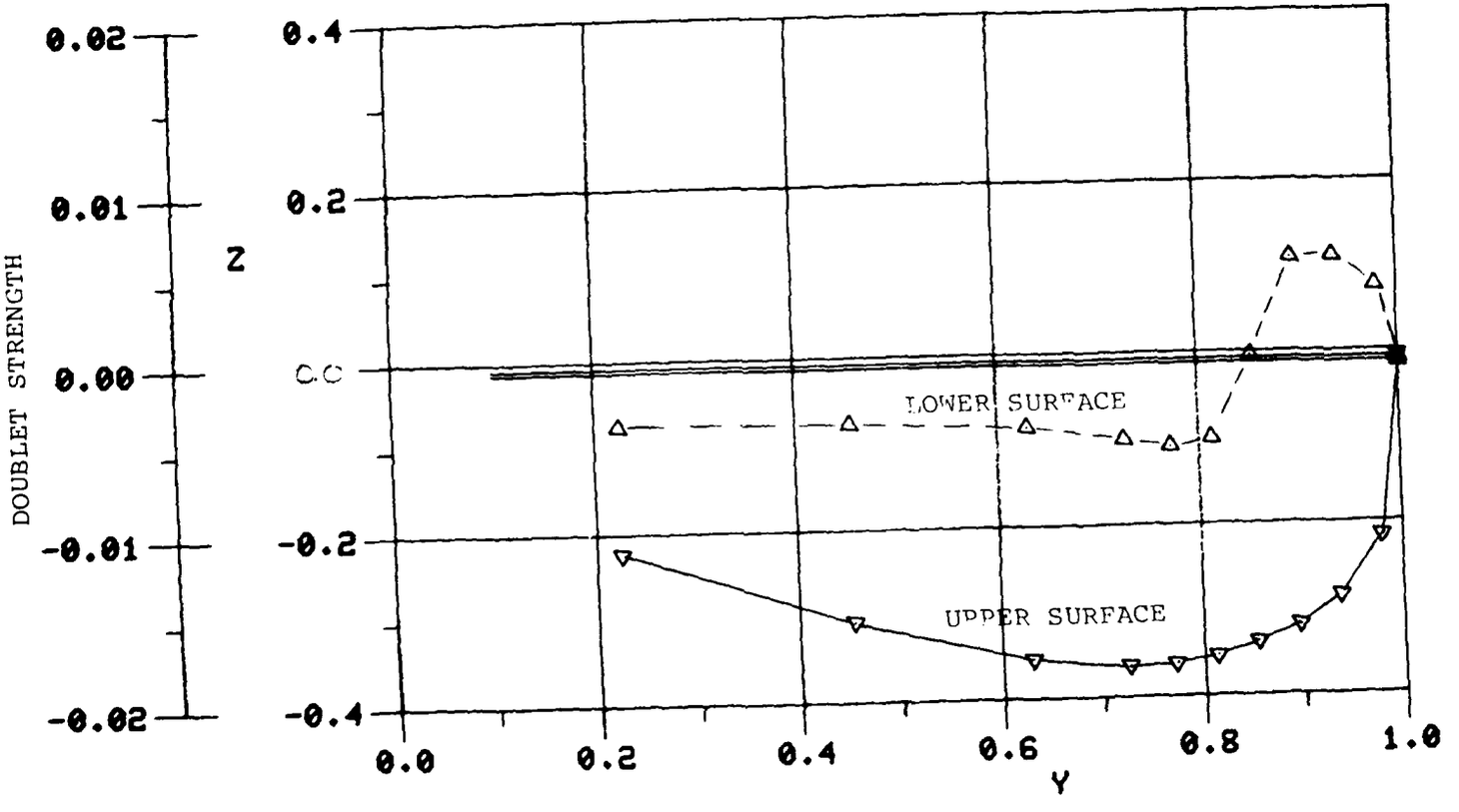


(a) Close Vortex Passage.

Figure 29. Radial Variation of Surface Doublet Distribution (Station Cut Near Trailing Edge, x = 0.04).

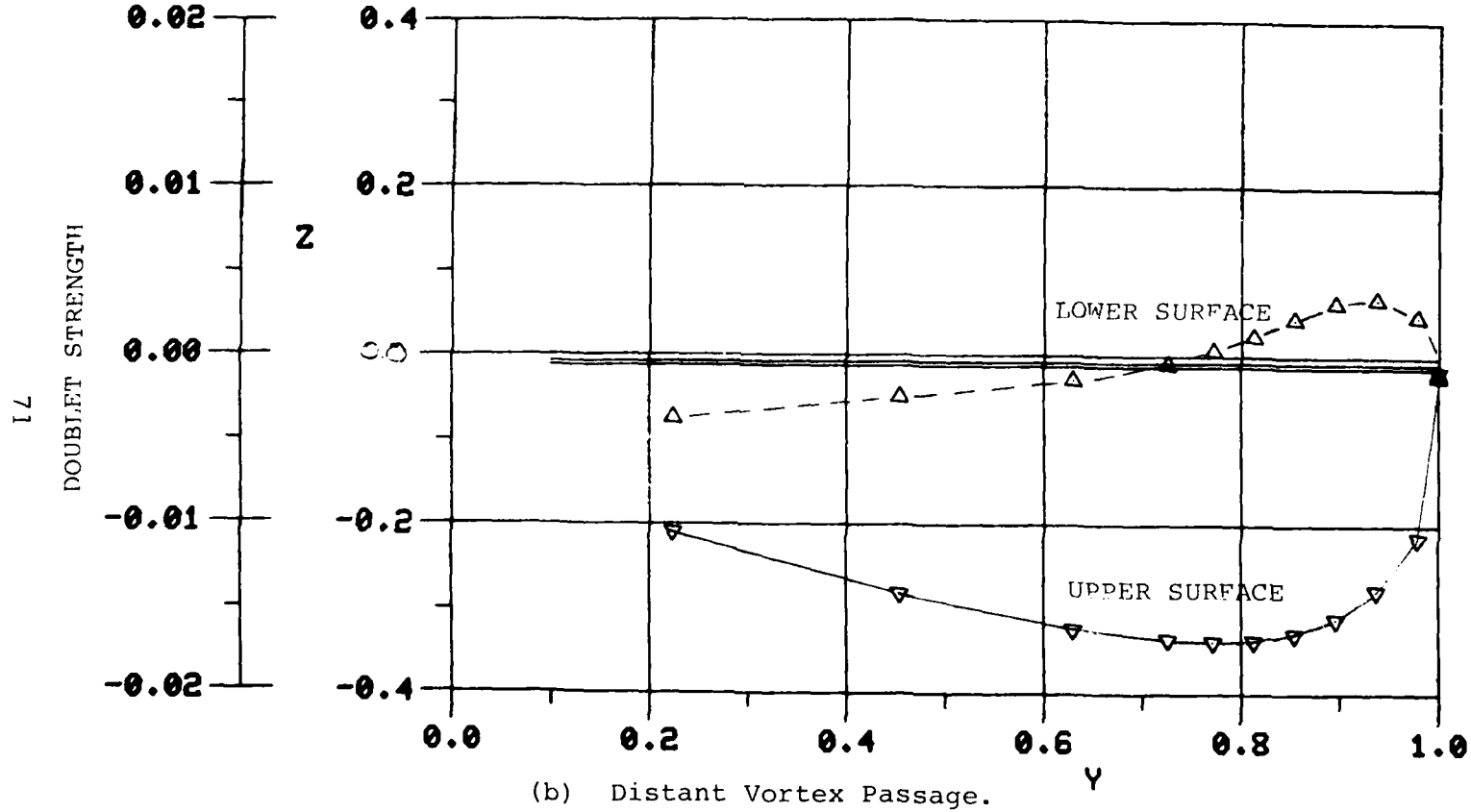


(b) Distant Vortex Passage.

Figure 29. Concluded.

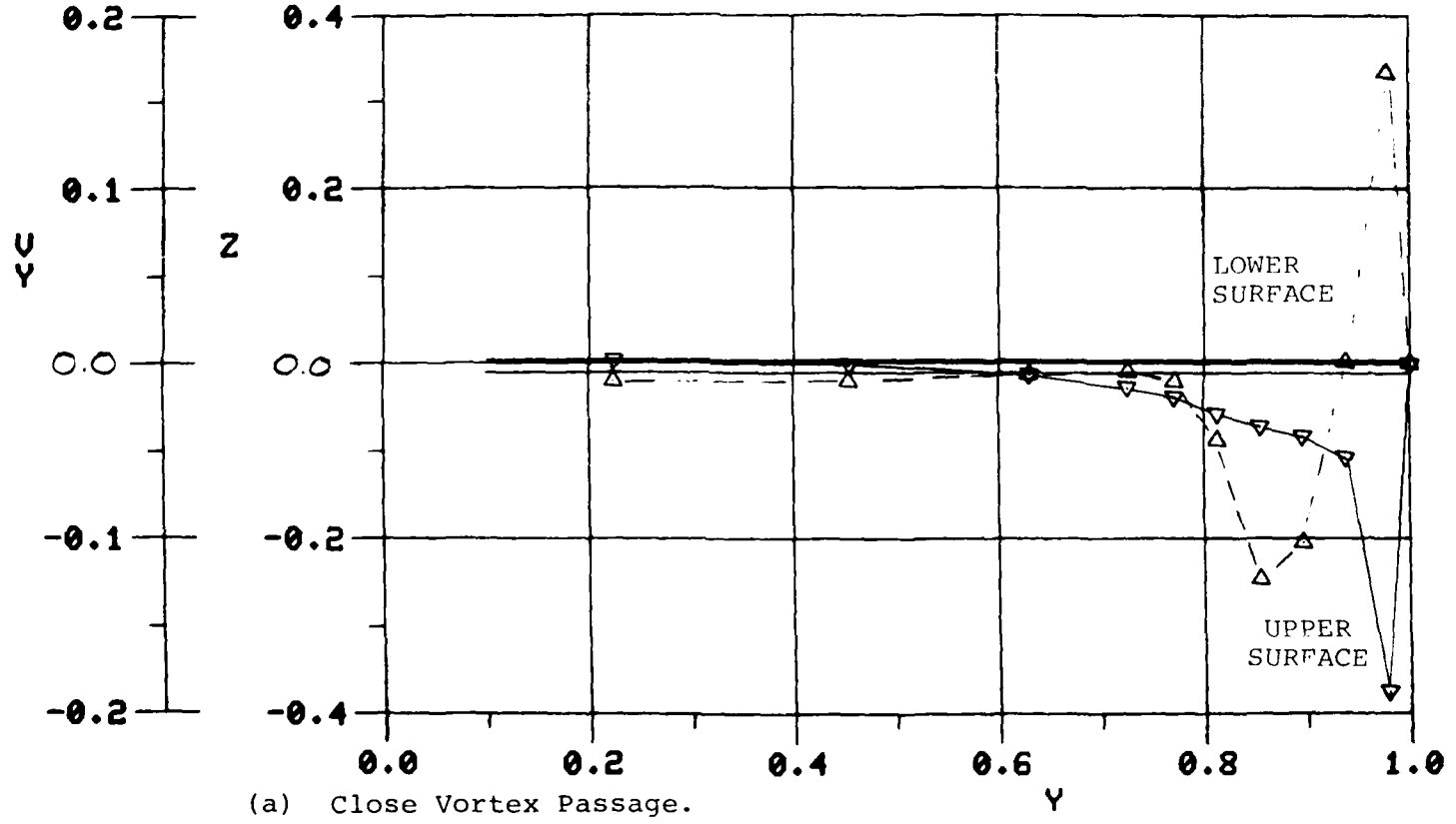


(a) Close Vortex Passage.

Figure 30. Radial Variation of Spanwise (VY) Velocity Component (Station Cut Near Leading Edge, x = -.03)

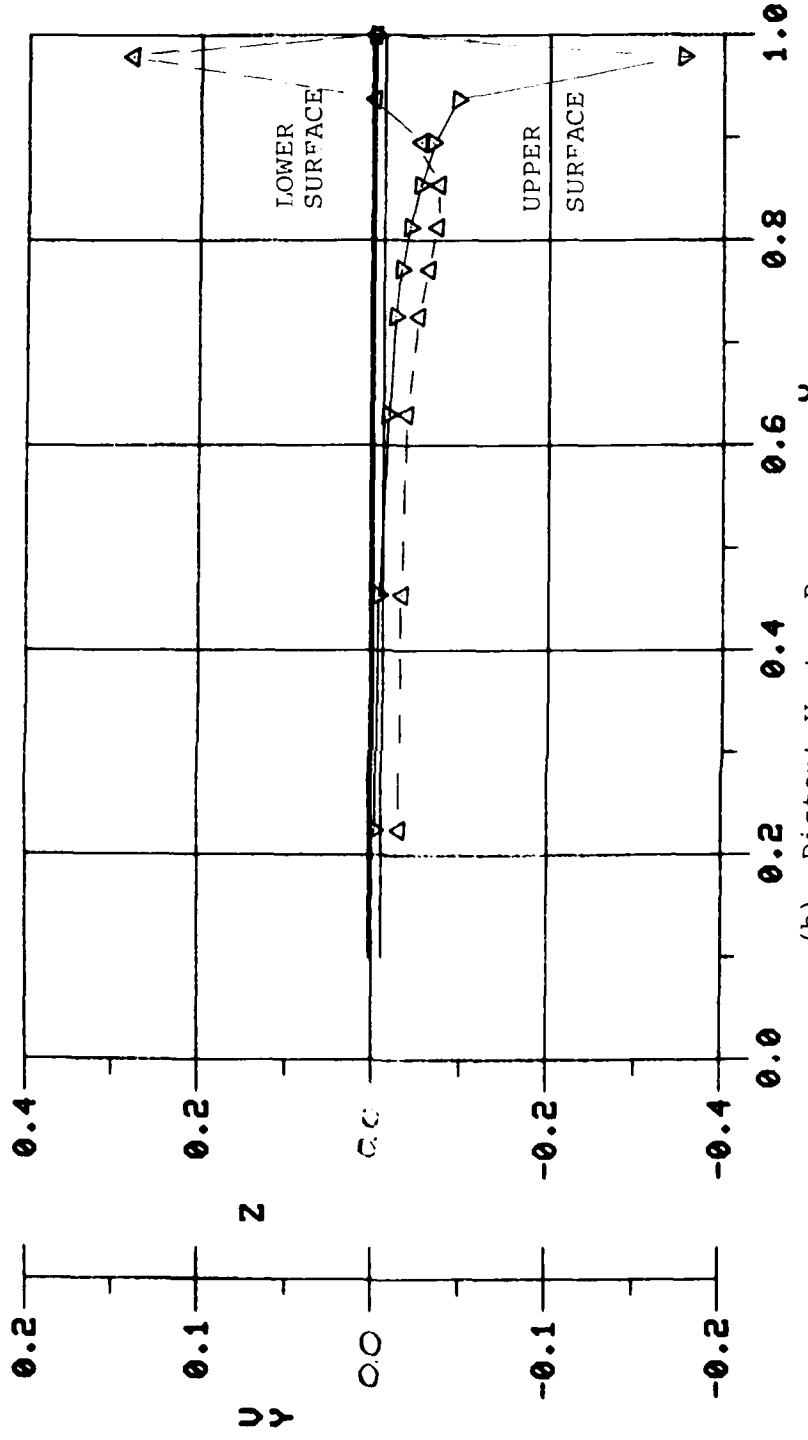


(b) Distant Vortex Passage.

Figure 30. Concluded.

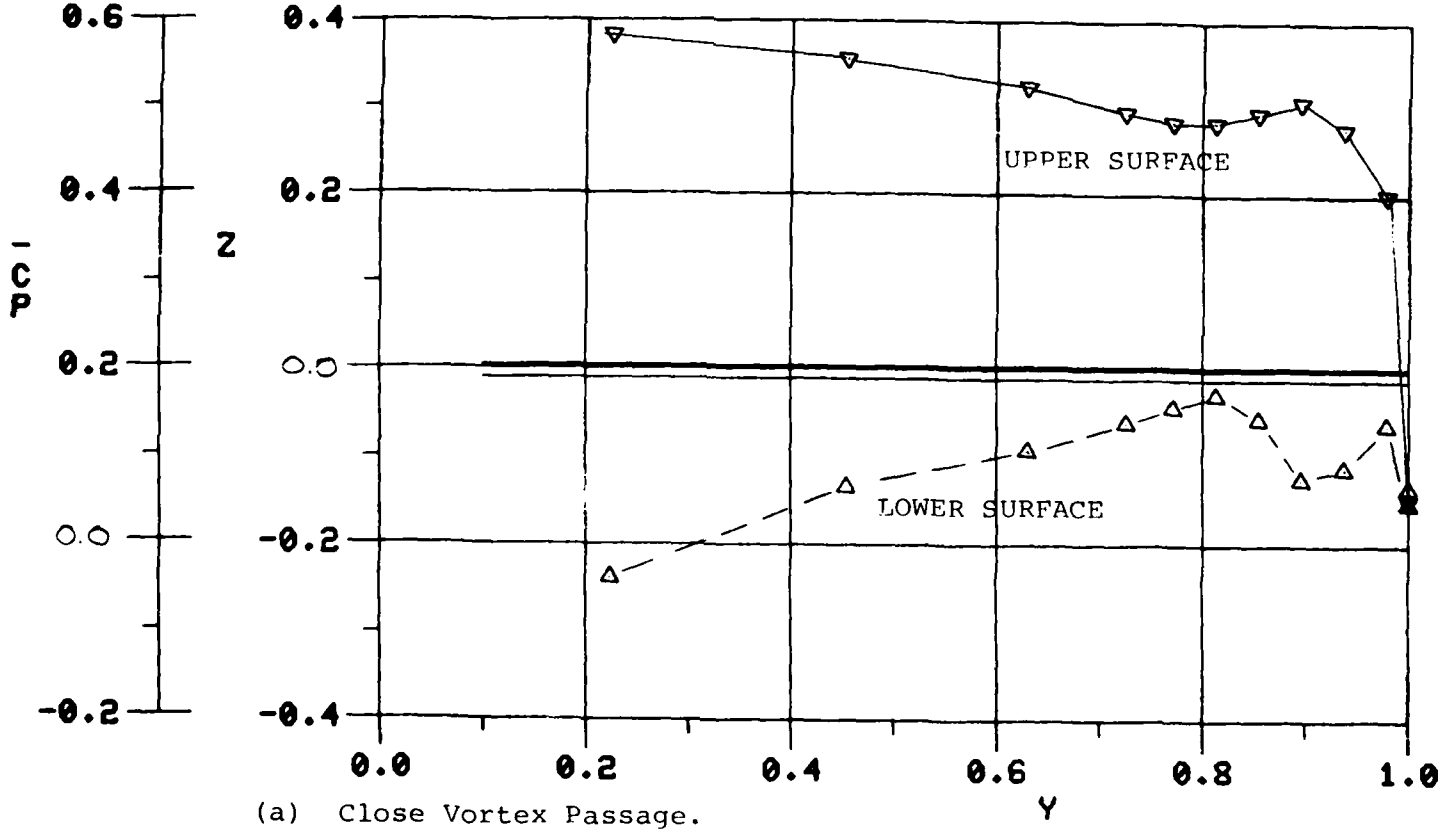


(a) Close Vortex Passage.

Figure 31. Radial Variation of Minus C (Station Cut near Leading Edge, x = -.03).

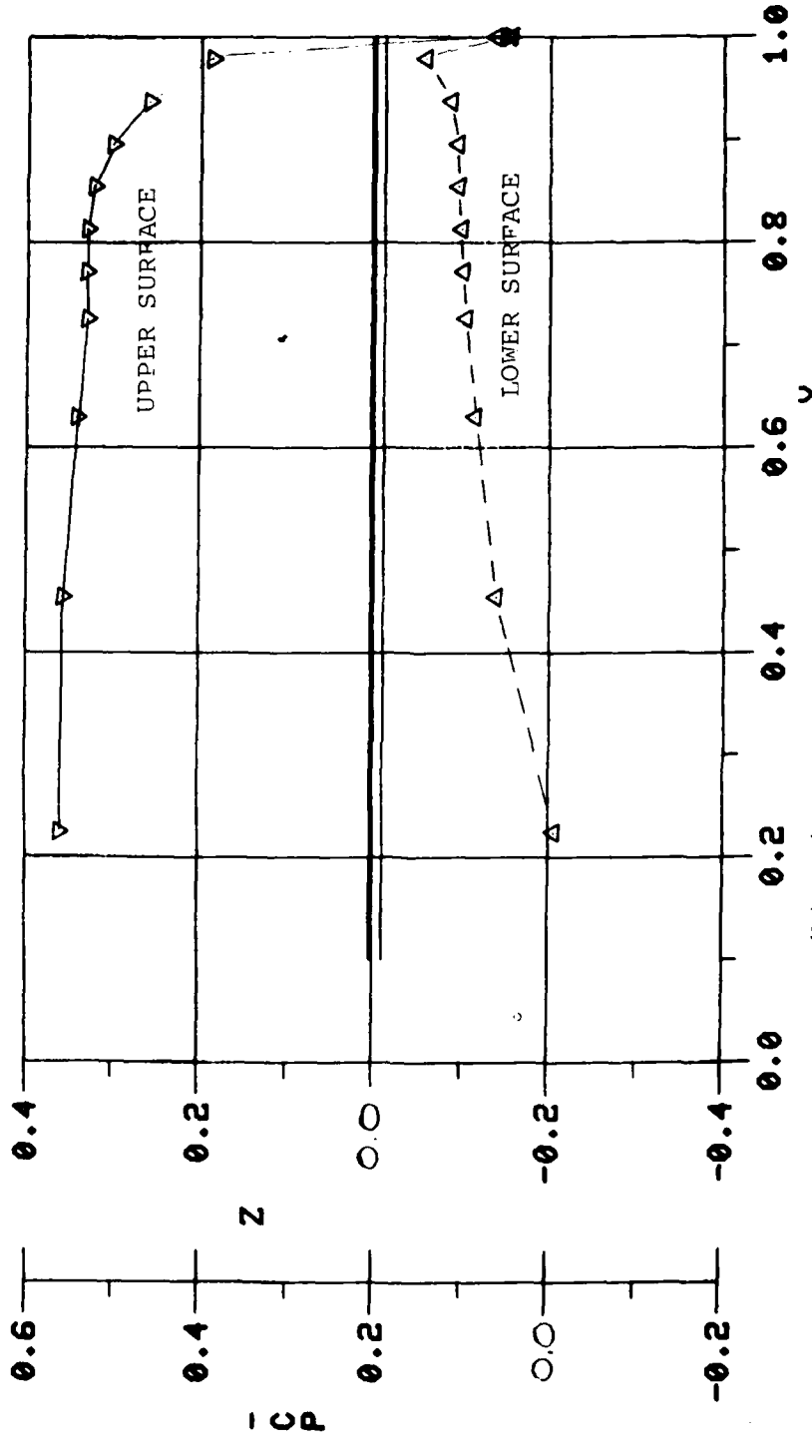


(b) Distant Vortex Passage.

Figure 31. Concluded.

UTRC[3] and HOVER[8] programs have already been reported in Reference 8. Calculations by these programs have proven very useful in validating ROTAIR in examining the convergence behavior of ROTAIR with panel number.

The blade surface panelling of this rotor is shown in Figure 32(a) and (b). In this case, the rotor collective angle is 5.75°, and the blade coning angle is 3° to correspond to the previous calculations. Additionally, the radial panelling distribution (15 columns) is equivalent to the panelling of the simpler methods, and the Landgrebe[3] wake constants were set for a thrust coefficient of 0.0022. Therefore, the wake geometry should be approximately equal for the three methods.

### 6.4.1 Far-Wake Convergence

ROTAIR was first run with different wake lengths to determine the convergence behavior of the new far-wake velocity potential model. With only ten panels around the airfoil (i.e., 10 rows) and 30° wake segments, the convergence of several key performance properties was as follows:

| | $\psi_{f_1} = 720$ <br> $\psi_{f_2} = 900$ | $\psi_{f_1} = 630$ <br> $\psi_{f_2} = 670$ | $\psi_{f_1} = 480$ <br> $\psi_{f_2} = 520$ | $\psi_{f_1} = 270$ <br> $\psi_{f_2} = 300$ |
|---|---|---|---|---|
| CIRC(MAX) | .008672 | .008603 | .008550 | .008251 |
| CTEAM | .002106 | .002108 | .002085 | .002090 |
| CT | .002665 | .002668 | .002639 | .002648 |
| CQ | .0001873 | .0001874 | .0001877 | .0001885 |
| FM | .42 | .42 | .41 | .41 |

These changes are mostly due to the loss in ultimate wake contraction as $\psi_{f_1}$ is shortened. Apparently, the far-wake model

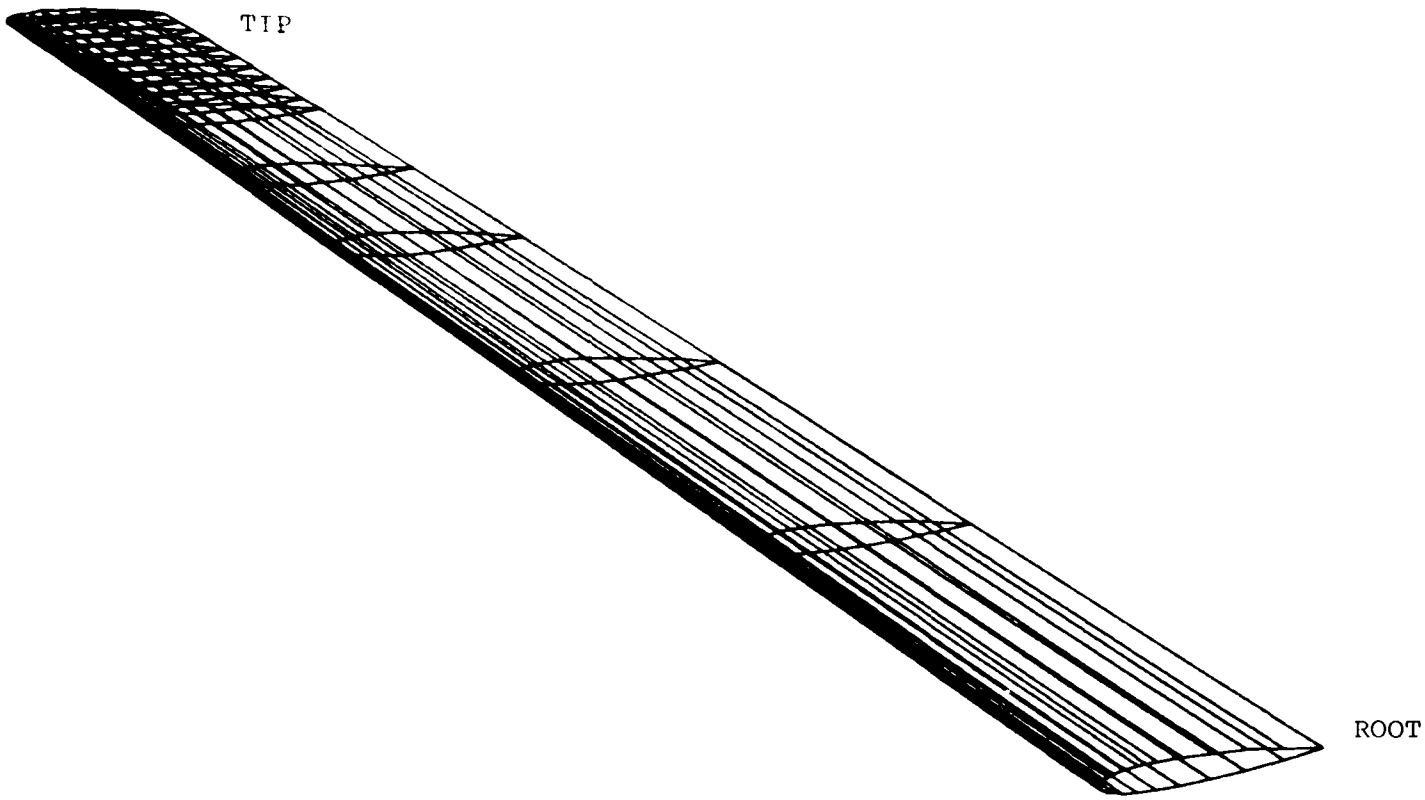


(a) Oblique View from Ahead of the Blade Leading Edge.

Figure 32. OH-58A Blade Panelling.

(b) View from Behind the Rotor Trailing Edge.

Figure 32. Concluded.

could almost be taken right up to the blade surface for prescribed wake calculations! This also indicates that for most of the wake, a relaxed wake scheme based on sheaths of vorticity (iterating on vorticity) might be possible. At any rate, for further calculations, the wake length could be set for $\psi_{f_1} = 480°$ and $\psi_{f_2} = 520°$ with little loss in accuracy.

### 6.4.2 Circulation Distribution Comparisons

The circulation distributions computed by three codes are compared in Figure 33. For this figure, all of the calculated circulation data are scaled by the maximum circulation predicted by ROTAIR (CIRC(MAX) = 0.008672). All the methods agree reasonably over the inner portion of the blade (the thick blade solution indicates lower circulation values again (see Section 6.2)). Finally, as reported in Reference 8, the lifting line program, UTRC, overpredicts the circulation values in the tip region compared to the ROTAIR and HOVER results which agree favorably.

### 6.4.3 Convergence with Panel Number

The convergence behavior of integrated performance parameters obtained by integration of the surface pressures is much too slow in the current code. Figure 34 illustrates the variation of the thrust coefficient computed by surface pressures and computed by circulation values for chordwise panel numbers (2 x NPC) ranging from 10 to 30. In all these calculations, $\psi_{f_1} = 480°$ and $\psi_{f_2} = 520°$. As usual, the circulation computed value converges from below, while the pressure computed value converges from above. Also, the circulation based thrust converges much faster, but is more restricted in its use. That is, regions of high radial velocities or arbitrary geometries invalidate the circulation base thrust. In fact, even for this case with $Z_{\psi_b}$ 0.03, the two thrust calculations seem to be converging on slightly different asymptotic values.

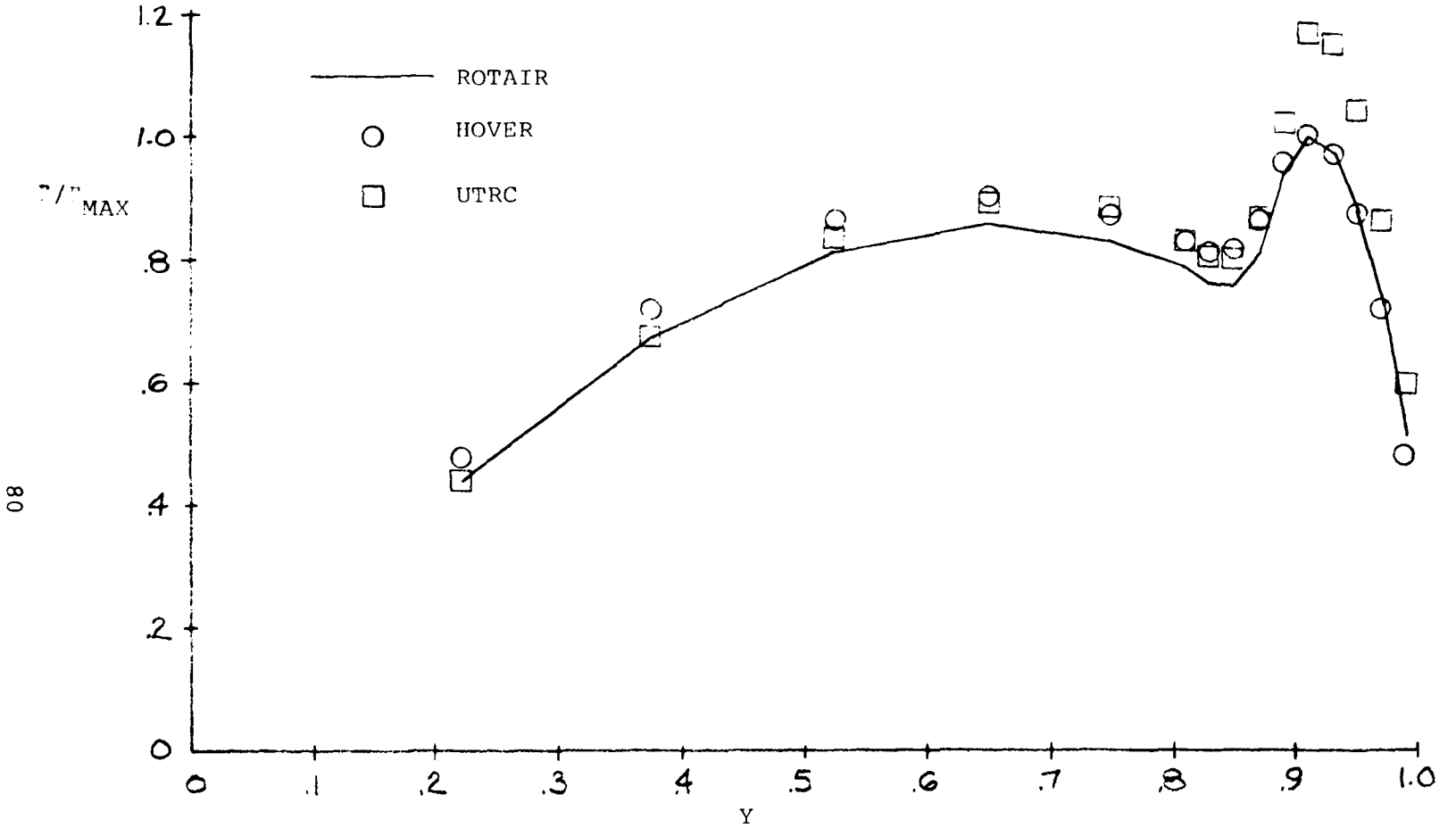


Figure 33. Calculated Circulation Distribution Comparisons for the OH-58A Rotor (Normalized by the Maximum Circulation Value Computed by ROTAIR).

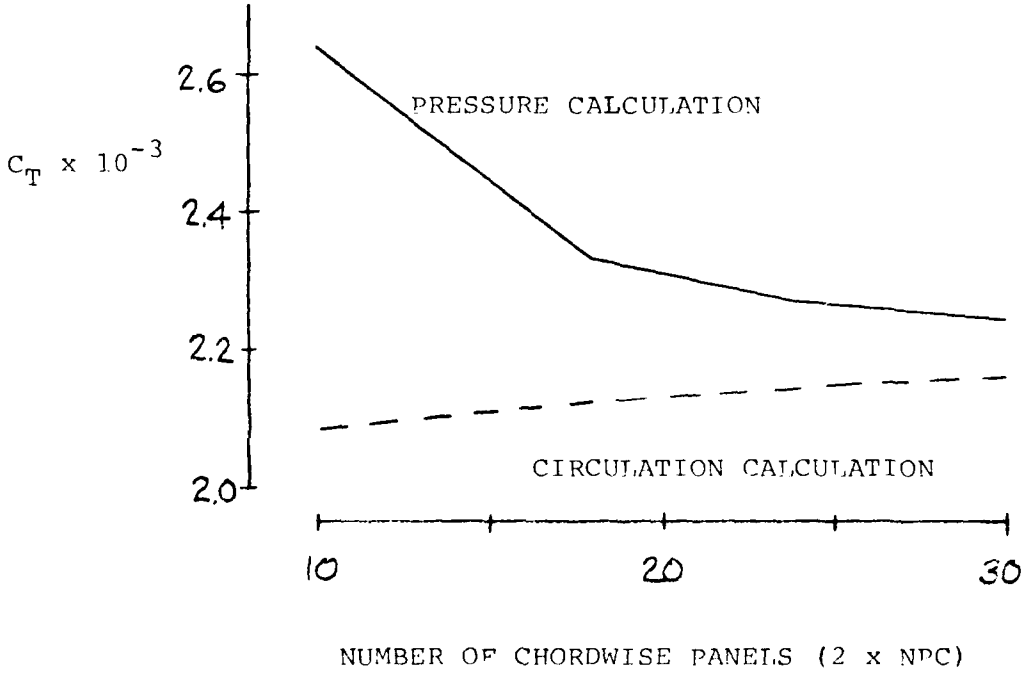


Figure 34. Effect of Number of Chordwise Panels (NROW) on Thrust Coefficient.

Figure 35 illustrates the convergence behavior of several key rotor performance quantities for chordwise panel number. In this figure, each of the ordinate values are scaled by their respective ultimate values achieved with 30 chordwise panels; hence, all the quantities approach a value of 1.0 at 30 panels. The values for these quantities with 30 panels are

| | | |
|---|---|---|
| CIRC(MAX) | = | 0.08853 |
| CT | = | 0.002242 |
| CTGAM | = | 0.002160 |
| CQ | = | 0.00009273 |
| FM | = | 0.554 |

Obviously, the induced torque, or section drag variation with panel number is quite large, and, even with 30 panels, the error in the induced torque is not acceptable for efficient computation.

This is an area of ROTAIR that needs additional work. Presently, loadings are obtained by summing $C_p^*$ x area for all of the panels. This can be improved by using the surface arc length around each given section along with a higher-order interpolation through $C_p^*$ values. 11 B

An additional method to obtain a highly accelerated convergence of the sectional properties would include a two-dimensional program in ROTAIR. Once the section panelling is complete, the two-dimensional program could be used to generate appropriate factors that could be applied later for the three-dimensional calculations. For example, the inviscid two-dimensional drag should be zero for all $C_\ell$'s. For a given airfoil panelling, the two-dimensional results would provide the $\Delta CD$ that should be subtracted, section by section, for the three-dimensional calculation. The more panels used, the smaller the $\Delta CD$'s. The lift values could be corrected in a similar manner. Finally, the additional computing time for the two-dimensional calculations would be very small.

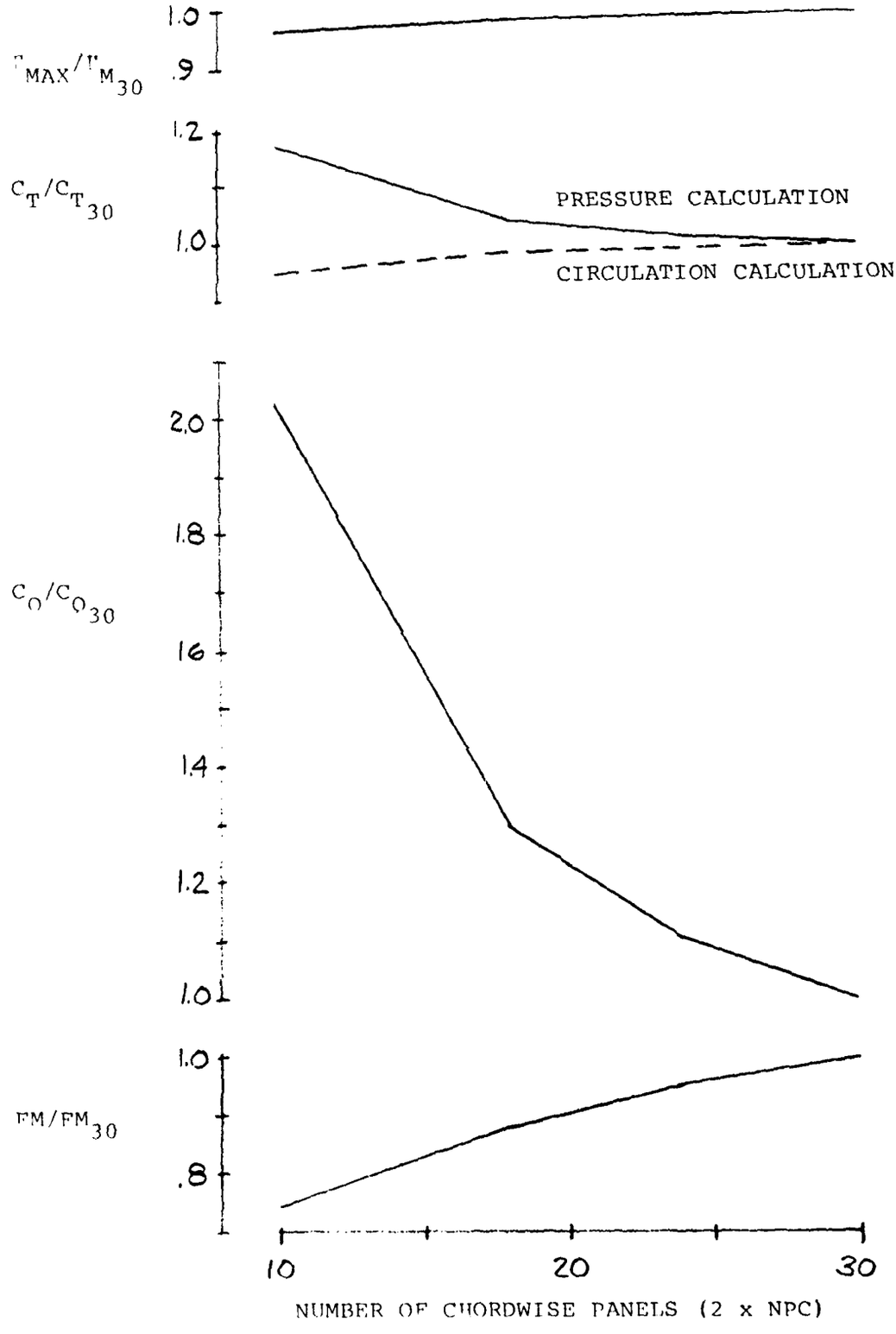


Figure 35. Effect of Number of Chordwise Panels (ROW) on Key Performance Parameters.

### 6.4.4 Pressure Distributions

Although the completed integrated loads by pressure integration converges slowly in the current program, the actual surface pressure values converge rapidly, even for as few as a total of eight panels around the airfoil (see Ref. 11), and detailed pressure distribution calculations will prove very useful in the analysis of the newer rotor tip shapes.

Figures 36 (a), (b), (c) and (d) demonstrate the calculated chordwise pressure distributions for the 30 panel case of Section 6.4.3 at several radial locations. The airfoil panelling shapes (seen in the H.C.S.) are superimposed on these figures and illustrate the linear twist of the blade geometry and the blade coning.

## 6.5 AMES MODEL ROTOR

The ultimate validation of the calculated pressure distribution is a direct comparison with measured surface pressure data. Here, we present a comparison of the calculated surface pressure distribution on a low aspect ratio blade with those measured by Caradonna and Tung.[6]

The actual blade surface, including blade-tip closure, is represented by quadrilateral panels as shown in Figure 37. To compare with the detailed measurements, a row of 18 panels was used around the airfoils and 15 columns across the blade radius. In addition, 27 panels were employed to close the rotor tip for a total of 297 panels. For production calculations, about half this number, or 150 panels, are sufficient. The wake constants were set for a far-wake radius, RFAR, equal to 0.88. This ultimate contraction radius was taken from the measured wake data.

Figures 38 (a), (b) and (c) illustrate the surface pressure comparisons at the radial stations where the experimental data was collected and excellent agreement is shown at all stations. Furthermore, the cost of these calculations on a commerical CYBER 176 was only $25 (approximately $12 on the Langley 175).

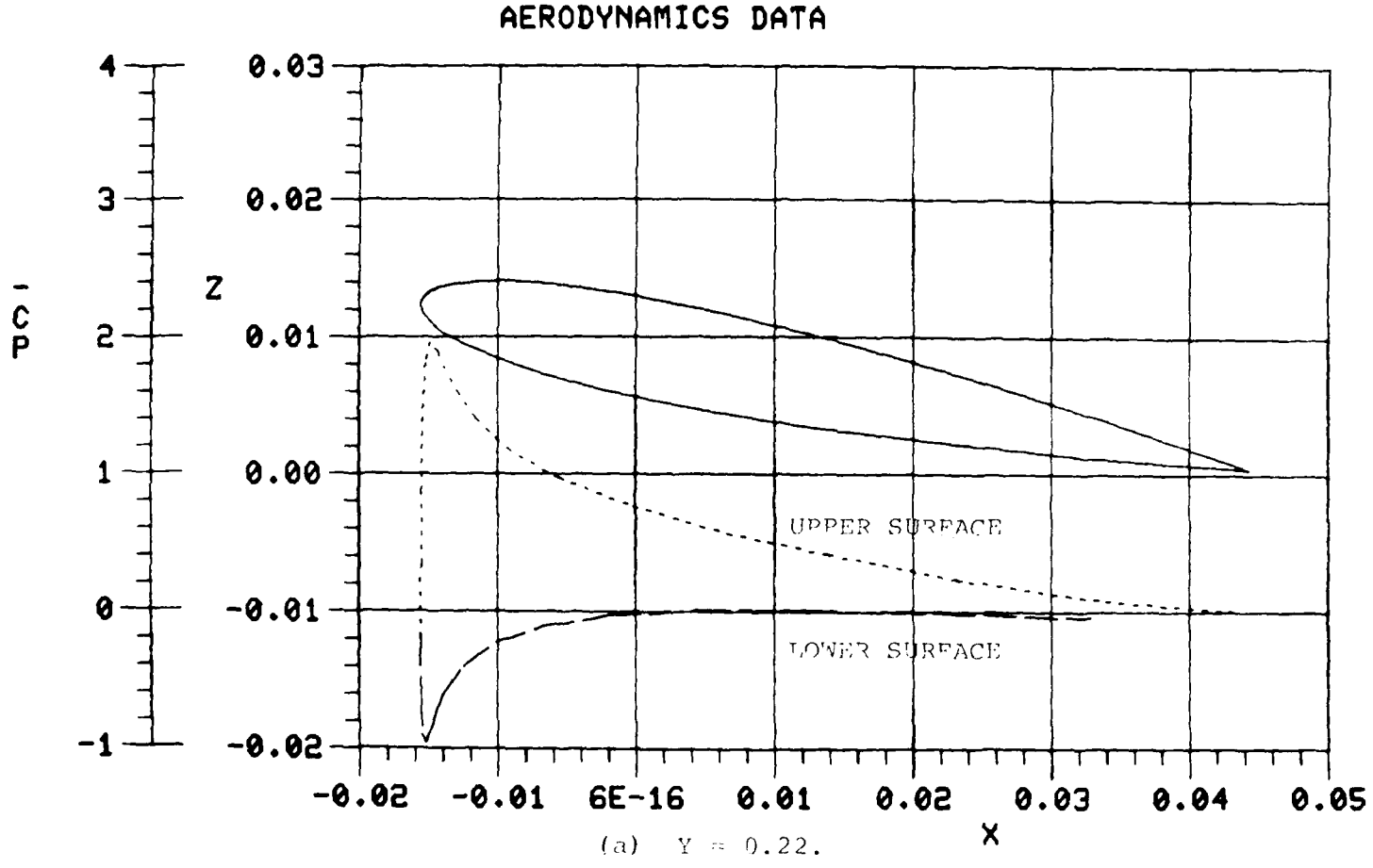


(a) Y = 0.22.

Figure 36. Chordwise Surface Pressure Distributions (Minus $C_p$) for the OH-58A.

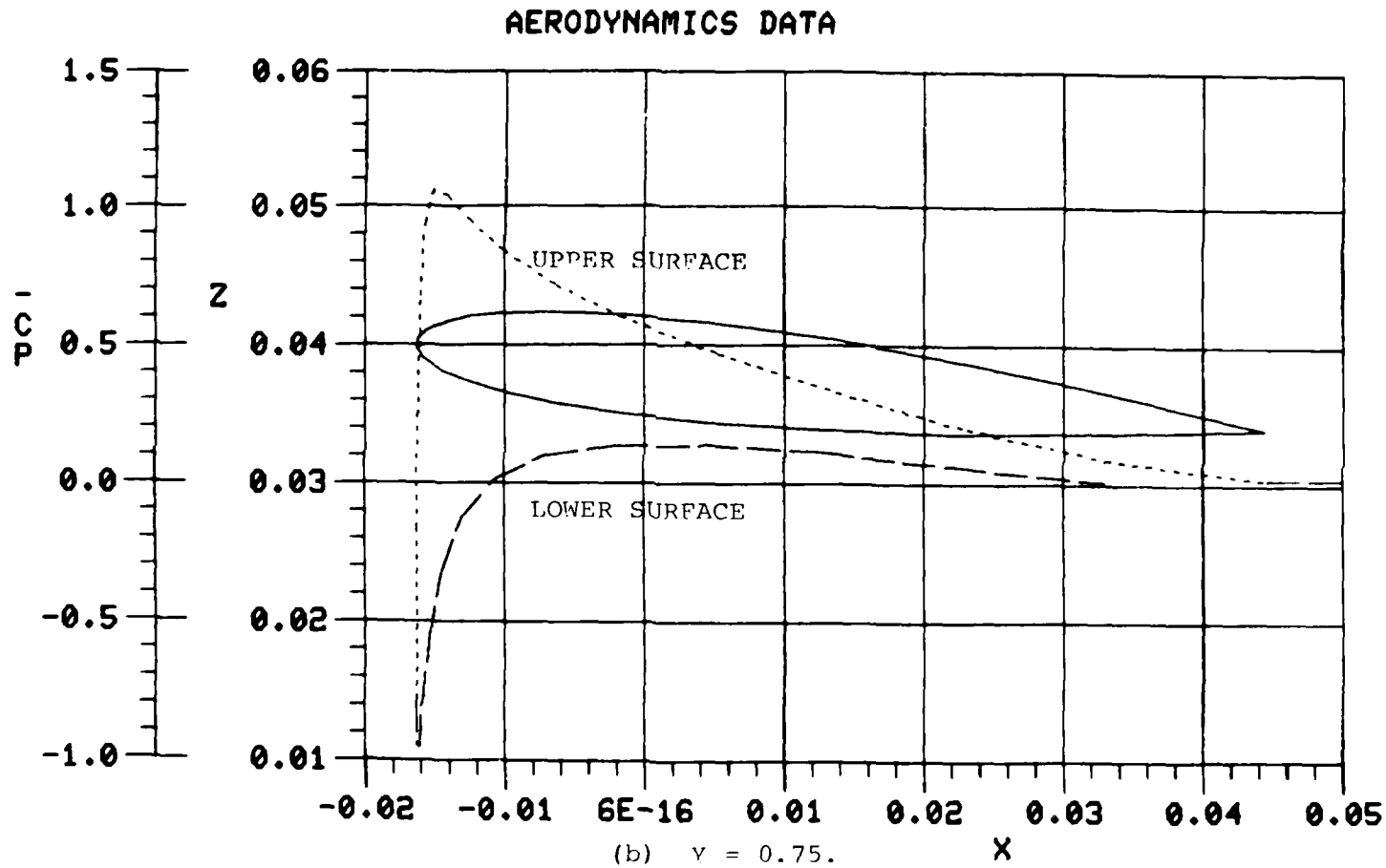


(b) Y = 0.75.

Figure 36. Continued.

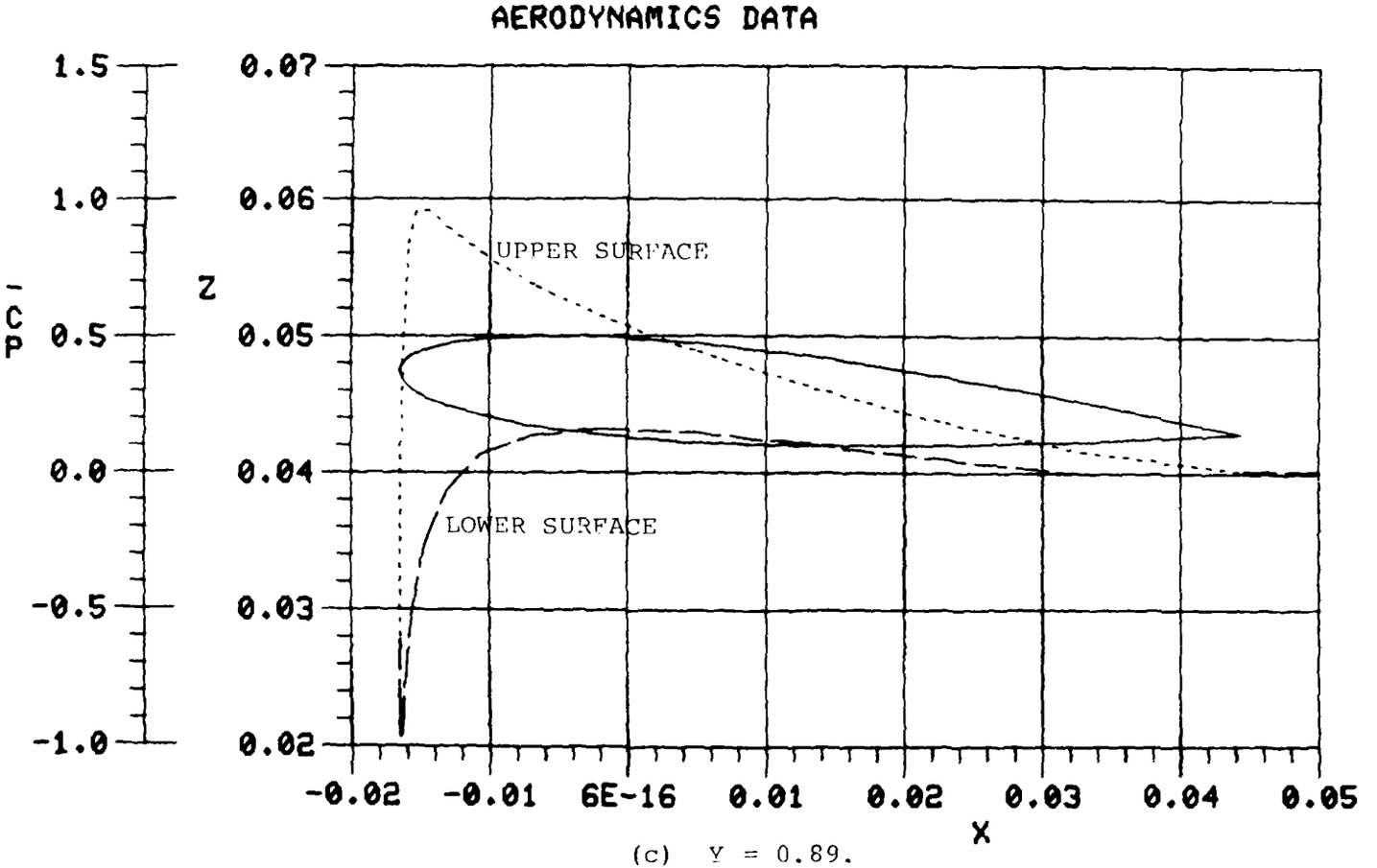


(c) Y = 0.89.

Figure 36. Continued.

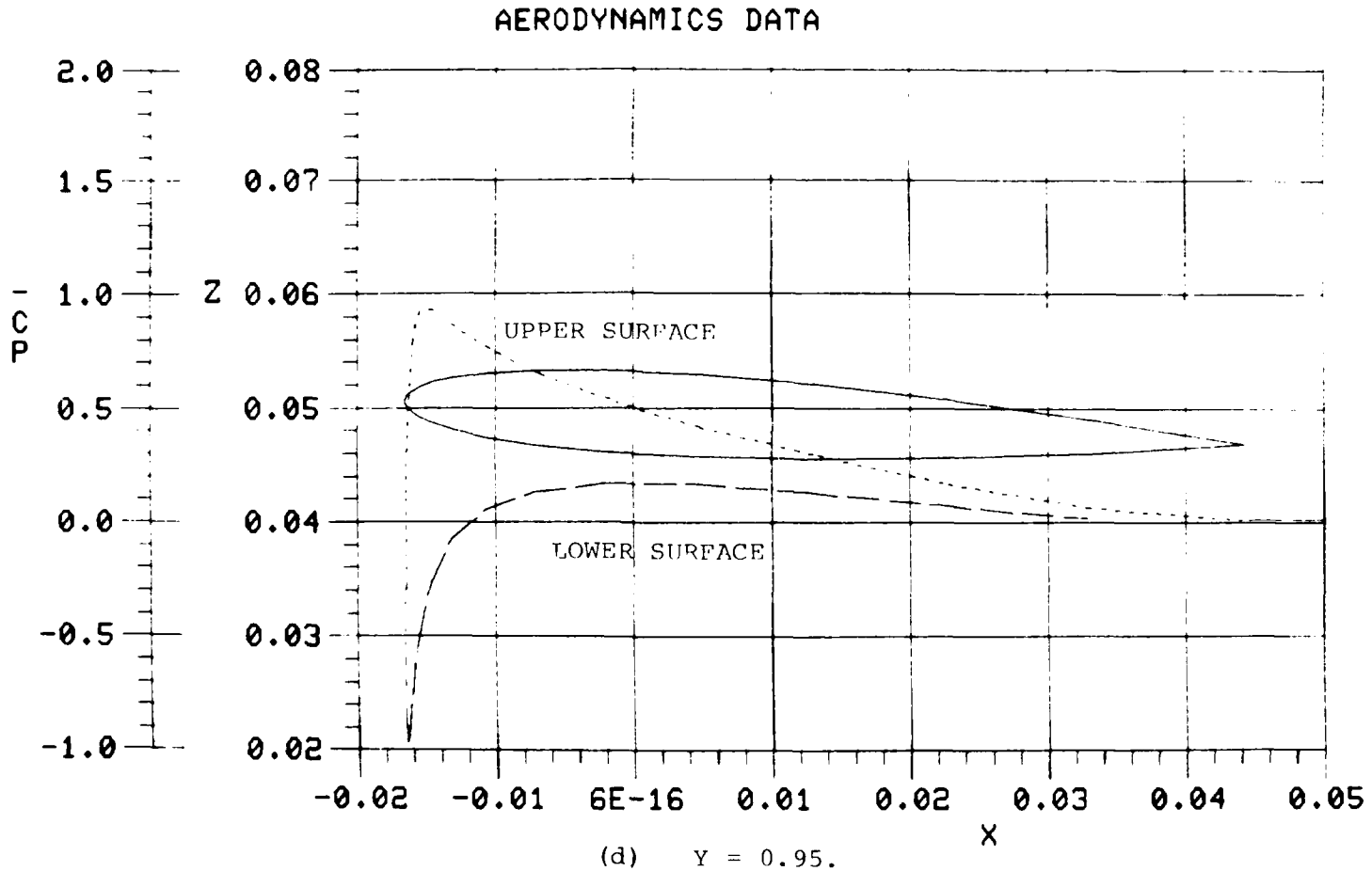


(d) Y = 0.95.

Figure 36. Concluded.

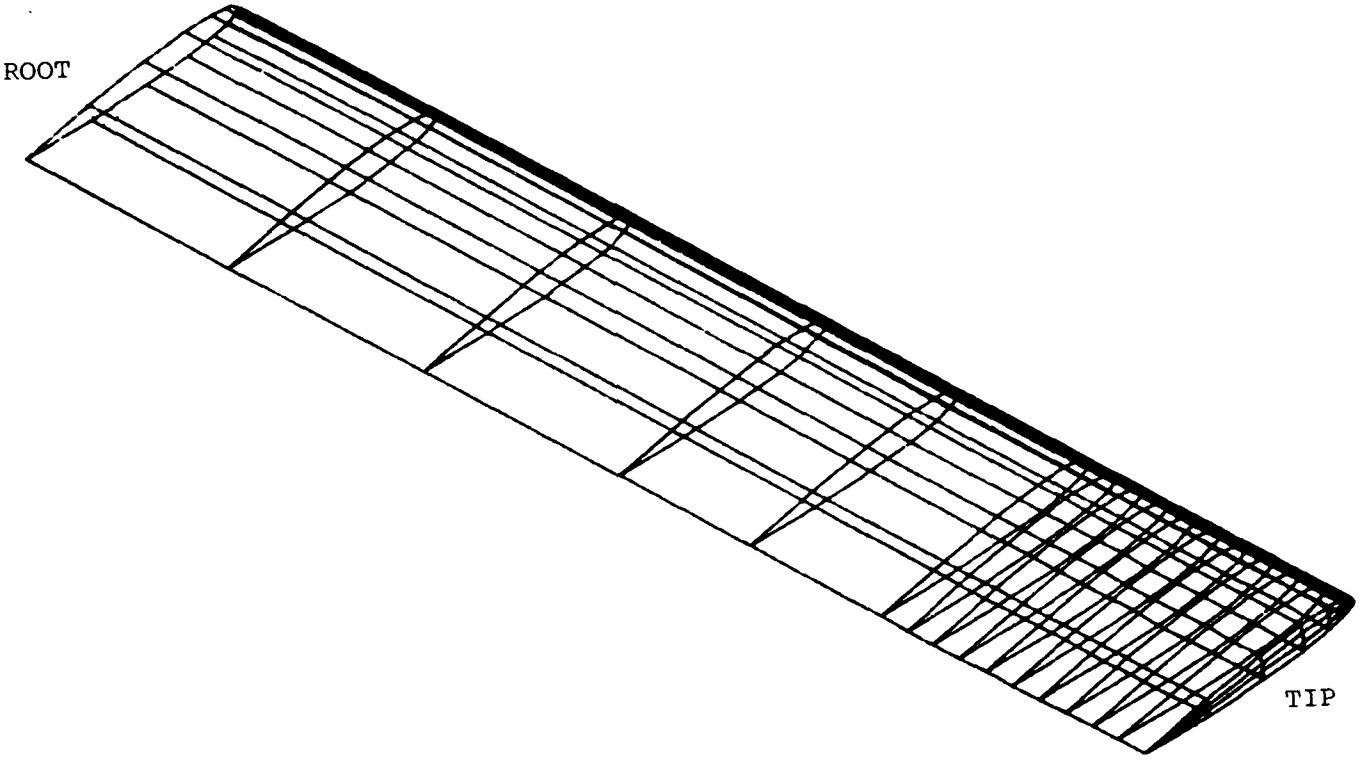


Figure 37. Blade Surface Panelling of Ames Two-Bladed Rotor.

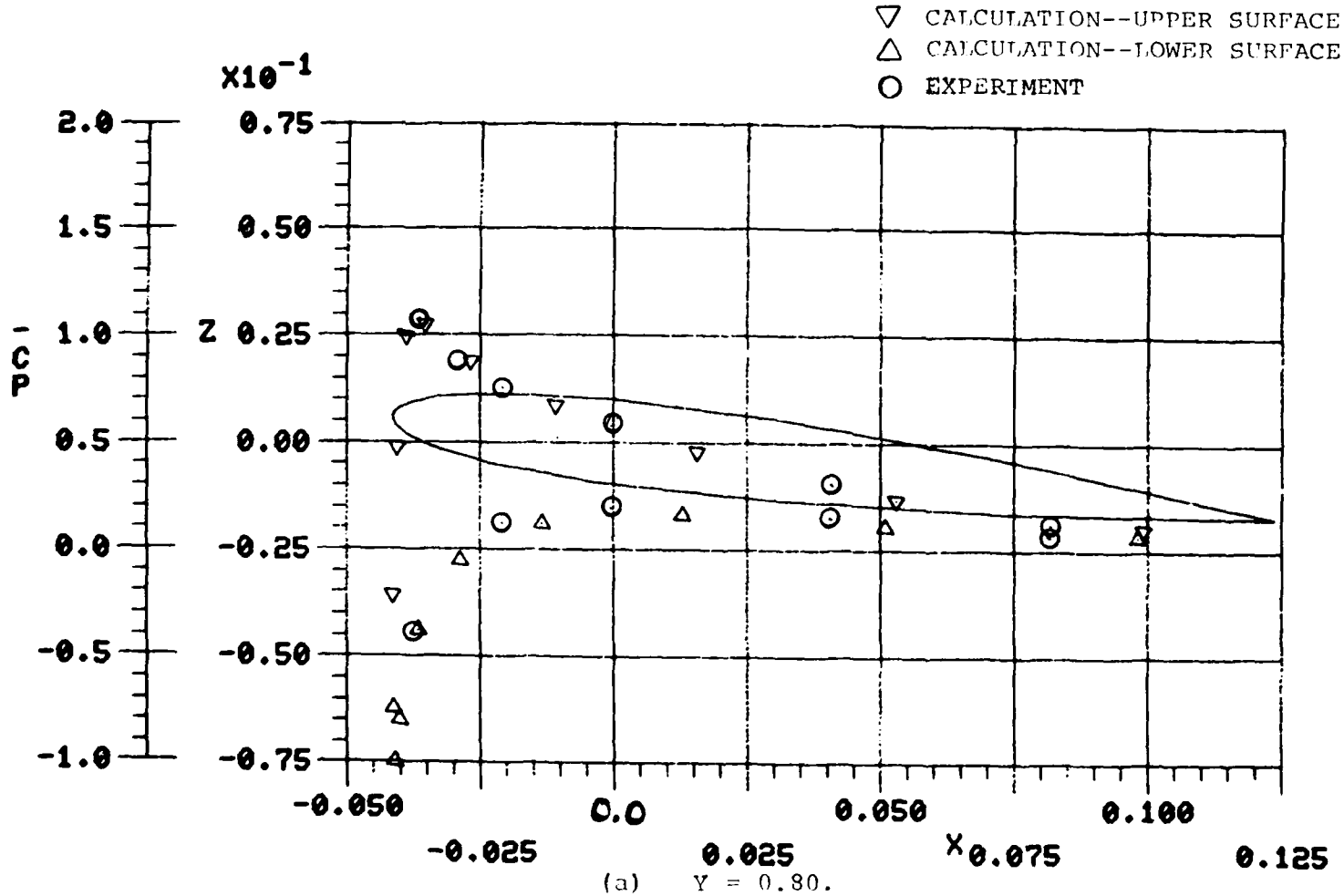


(a) Y = 0.80.

Figure 38. Comparisons of Calculated Chordwise Pressures (minus $C_p$) with Experimental Data for Ames Model Rotor.

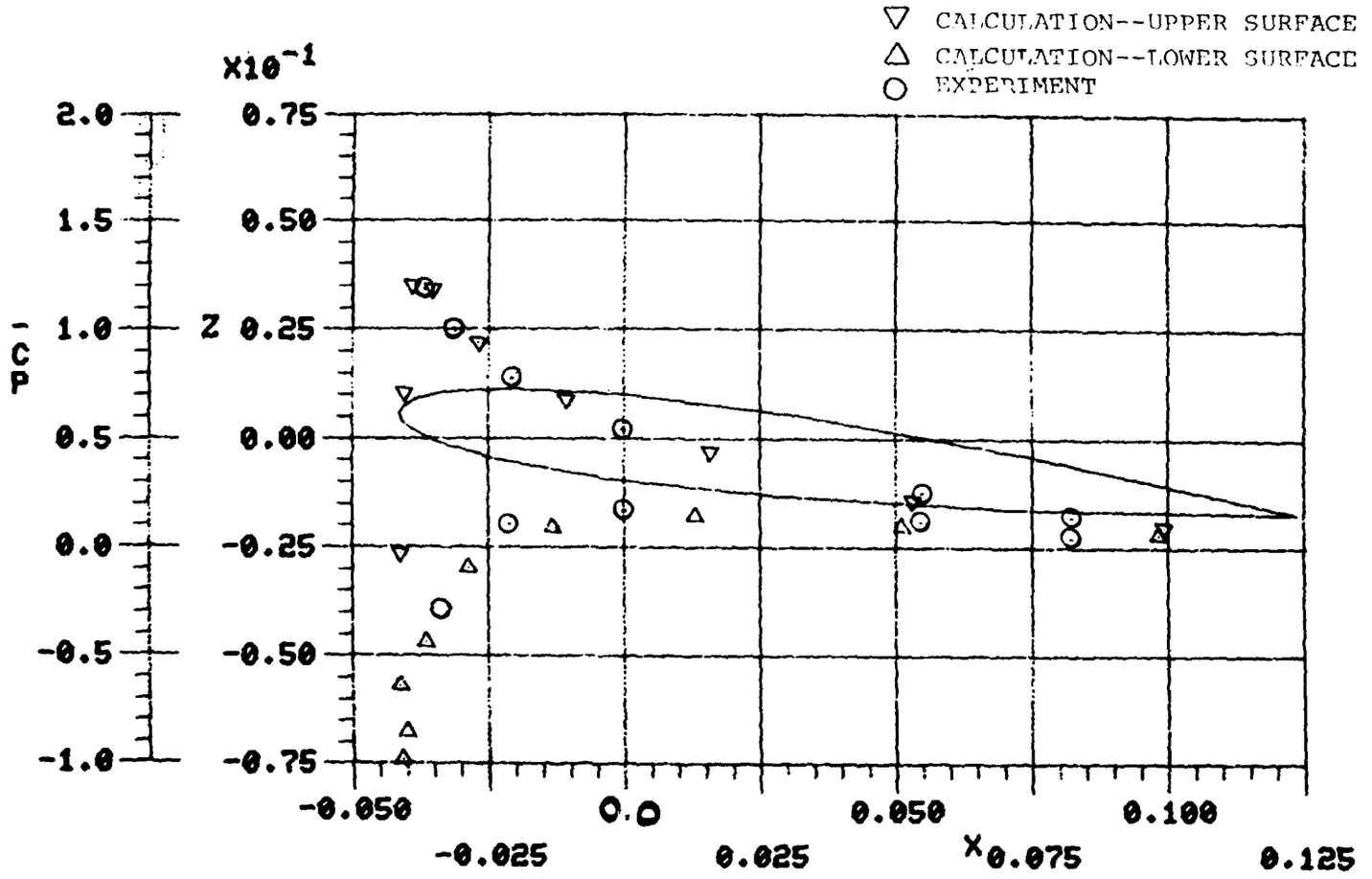


(b) Y = 0.89.

Figure 38. Continued.

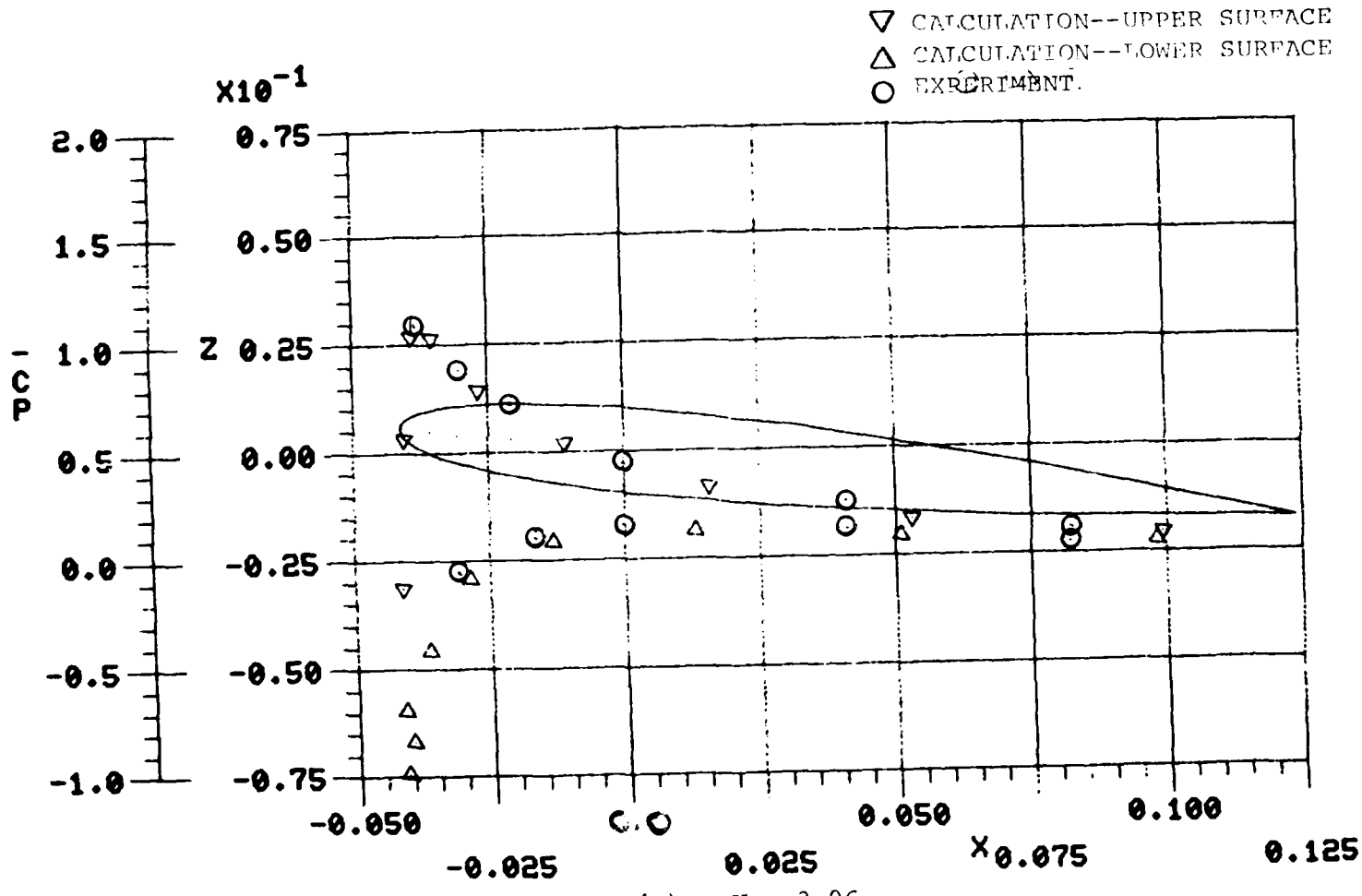


(c) Y = 0.96.

Figure 38. Concluded.

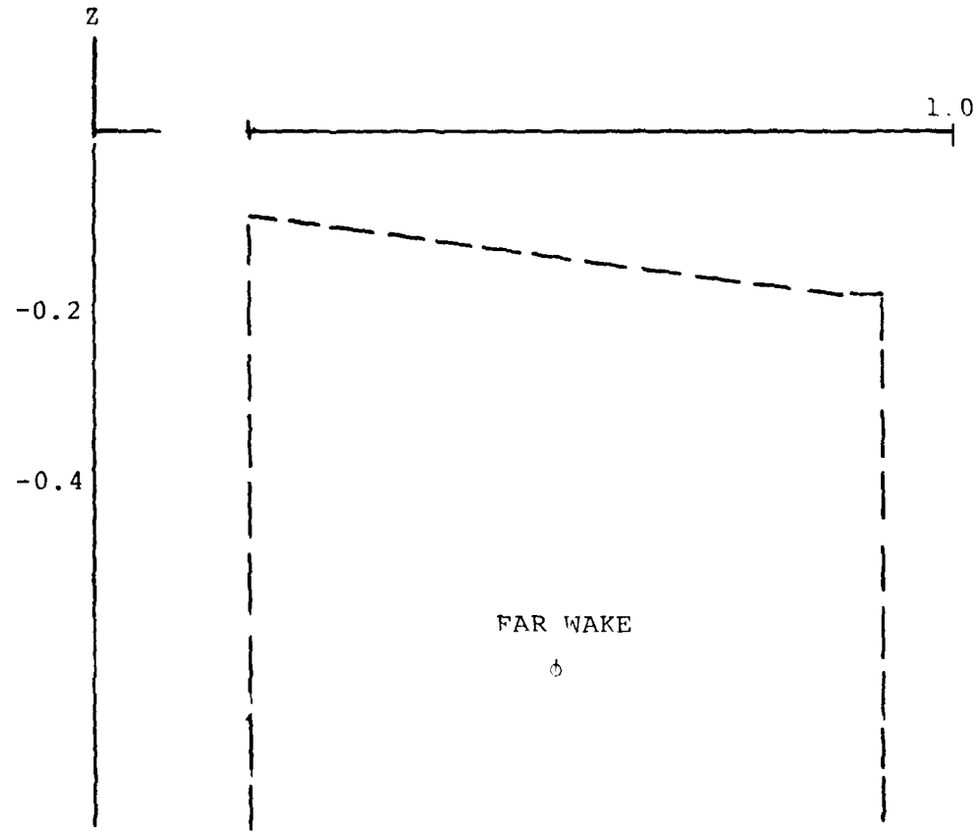


Figure 39. Far-Wake Boundary for Ames Model Rotor.

This was achieved because of the very accurate far-wake doublet model. In fact, since most all of the contraction occurs before first blade passage for this case, only 270° of total detailed wake were needed for this two-bladed rotor. Figure 39 illustrates the boundary where the "far-wake" analytical model was included.

## 6.6 RELAXED WAKE CALCULATIONS

A relaxed wake calculation in ROTAIR is demonstrated in Figure 40 for the OH-58A blade. Since the basic free-wake methodology has been carried over from Reference 8, the convergence of the axial coordinates should follow the same approximate trends obtained with HOVER. Of course, the wake structure is not exactly equal for the two codes since ROTAIR includes exact blade twist and coning, and has a slightly different far-wake model (see Section 4). The calculations in Figure 40 do show the highly convergent behavior found with HOVER, but the first blade passage axial distance, $Z_{\psi_b}$, converges at a much slower rate than the HOVER calculations. Detailed velocity scan comparisons for the two programs have demonstrated that ROTAIR predicted wake induced velocities are correct when the wake vortex strengths are equal. For this calculation, NPC = 5 so that only 10 panels were used around the airfoil. As shown in Section 6.4.3, there are errors in the circulation values for so few panels; consequently, more chordwise panels should always be used if relaxation is desired. Additional relaxation runs with dense panelling should be undertaken to completely validate this part of the code. Also, the method utilized in HOVER for storing the influence coefficients for the rigid wakes needs to be added to ROTAIR to reduce relaxation costs.

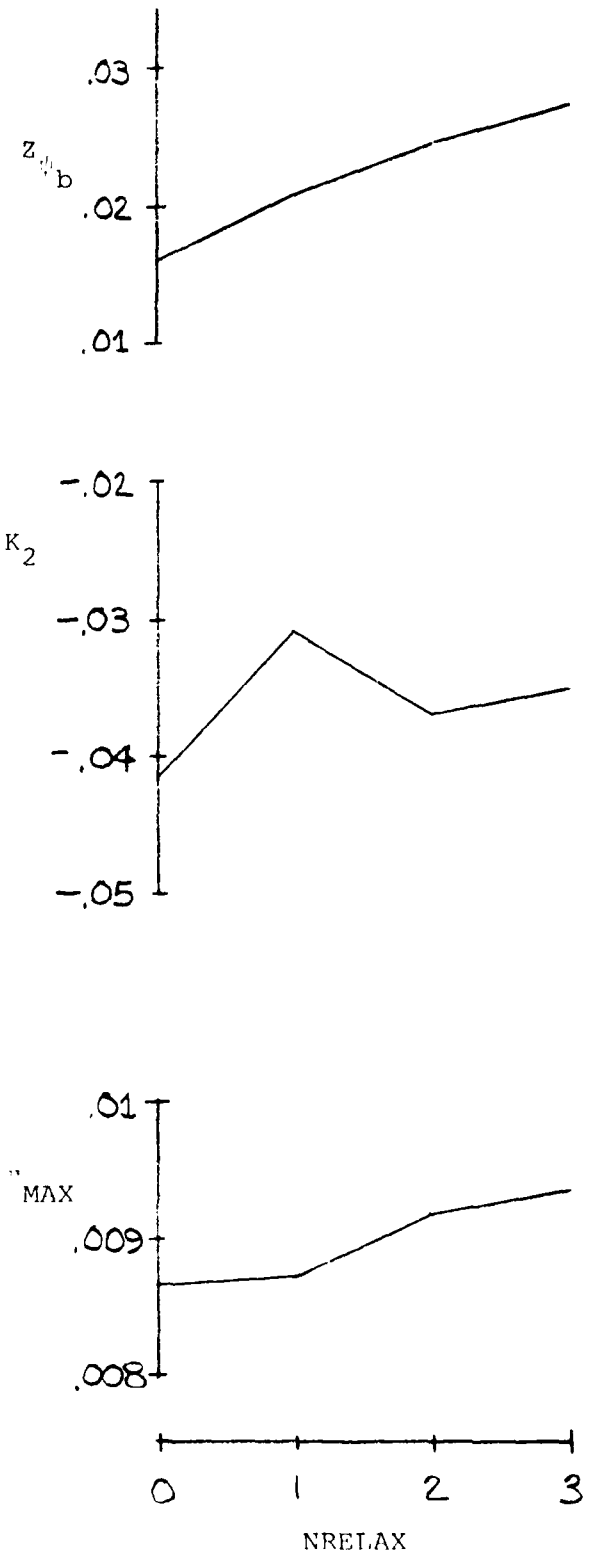


Figure 40. Variation of Key Rotor Properties with Wake Relaxation for the OH-58A.

AD-A109 687 ANALYTICAL METHODS INC REDMOND WA F/G 20/4
A SURFACE SINGULARITY METHOD FOR ROTORS IN HOVER OR CLIMB.(U)
DEC 81 J M SUMMA, B MASKEW DAAJ02-76-C-0069
UNCLASSIFIED AMI-8103 USAAVRADCOM-TR-81-D-23 NL

2 : 2

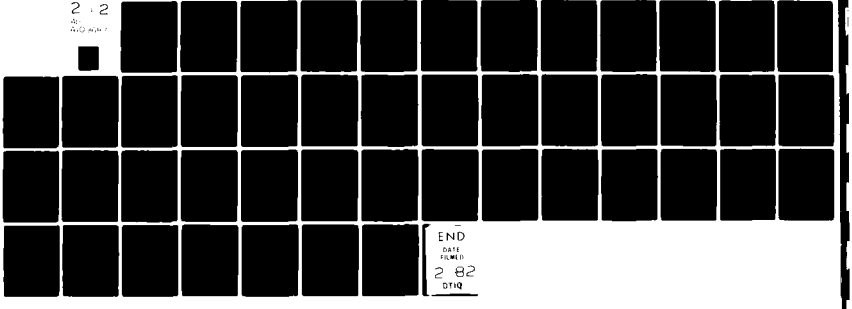

END
DATE FILMED
2 82
DTIC

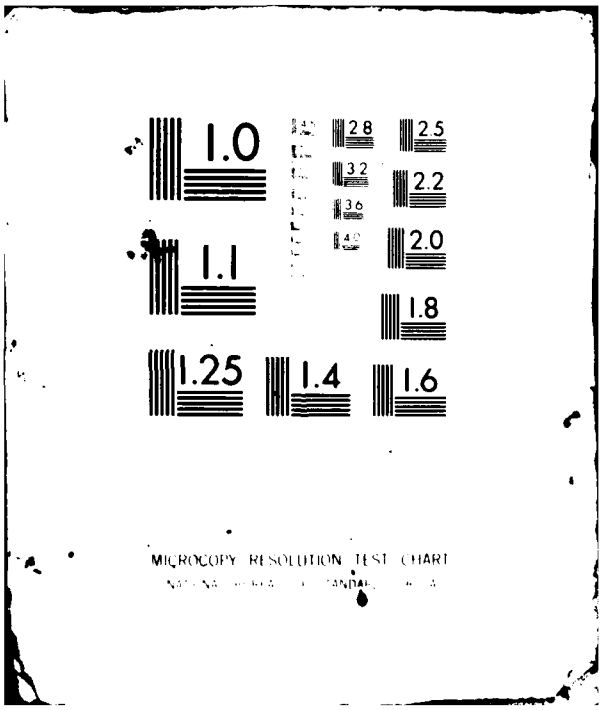
1.0
1.1
1.25
1.4
1.6
1.8
2.0
2.2
2.5
2.8
3.2
3.6
4.0
MICROCOPY RESOLUTION TEST CHART

## 7.0 SUMMARY AND FUTURE DEVELOPMENT

A surface singularity potential flow code, ROTAIR, has been assembled for the calculation of detailed surface pressures on rotors in hover or climb. This method is basically a marriage of two codes developed at AMI: the fixed-wing surface singularity doublet code[9] and the rotor lifting-surface code.[8] The program includes a tip vortex separation model. Also, the rotor tip surface is panelled so that pressures are calculated right around the tip-edge surface.

Preliminary calculations have verified the capabilities of the program for computing blade surface properties in the presence of a close-vortex passage. Additionally, calculated pressure distributions compare favorably with experimental data for a low aspect ratio two-bladed rotor, and the calculated circulation distribution is consistent with that computed earlier with the lifting-surface code. Finally, the newly developed far-wake doublet model promises to keep computing efforts practical.

Meanwhile, further development of the methods is continuing. The rotor wake relaxation schemes are being modified to allow for free contraction boundaries and to reduce computing effects. Elastic modelling and collective iterations are also being added to the program.

In the immediate future, thickness effects should be investigated in more detail; the extent of tip-edge separation and tip vortex formation needs additional work; the convergence of integrated pressure data with panel number must be improved for practical computation; influences of compressibility on the surface singularity method should be examined; and, eventually, the addition of a boundary layer method should be considered to eliminate the two-dimensional profile approximations and to more realistically study the rotor tip problem.

## 8.0 REFERENCES


1. Gray, R.B., "On the Motion of the Helical Vortex Shed from a Single-Bladed Hovering Helicopter Rotor and its Application to the Calculation of the Spanwise Aerodynamic Loading", Princeton University Aero. Engr. Dept., Report No. 313, September 1955.

2. Gray, R.B., "An Aerodynamic Analysis of a Single-Bladed Rotor in Hovering and Low Speed Forward Flight as Determined from Smoke Studies of the Vorticity Distribution in the Wake", Princeton University Aero. Engr. Dept., Report No. 356, September 1956.

3. Landgrebe, A.J., "An Analytical and Experimental Investigation of Helicopter Rotor Hover Performance and Wake Geometry Characteristics", USAAMRDL Tech. Rept. 71-24, Eustis Directorate, U.S. Army Air Mobility Research and Development Laboratory, Fort Eustis, VA, June 1971, AD 728835.

4. Landgrebe, A.J., Moffit, R.C., and Clark, D.R., "Aerodynamic Technology for Advanced Rotorcraft--Part I", J. Am. Hel. Soc., Vol. 22, No. 2, April 1977.

5. Kocurek, J.D., "Hover Performance Methodology at Bell Helicopter Textron", 36th Annual Forum of the American Helicopter Society, Preprint No. 80-3, May 1980.

6. Caradonna, F.X., and Tung, C., "Experimental and Analytical Studies of a Model Helicopter Rotor in Hover", Sixth European Rotorcraft and Powered Lift Aircraft Forum, Paper NO. 25, Briscol, England, September 1980.

7. Summa, J.M., and Clark, D.R., "A Lifting-Surface Method for Hover/Climb Airloads", 35th Annual National Forum of the American Helicopter Society, Preprint No. 79-3, May 1979.

8. Summa, J.M., "Evaluation of Blade Tip Planform Effects on Hover Performance", Contract DAAJ02-76-C-0069, Applied Technology Laboratory, U.S. Army Research and Technology Laboratories (AVRADCOM), Fort Eustis, VA, to be published.

9. Maskew, B., "Unsteady Potential Flow Analysis of Rotor Blade Tip Shapes", Interim Report and Program User Guide (Contract NAS1-15472), NASA Langley Research Center, April 1980.

10. Maskew, B., "Influence of Rotor Blade Tip Shape on Tip Vortex Shedding--An Unsteady, Inviscid Analysis", Presented at the 36th Annual Forum of the American Helicopter Scoeity, Preprint No. 80-6, May 1980.

11. Maskew, B., "Prediction of Subsonic Aerodynamic Characteristics--A Case for Low-Order Panel Methods", AIAA 19th Aerospace Sciences Meeting, AIAA-81-0252, January 1981.

12. Morino, L., Chen, L.T., and Sucio, E.O., "Steady and Oscillatory Subsonic and Supersonic Aerodynamics Around Complex Configurations", AIAA J., Vol. 13, No. 3, pp. 368-374, March 1975.

13. Maskew, B., and Dvorak, F.A., "The Prediction of $C_{LMAX}$ Using a Separated Flow Model", J. Am. Hel. Soc., April 1978.

14. Kocurek, J.D., and Tangler, J.L., "Prescribed Wake Lifting Surface Hover Performance Analysis", Presented at the 32nd Annual National VSTOL Forum of the American Helicopter Society, Washington, D.C., May 1976.

## APPENDIX A: SUBROUTINE MAP

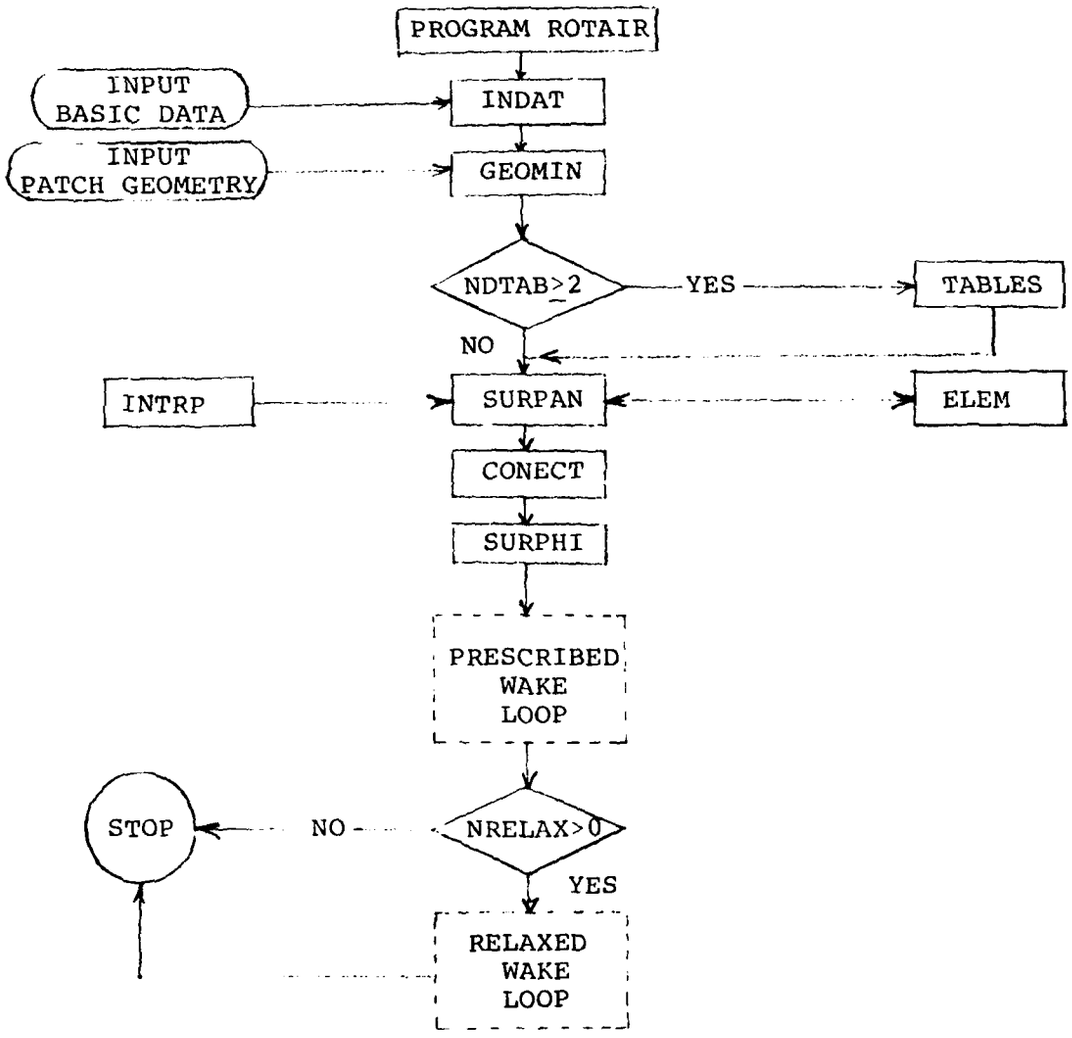


Figure A-1. Complete Subroutine Map.

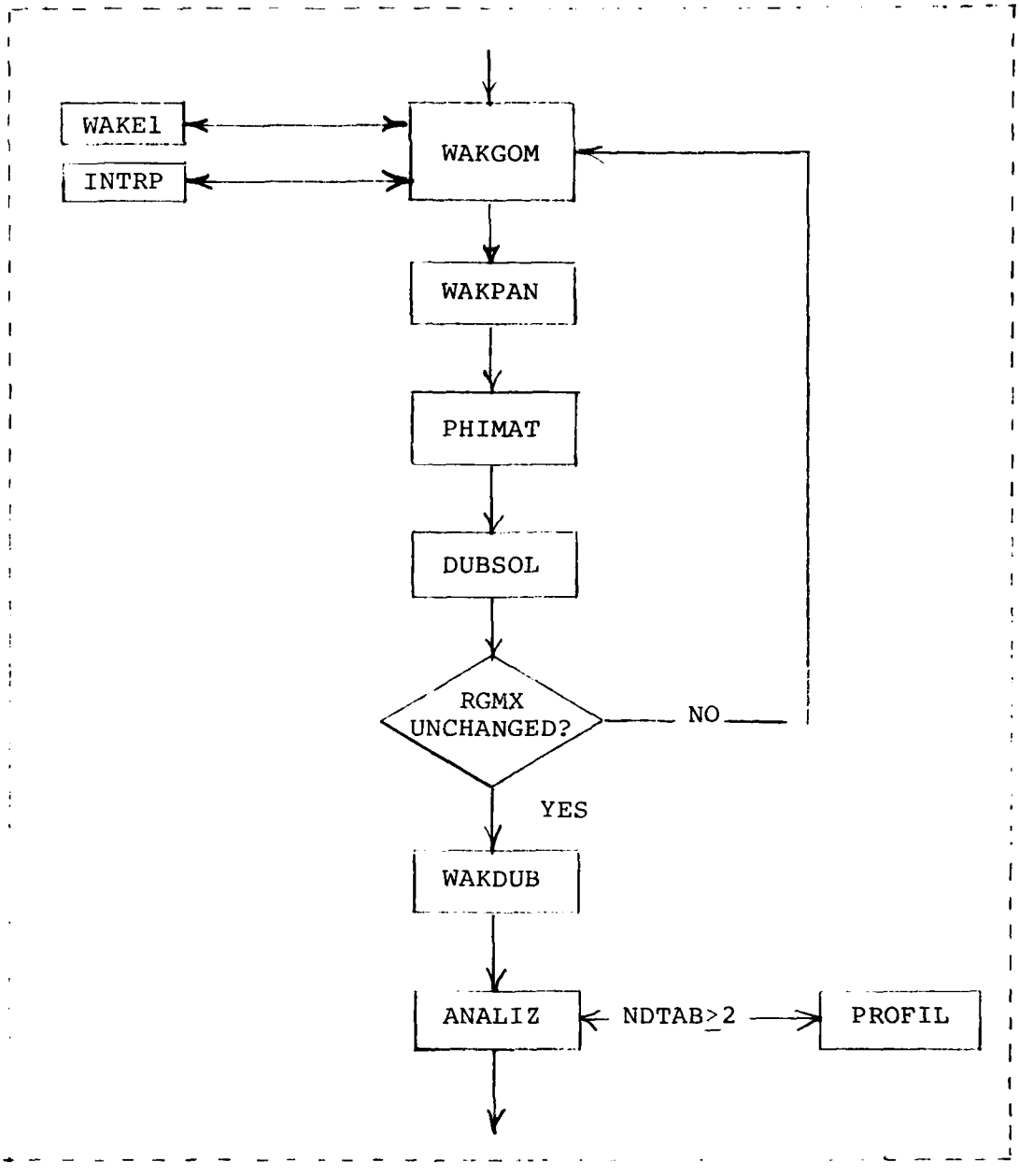


Figure A-2. Prescribed Wake Loop.

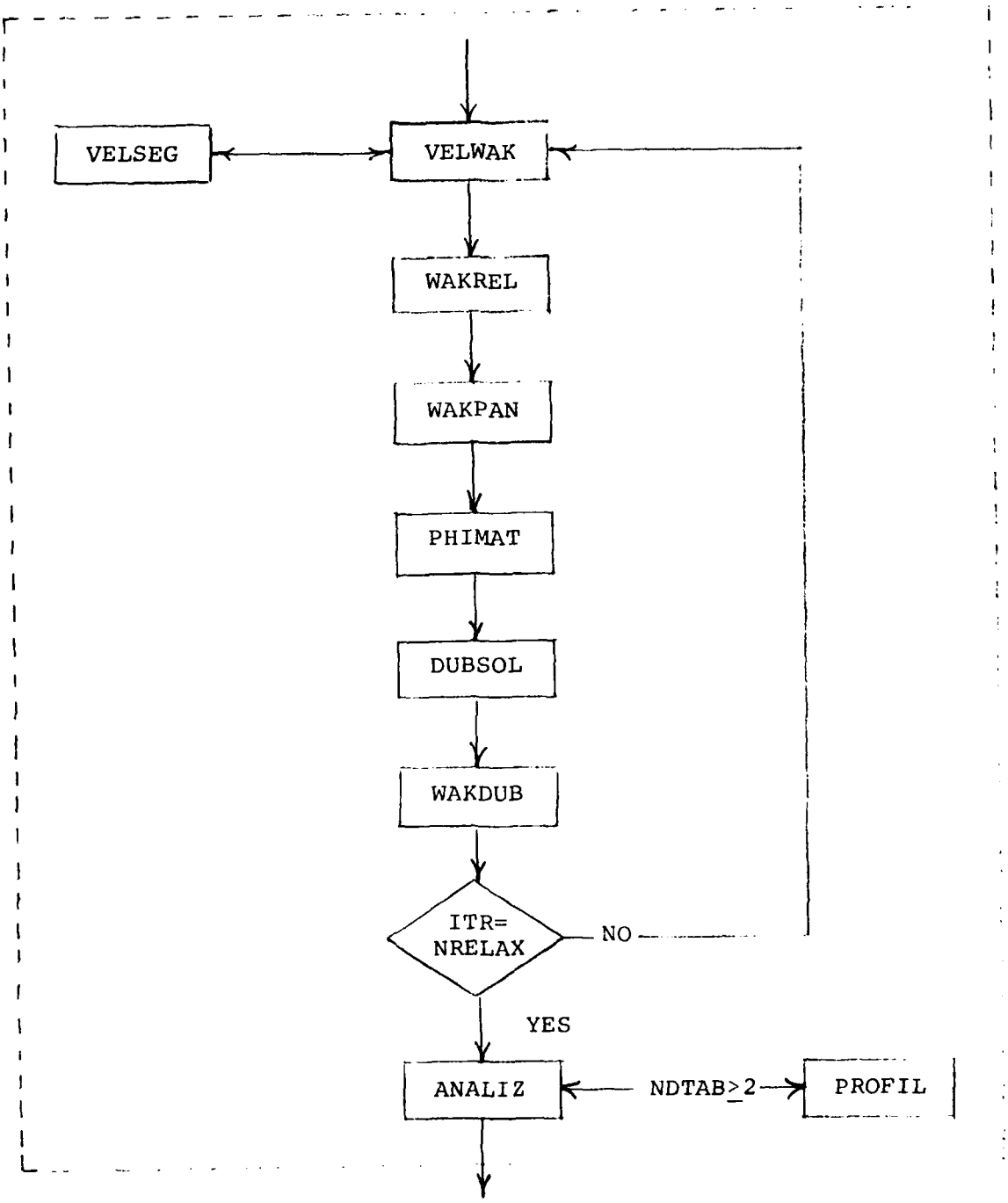


Figure A-3. Relaxed Wake Loop.

## APPENDIX B: INPUT DESCRIPTION

The input is in five main parts: Basic Data, Wake Data, Blade Orientation, Geometry and Aerodynamic Data Tables. Figure B-1 shows the assembly of the input cards.

### BASIC DATA

CARD 1: General Identification.

| Columns | Variable | Description | Format |
|---|---|---|---|
| 1-80 | TEXT | Any identifying information for the case | 8A10 |

CARD 2: Print Control.

| Columns | Variable | Value | Description | Format |
|---|---|---|---|---|
| 1-5 | IPRI | 1 | All the input data is printed in the same order as it is read | 2I5 |
| | | 0 | Input data print-off | |
| 6-10 | IPRLEV | 0 | Basic print level (see Appendix C) | |
| | | 1 | Panel corner points are printed | |

CARD 3: Mode Card.

| Columns | Variable | Value | Description | Format |
|---|---|---|---|---|
| 1-5 | NPNMAX | | Upper limit on number of panels the user expects to be generated (default 1000) | 2I5 |
| 6-10 | MSTOP | 0 | Complete run | |
| | | 2 | Calculations stop after SURPAN for examination of panel corner points (set IPRLEV=1) | |

CARD 4: Number of Aerodynamic Table Stations.

| Columns | Variable | Value | Description | Format |
|---|---|---|---|---|
| 1-5 | NDTAB | 0,2-20 | Number of 2-D sectional data table input stations | I5 |

CARD 5: General Rotor Information.

| Columns | Variable | Value | Description | Format |
|---|---|---|---|---|
| 1-5 | NB | 1-8 | Number of blades | I5,F10.0 |
| 6-15 | RADIUS | | Rotor radius as defined in the geometry input | |

Note: RADIUS must equal YFLAP plus STY of the last geometric defining section; therefore, RADIUS sets the length units for geometry input.

CARD 6: Velocity Requests.

| Columns | Variable | Description | Format |
|---|---|---|---|
| 1-10 | VCLIMB | Rotor climb speed | 3F10.0 |
| 11-20 | VTIP | Rotor rotation tip speed | |
| 21-30 | VSOUND | Speed of sound | |

Note: Any consistent units of length/sec. or dimensionless.

CARD 7: Performance Card.

| Column | Variable | Value | Description | Format |
|---|---|---|---|---|
| 1-10 | CTO | | Requested thrust coefficient; i.e., used to set the prescribed wake constants | 2F10.0 |
| 11-20 | RGMX | | Estimated ratial position of maximum circulation. Same units as *RADIUS* | |

WAKE DATA

CARD 8: Basic Constants.

| Column | Variable | Value | Description | Format |
|---|---|---|---|---|
| 1-10 | RFAR | 0-1.0 | Ultimate contracted radius. "A" in Landgrebe's notation. Default value is 0.78 | 2F10.0 |
| 11-20 | PSIO | $<\psi_b$ | Azimuth for the start of axial descent of the inner sheet at the axis of rotation. In the original equations, PSIO=90 (degrees) | |

CARD 9: Wake Azimuthal Boundaries

| Column | Variable | Value | Description | Format |
|---|---|---|---|---|
| 1-10 | PSIF1 | $\geq 0$ | Azimuth of start of intermediate wake (degrees) | 3F10.0 |
| 11-20 | PSIF2 | $\geq$PSIF1 | Azimuth of start of far wake (degrees) | |
| 21-30 | PSIMRG | $< \psi_b$ $\geq$DPSIT1 | Azimuth at which tip vortex merger occurs (degrees) | |

CARD 10: Wake Azimuthal Increments.

| Column | Variable | Value | Description | Format |
|---|---|---|---|---|
| 1-10 | DPSIT1 | arbitrary | Azimuthal increment of tip vortex to first blade passage (degrees) | 4F10.0 |
| 11-20 | DPSIT2 | arbitrary | Azimuthal increment of tip vortex after first blade passage (degrees) | |
| 21-30 | DPSIS1 | arbitrary | Azimuthal increment of inner sheet to first blade passage (degrees) | |
| 31-40 | DPSIS2 | arbitrary | Azimuthal increment of inner sheet after first blade passage (degrees) | |

14
F

Note: Unless NRELAX>0, all can be set to 30 degrees for preliminary work.

CARD 11: Tip Vortex Constants.

| Columns | Variable | Value | Description | Format |
|---|---|---|---|---|
| 1-10 | TK1 | $<0.0$ | Pitch constant of the tip vortex to first blade passage. Normally identified as $k_1$ | 3F10.0 |
| 11-20 | TK2 | $<0.0$ | Pitch constant of the tip vortex after first blade passage. Normally identified as $k_2$ | |
| 21-30 | TLAMDA | $\geq 0.0$ | Wake contraction constant. Normally identified as $\lambda$ | |

CARD 12: Inner Sheet Constants.

| Columns | Variable | Value | Description | Format |
|---|---|---|---|---|
| 1-10 | SKT1 | $<0.0$ | Pitch constant of inner sheet at r = 1.0 to PSIO. Normally identified as $k_{1_{\bar{r}=1}}$ | 4F10.0 |
| 11-20 | SKT2 | $<0.0$ | Pitch constant of inner sheet at r = 1.0 after PSIO. Normally identified as $k_{2_{\bar{r}=1}}$ | |
| 21-30 | SKR1 | $\leq 0.0$ | Pitch constant of inner sheet at r = 0 to PSIO. Normally identified as $k_{1_{\bar{r}=0}}$ and taken as 0.0 | |
| 31-40 | SKR2 | $<0.0$ | Pitch constant of inner sheet at r = 0 after PSIO. Normally identified as $k_{2_{\bar{r}=0}}$ | |

14
B

CARD 13: Tip Vortex Formation.

| Columns | Variable | Value | Description | Format |
|---|---|---|---|---|
| 1-5 | NSEP | $\geq 0$ | The number of tip panels from the trailing edge for which vortex shedding occurs | I5,2F10.0 |
| 6-15 | DELZ | | The distance above the trailing edge that the tip vortex passes through. Same units as RADIUS (Figure 19) | |
| 16-25 | DELR | | The distance that the tip vortex is shifted inboard from the rotor tip. Same units as RADIUS (Figure 19) | |

CARD 14: Wake Relaxation.

| Columns | Variable | Value | Description | Format |
|---|---|---|---|---|
| 1-5 | NRELAX | $\geq 0$ | Number of wake relaxation iterations | I5 |

ROTOR BLADE ORIENTATION

(B.C.S. to H.C.S. Transformation)

CARD 15: Blade Orientation.

| Columns | Variable | Value | Description | Format |
|---|---|---|---|---|
| 1-10 | YFLAP | $\geq 0.0$ | Rotor flapping axis radius location. Same units as RADIUS | 3F10.0 |
| 11-20 | THTA75 | | Blade collective (degrees) | |
| 21-30 | CONE | | Blade coning angle (degrees) | |

Note: (1) RADIUS = YFLAP + STY of last section;
(2) see Section 3, Figure 3

## PATCH GEOMETRY

Repeat the following group of cards, 16 through 21 (where applicable), for each patch.

CARD 16: Patch Card.

| Columns | Variable | Value | Description | Format |
|---|---|---|---|---|
| 1-5 | IDENT | 1 | Gives wing-type printout of pressure data (see Appendix C) | 2I5 |
| | | 2 | Simplified pressure printout (tip closure patch) | |
| 6-10 | MAKE | 0 | Regular patch input. Requires CARD 17 and CARDS 18, 19 and 20 where applicable | |
| | | M | Automatic patch closing end of Patch M. Requires CARD 21 only. See Section 3.3.2 | |

CARD 17: Section Card.

| Columns | Variable | Value | Description | Format |
|---|---|---|---|---|
| 1-10 | STX | | Location of the section leading-edge in the blade reference frame (see Figures 6 and 7) | 6F10.0, 10X, 4I5 |
| 11-20 | STY | | | |
| 21-30 | STZ | | | |
| 31-40 | SCALE | $\neq 0$ | Scaling factor on section chord length | |
| 41-50 | ALF | | Section twist angle in degrees | see Fig. 6 |
| 51-60 | THETA | | Section rotation angle in degrees | |

| Columns | Variable | Value | Description | Format |
|---|---|---|---|---|
| 61-65 | INMODE | | Type of section input (see Figure 8) | |
| | | 0 | Copies the previously defined section as originally specified; i.e., the basic coordinates before scaling, etc. | |
| | | -M | Copies the basic coordinates of section M (absolute subscript) | |
| | | 1 | Input y,z coordinates of SECTION. Requires CARD SET 18A | |
| | | 2 | Input x,z coordinates of SECTION. Requires CARD SET 18A | |
| | | 3 | Input x,y coordinates of SECTION. Requires CARD SET 18C | |
| | | 4 | Input x,y,z coordinates of SECTION. Requires CARD SET 18D | |
| | | 5 | Generates coordinates on an NACA 4-digit section. Requires CARD 20 only | |
| 66-70 | NODS | 0 | First or interior section on a patch | |
| | | 1<br>2 | End of a spanwise region within a patch with continuous (1) or discontinuous (2) slope on the spanwise generators onto the next spanwise region (Figure 11) | |
| | | 3 | This section completes the present PATCH | |
| | | 5 | This section completes the last patch in the configuration | |

| Columns | Variable | Value | Description | Format |
|---|---|---|---|---|
| 71-75 | NPS | | Only active if NODS $\neq$ 0 | |
| | | 0 | Manual panelling in spanwise region just completed; defined sections are used as panel edges in this region | |
| | | $>$0 | Number of panels to be generated in the spanwise region just completed | |
| 76-80 | INTS | | (Only active if NODS $\neq$ 0 and NPS $>$ 0) | |
| | | 0<br>1<br>2<br>3 | Form of spanwise interval spacing for the generated panels. See Section 3 and Figure 10 | |

CARD SET 18: SECTION Coordinates. (Present if INMODE = 1, 2, 3 or 4). In each set use one card per point. Insert NODE CARD(S) 19 to control panelling and to complete a set; see Figures 8 and 9.

CARD SET 18A (INMODE = 1)

| Columns | Variable | Value | Description | Format |
|---|---|---|---|---|
| 1-10<br>11-20<br>21-30 | BY<br>BZ<br>$\Delta$X | | y,z coordinates of a point on the section. The x-stations are essentially constant (0.0); however, local deviations in x can be placed in $\Delta$x | 3F10.0 |

CARD SET 18B (INMODE = 2)

| Columns | Variable | Value | Description | Format |
|---|---|---|---|---|
| 1-10 | BX | | x,z coordinates of a point on the section. The y-stations are essentially constant (0.0); however, local derivations in y can be placed in Δy. Most rotors require this form | 3F10.0 |
| 11-20 | BZ | | | |
| 21-30 | ΔY | | | |

CARD SET 18C (INMODE = 3)

| Columns | Variable | Value | Description | Format |
|---|---|---|---|---|
| 1-10 | BX | | x,y coordinates of a point on the section. The z-stations are essentially constant (0.0); however, local derivations in Z can be placed in Δz | 3F10.0 |
| 11-20 | XY | | | |
| 21-30 | ΔZ | | | |

CARD SET 18D (INMODE = 4)

| Columns | Variable | Value | Description | Format |
|---|---|---|---|---|
| 1-10 | BX | | x,y,z coordinates of a point on an arbitrary skewed section | 3F10.0 |
| 11-20 | BY | | | |
| 21-30 | BZ | | | |

CARD 19: Chordwise Node Card

| Columns | Variable | Value | Description | Format |
|---|---|---|---|---|
| 30-35 | NODEC | 1 | Terminates a chordwise region having continuous (1) or discontinuous (2) surface slope onto the next chordwise region (for example, see Figure B-2) | 30X,3I5 |
| | | 2 | | |

| Columns | Variable | Value | Description | Format |
|---|---|---|---|---|
| 30-35 | NODEC (Continued) | 3 | Signifies a TERMINAL NODE CARD placed after the last point on a section | |
| | | -1, -2, -3 | Negative values initiate a copying routine. Use CARD 19A to define a string of points to be copied over to form part or all of present section. The last copied point is the end of a chordwise region with the corresponding action according to the modulus of the NODEC value | |
| | | -4 | The CARD 19A must be followed either with another negative NODE CARD or with further basic points | |
| 36-40 | NPC | 0 | Manual panelling in the chordwise region just completed (i.e., basic points correspond to panel corners) | |
| | | >0 | Number of panels to be generated in the chordwise region just completed | |
| 41-45 | INTC | 0, 1, 2, 3 | Form of chordwise interval spacing for the generated panels (see Figure 10) | |

CARD 19A: Copy Card. Defines a string of basic points to be copied over. Required only if NODEC < 0.

| Columns | Variable | Value | Description | Format |
|---|---|---|---|---|
| 1-5 | NPCH | | Patch number | 4I5 |
| 6-10 | NSEC | | Section number within that patch (local subscript) | |
| 11-15 | IB, LB | | First and last basic points on that section (local subscript) | |

CARD 20: NACA 4-Digit Section (INMODE=5).

| Columns | Variable | Description | Format |
|---|---|---|---|
| 1-10 | TC | Thickness/chord ratio of NACA 4-Digit section | F10.0, I5 |
| 11-15 | NPC | Number of panels to be generated across airfoil chord (i.e., total number of panels for upper plus lower surfaces = 2 x NPC) | |

Note: A section is generated having a unit chord length and having the leading edge at 0.0, 0.0. Set the STX,STY, STZ and SCALE values on CARD 17 to the required location and size for the section.

15 F CARD 21: Automatic Patch Card (only if MAKE≠0 on CARD 16). See Figure 12.

| Columns | Variable | Value | Description | Format |
|---|---|---|---|---|
| 36-40 | NPC | | Number of panels "chordwise" on patch | 35X, 3I5, 15X, 3I5 |
| 41-45 | INTC | 0<br>1<br>2<br>3 | Form of panel spacing "chordwise". See Figure 10 | |
| 46-50 | KURV | 0 | Flat tip | |
| | | 1 | Semicircular tip section | |
| 66-70 | NODS | 5 | Last patch | |

| Columns | Variable | Value | Description | Format |
|---|---|---|---|---|
| 71-75 | NPS | 0 | Basic points of tip section used as panel points in "spanwise" direction. NPS should not be set to zero if NPC>0 on the tip section (i.e., on CARD 19). If CARD 20 is used for the tip section, NPS = 0 is required | |
| | | >0 | Number of panels to be generated "spanwise" | |
| 76-80 | INTS | 0<br>1<br>2<br>3 | Spacing options, see Figure 10. Inactive if NPS = 0 | |

## AERODYNAMIC SECTION DATA

15
B

These data tables are input in the standard format currently used in the Rotorcraft Flight Simulation Program, C-81.

Repeat the following cards, 22 through 26 (where applicable), for each NDTAB stations. If NDTAB=0, skip this entire card set.

CL and CD tables are all that are allowed.

CARD 22: Copy Control and Defining Station.

| Columns | Variable | Value | Description | Format |
|---|---|---|---|---|
| 1-10 | ICOPY | 0 | Complete aerodynamic tables are read in for this section | I10,F10.0 |
| | | ID | Sectional aerodynamic data is copied over from previously defined section ID | |
| 11-20 | YR | | The radius location of the table defining station. Same units as RADIUS (with respect to axis of rotation) | |

Note: If ICOPY>0, the rest of the card set (23 through 26) is omitted for this section.

CARD 23: Title and Control Card.

| Columns | Variable | Value | Description | Format |
|---|---|---|---|---|
| 1-30 | TITLE | any | Alphanumerical title of sets of tables | 6A5,6I2 |
| 31-32 | NMACH(1) | 3-18 | Number of Mach number entries in $C_\ell$ table | |
| 33-34 | NALPHA(1) | 3-125 | Number of angle-of-attack entries in $C_\ell$ table | |
| 35-36 | NMACH(2) | 3-18 | Number of Mach number entries in $C_d$ table | |
| 37-38 | NALPHA(2) | 3-125 | Number of angle-of-attack entries in $C_d$ table | |

Note: Card sets 24 through 26 are repeated as a group two times for $C_\ell$ and $C_d$; that is, in the following descriptions

K = 1 ----- $C_\ell$

K = 2 ----- $C_d$

CARD 24: Mach Number Entries.

| Columns | Variable | Value | Description | Format |
|---|---|---|---|---|
| 8-14 | MACH(1) | arbitrary | Lowest Mach number | 7X,9F10.0 |
| 15-21 | MACH(2) | " | Next highest Mach number | |
| 22-28 | MACH(3) | " | " | |
| . | . | | | |
| . | . | | | |
| . | . | | | |
| 64-70 | MACH(9) | " | " | |

Note: Additional card may be required with same format to input NMACH(K) values of Mach numbers.

CARD 25: Angle-of-Attack/Coefficient Data.

| Columns | Variable | Value | Description | Format |
|---|---|---|---|---|
| 1-7 | ALPHAI(K) | arbitrary | Angle of attack, degrees | 10F7.0 |
| 8-14 | COI(K,1) | arbitrary | Coefficient at MACH(1) | |
| 15-21 | COI(K,2) | " | Coefficient at MACH(2) | |
| 22-28 | COI(K,3) | " | Coefficient at MACH(3) | |
| . | . | | | |
| . | . | | | |
| . | . | | | |
| 64-70 | COI(K,9) | " | Coefficient at MACH(9) | |

CARD 26: Continued Coefficient Data.

| Columns | Variable | Value | Description | Format |
|---|---|---|---|---|
| 8-14 | COI(K,10) | arbitrary | Coefficient at MACH(10) | 7X,9F7.0 |
| . | . | | | |
| . | . | | | |
| . | . | | | |
| 64-70 | COI(K,18) | " | Coefficient at MACH(18) | |

Note: 1. CARD 26 included only if NMACH(K)>9.

2. CARDS 25 and 26 repeated NALPHA(K) times for each angle of attack.

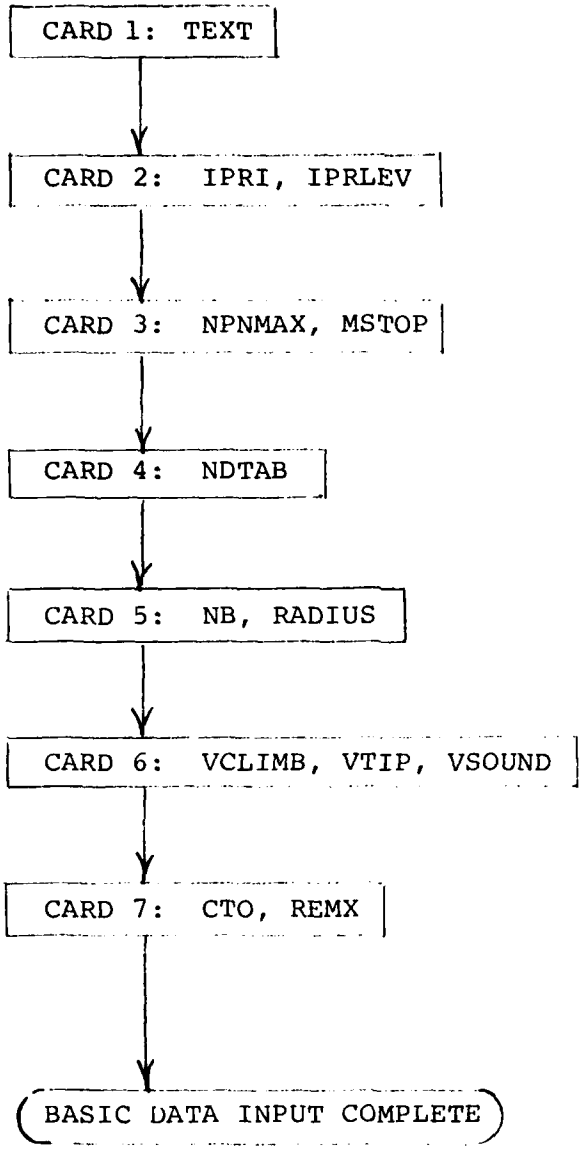


(a) Basic Data.

Figure B-1. Flow Chart for Input Card Deck.

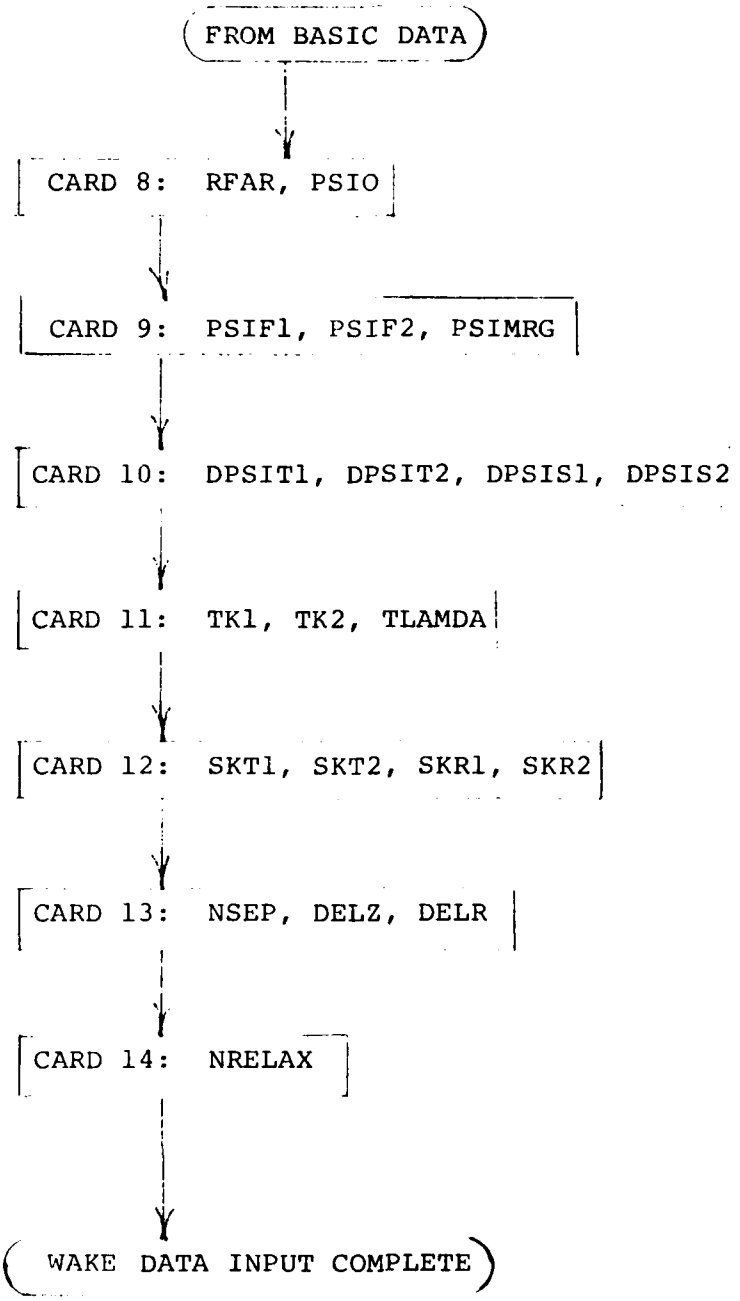


(b) Wake Data.

Figure B-1. Continued.

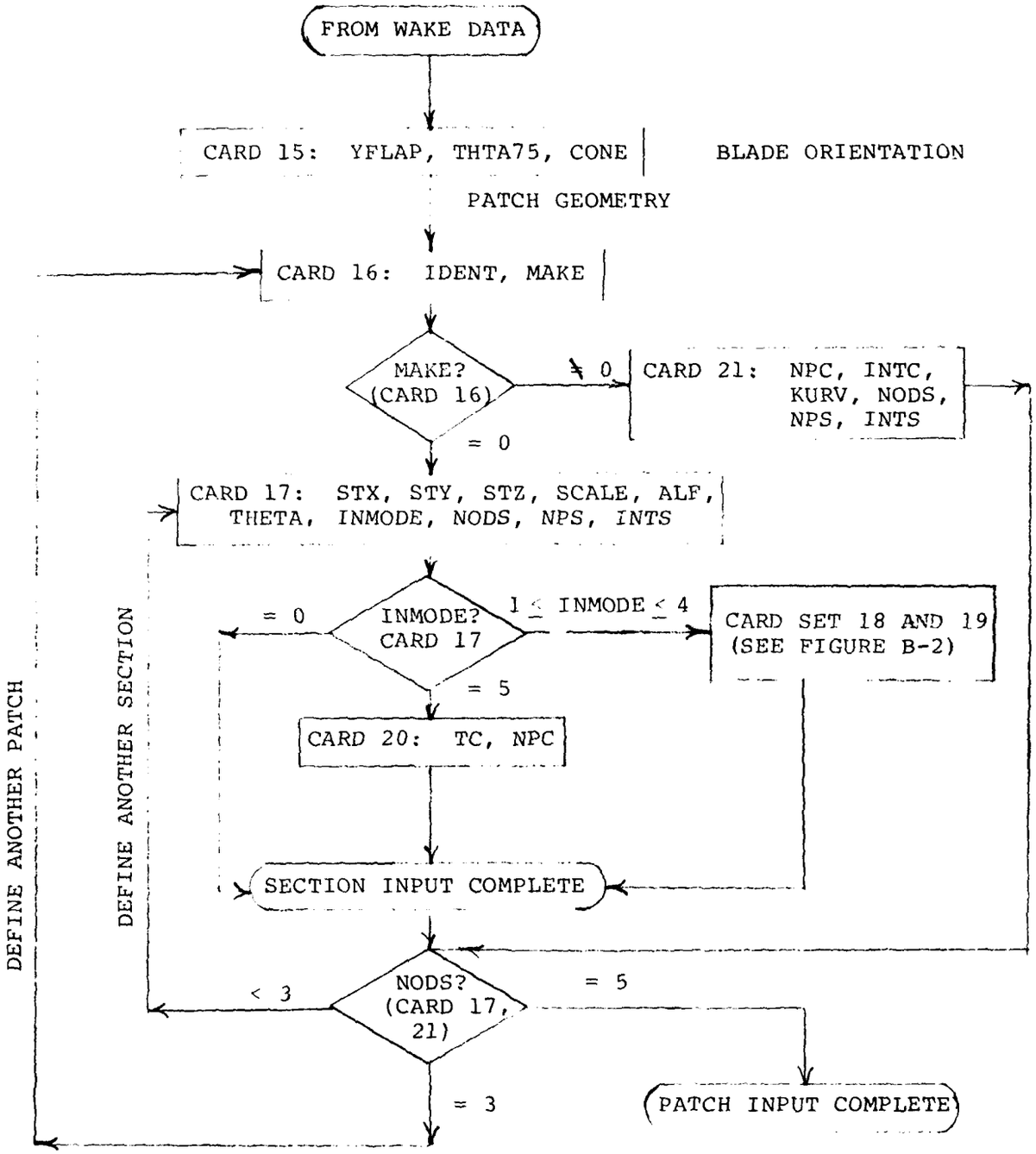


(c) Blade Geometry.

Figure B-1. Continued.

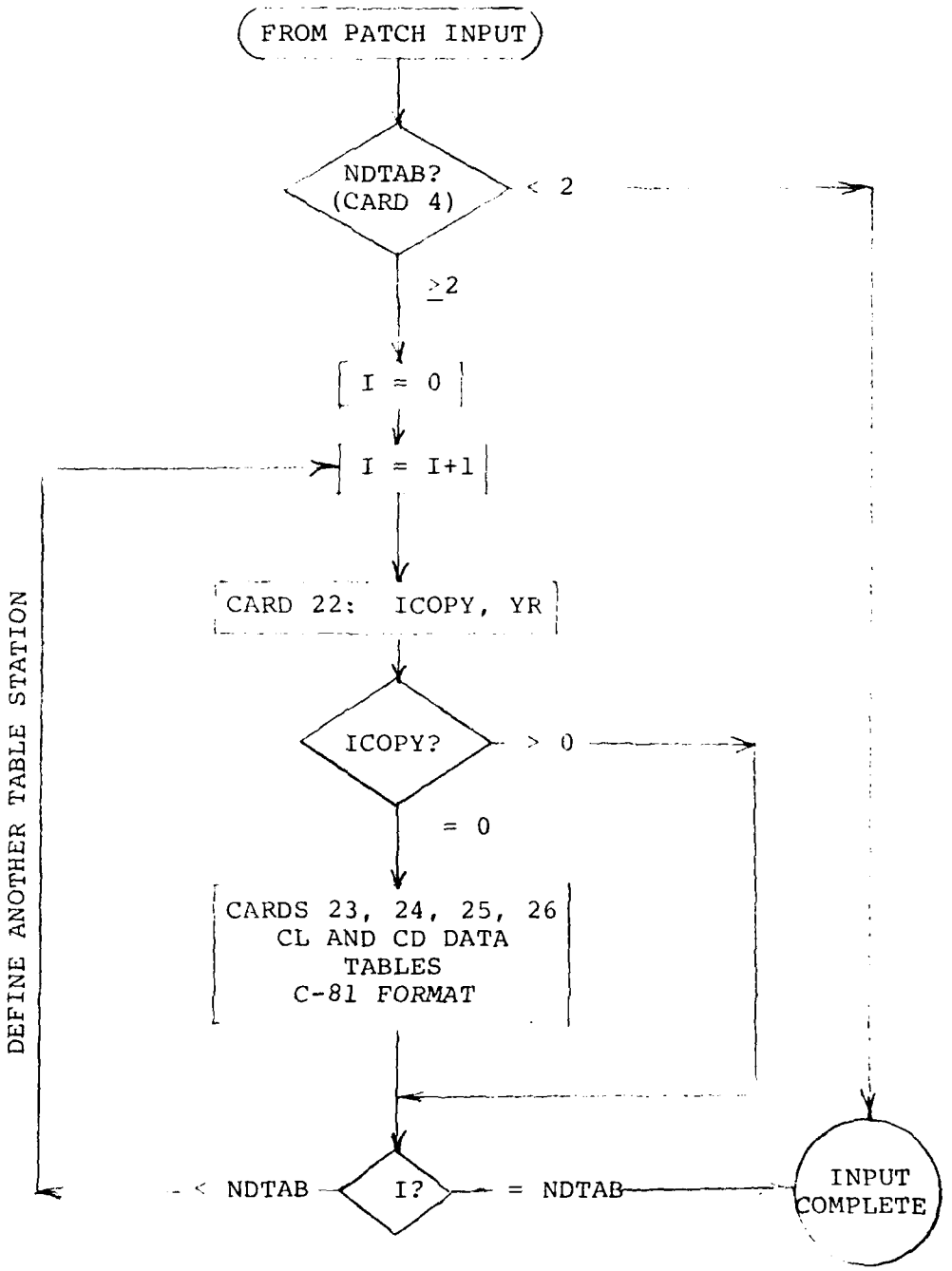


(d) Aerodynamic Tables.

Figure B-1. Concluded.

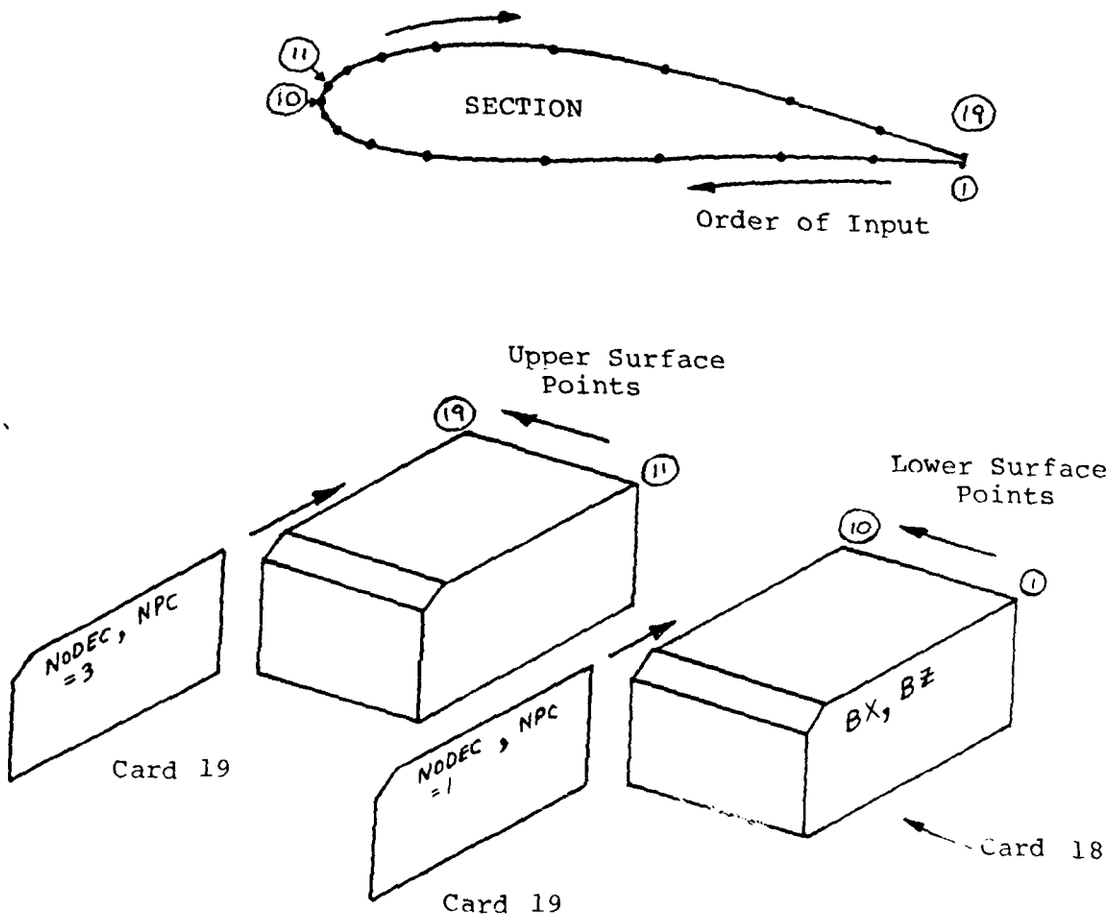


16
B

Figure B-2. Card Set 18/19. Section Coordinates for a Simple Airfoil.

## APPENDIX C: OUTPUT DESCRIPTION

Since ROTAIR is a preliminary code, some of the basic printed output is included until the program has been thoroughly validated. Consequently, only the basic printed output is described here. Also, for the present purposes, the prescribed wake geometry is always printed and, if NRELAX>0, the relaxed wake geometry is printed for each iteration.

The program output starts with the program header followed by the user's TEXT identification. If IPRI has been set to 1, all the input data is printed in the order of input and each variable is identified in parentheses. The input lists for the Basic Data and Patch Geometry are printed first. The input print is then interrupted by patch basic data from subroutine GEOMIN. This includes:

| M | IDENT | KLASS | KOMP | NROW | NCOL | IPAN | LPAN |
|---|---|---|---|---|---|---|---|
| . | . | . | . | . | . | . | . |
| . | . | . | . | . | . | . | . |
| . | . | . | . | . | . | . | . |

where M is the patch number; IDENT is the patch identifier (1 or 2); KLASS and KOMP are not used in the present application; NROW and NCOL are the number of panel rows and columns, respectively, on each patch, and IPAN, LPAN are the first and last panel subscripts on each patch.

If IPRLEV=1, the above is followed by the panel corner point coordinates:

| K | $X_1$ | $Y_1$ | $Z_1$ | $X_2$ | $Y_2$ | $Z_2$ | $X_3$ | $Y_3$ | $Z_3$ | $X_4$ | $Y_4$ | $Z_4$ |
|---|---|---|---|---|---|---|---|---|---|---|---|---|
| . | . | . | . | . | . | . | . | . | . | . | . | . |
| . | . | . | . | . | . | . | . | . | . | . | . | . |
| . | . | . | . | . | . | . | . | . | . | . | . | . |

where K is the panel subscript, and $X_i$, $Y_i$, $Z_i$ are the normalized coordinates in the G.C.S.. The points are assembled in a set for each patch.

If IPRI=1, the input list continues with a printout of the basic wake data. The prescribed wake geometry is printed in the same form as for the HOVER code. However, actual normalized coordinates are defined with respect to the G.C.S.

The printout of the pressure distribution, etc., is as follows:

(a) MODE = 1. The pressure distribution is printed according to the type of patch (IDENT). If IDENT = 1, the following is printed for each column of panels.

| K | X | Y | Z | DUB | VX | VY | VZ | V | $C_p$ | X/C | $C_p^*$ |
|---|---|---|---|---|---|---|---|---|---|---|---|
| . | . | . | . | . | . | . | . | . | . | . | . |
| . | . | . | . | . | . | . | . | . | . | . | . |
| . | . | . | . | . | . | . | . | . | . | . | . |

where K is the panel subscript; X, Y, Z is the control point location, and DUB the doublet value; VX, VY, VZ and V are the velocity vector components and magnitude; $C_p$ is the usual pressure coefficient, X/C is the location of the point relative to the local chord line, and $C_p^*$ is the pressure coefficient normalized by VTIP.

Each column is followed by the integrated section force and moment coefficients defined in the G.C.S.

CIRC CX CY CTS CTSGAM CLGAM CL CD CMX CMY CQS

where CIRC is the normalized section circulation; CX, CY are the force coefficients along the X- and Y-axes of the G.C.S.; CTS, CTSGAM are the section thrust coefficients by pressure integration and circulation, respectively; CLGAM, CL are the section lift coefficients by circulation and pressure integration, respectively; CD is the section drag coefficient by pressure integration; CMX, CMY are the moment coefficients about the X- and Y-axes of the G.C.S.; and CQS is the section torque coefficient. CHORD is the local chord length with leading edge at XLE, YLE, ZLE. The coordinates are given in the same units as originally specified.

For type 2 patches (IDENT = 2), the pressure printout is shortened by omitting X/C, $C_p^*$.

A summary of the patch force and moment coefficients normalized by the reference quantities in the basic data is printed after each patch and the total force and moment coefficients are printed after the last patch.

If NDTAB>2, then the profile losses calculated by the user-supplied two-dimensional tables are printed in the following manner.

| COL | Y | MACH | CL2D | CDO | CXO | CTSO | CQSO |
|---|---|---|---|---|---|---|---|
| . | . | . | . | . | . | . | . |
| . | . | . | . | . | . | . | . |
| . | . | . | . | . | . | . | . |

COL is the column identified; Y is the normalized radial position of the section in the G.C.S.; MACH is the section Mach number; CL2D is the interpolated table, CL (should equal the surface singularity, CL); CDO is the corresponding interpolated profile drag coefficient; CXO is the resultant sectional inplane profile force coefficient; CTSO is the resultant sectional profile thrust coefficient loss; and CQSO is the resultant sectional profile torque coefficient.

Finally, the integrated total rotor performance properties (based on pressure integration) including the figure of merit are printed.

## APPRENDIX D: SAMPLE INPUT DATA CASES

### CASE 1: HYPOTHETICAL ROTOR GEOMETRY

Geometric Description (scaled by R):

| | |
|---|---|
| Tip Taper Ratio | = 1.5 |
| % Radius: Start of Taper | = 85 |
| Blade Chord Root to Start of Taper | = .06 |
| Tip Chord | = .04 |
| Sweepback of c/4 | = 20° |
| % Radius: Start of Sweep | = 85 |
| Anhedral of c/4 | = 10° |
| % Radius: Start of Anhedral | = 85 |
| Airfoil | = NACA 0012 |
| Linear Twist about c/4 | = -10° |

(CASE 1: Continued)

Sample Geometric Patch Input

| DESCRIPTION | CARD COLUMNS (10 PER DIVISION) | | | | | | | |
|---|---|---|---|---|---|---|---|---|
| | 1 | 2 | 3 | 4 | 5 | 6 | 7 | 8 |
| PATCH CARD | 1 0 | | | | | | | |
| SECTION CARD | -.01484 | .15 | .00222 | 0.06 | 8.5 | 0.0 | 5 | |
| NACA SECTION | 0.12 | 5 | | | | | | |
| SECTION CARD | -.01499 | .85 | .00039 | 0.06 | 1.5 | 0.0 | 0 3 | 8 2 |
| PATCH CARD | 1 0 | | | | | | | |
| SECTION CARD | -.01499 | .85 | .00039 | 0.06 | 1.5 | 0.0 | 5 | |
| NACA SECTION | 0.12 | 10 | | | | | | |
| SECTION CARD | .04460 | 1.00 | -.02645 | 0.04 | 0.0 | 0.0 | 0 3 | 10 0 |
| PATCH CARD | 2 1 | | | | | | | |
| AUTO PATCH CARD | | | | 3 | 3 | | 5 | |

CASE 2: COMPLETE OH-58A INPUT

| DESCRIPTION | CARD COLUMNS (10 PER DIVISION) 1 | 2 | 3 | 4 | 5 | 6 | 7 | 8 |
|---|---|---|---|---|---|---|---|---|
| IDENTIFICATION | OH-58A | ROTOR | | | | | | |
| PRINT CONTROL | 1 0 | | | | | | | |
| MODE CARD | 320 0 | | | | | | | |
| NDTAB | 2 | | | | | | | |
| ROTOR INFORMATION | 2 | 1.0 | | | | | | |
| VELOCITIES | 0.0 | 655.0 | 1157.0 | | | | | |
| PERFORMANCE | 0.0022 | 0.9 | | | | | | |
| WAKE BASIL | 0.78 | 180.0 | | | | | | |
| WAKE BOUNDARIES | 480.0 | 520.0 | 30.0 | | | | | |
| WAKE AZIMUTH | 30.0 | 30.0 | 30.0 | 30.0 | | | | |
| TIP VORTEX CONSTANTS | -.01149 | -.04181 | .20440 | | | | | |
| INNER SHEET CONSTANTS | -.07297 | -.08955 | 0.0 | -.03634 | | | | |
| TIP VORTEX FORMATION | 0 | | | | | | | |
| NRELAX | 3 | | | | | | | |
| BLADE ORIENTATION | 0.0 | 5.75 | 3.0 | | | | | |
| PATCH CARD | 1 0 | | | | | | | |
| SECTION CARD | -.01506 | .144 | .00240 | 0.061 | 9.07 | | 5 | |
| NACA SECTION | 0.12 | 5 | | | | | | |
| SECTION CARD | -.01512 | .300 | .00197 | 0.061 | 7.42 | | 1 | 1 3 |
| SECTION CARD | -.01521 | .600 | .00113 | 0.061 | 4.24 | | 1 | 2 3 |
| SECTION CARD | -.01524 | .800 | .00056 | 0.061 | 2.12 | | 1 | 2 3 |
| SECTION CARD | -.01525 | 1.000 | 0.0 | 0.061 | 0.00 | | 3 | 10 3 |
| PATCH CARD | 2 1 | | | | | | | |
| AUTO PATCH CARD | | | | 3 | 3 | | 5 | |
| TABLE COPY CARD | 0 | 0.144 | | | | | | |
| | | | AERODYNAMIC DATA TABLES CL AND CD IN C-81 FORMAT | | | | | |
| TABLE COPY CARD | 1 | 1.0 | | | | | | |

# APPENDIX E: SAMPLE OUTPUT DATA CASE

```
**********************************************************

                ANALYTICAL METHODS,INC.

                PROGRAM ROTAIR

          SURFACE POTENTIAL FLOW ANALYSIS METHOD

          FOR ROTORS IN HOVER OR CLIMB

17
F

**********************************************************
  UH58A ROTOR
**********************************************************
```

INPUT LIST FOR BASIC DATA AND PATCH GEOMETRY
**********

(VARIABLES ARE IDENTIFIED IN PARENTHESES FOR CONVENIENCE)

```
 (IPRT IPRLEV)
     1       0

 (NPNMAX  MSTOP)
  320       0

 (NDTAB)
     2

 (NB       RADIUS)
  2     1.0000

  (VCLIMB       VTIP    VSOUND)
  0.0000   655.0000 1157.0000

     (CTO       RGMX)
   .0022      .9000

    (REAR       PSIO)
    .780    180.000

   (PSIF1      PSIF2    PSIMRG)
  480.00     520.00      30.00

  (DPSIT1     DPSIT2     DPSIS1    DPSIS2)
   30.00       30.00      30.00     30.00

     (TK1        TK2    TLAMDA)
 -.01149    -.04181     .20440

    (STK1       STK2       SKR1      SKR2)
 -.07297    -.06955    0.00000   -.03634

    (NSEP       DELZ       DELR)
       0     0.0000     0.0000

    (NRELAX =     0)

   (YFLAP     THTA75       CONE)
 0.00000    5.75000    3.00000
```

```
 (IDENT    MAKE)
      1       0                          (NPATCH=    1 )

     (STX       STY       STZ       SCALE      ALF       THETA  INMODE  NODS  NPS  INTS)
   -.01506    .14400    .06240    .06100   9.07000   0.00000       5     0    0     0          (NDSEC=    1)

     (TC       NPC          NACA SECTION GENERATED)
     .120       5

     (STX       STY       STZ       SCALE      ALF       THETA  INMODE  NODS  NPS  INTS)
   -.01512    .30000    .00197    .06100   7.42000   0.00000       0     1    1     3          (NDSEC=    2)

     (STX       STY       STZ       SCALE      ALF       THETA  INMODE  NODS  NPS  INTS)
   -.01521    .60000    .00113    .06100   4.24000   0.00000       0     1    2     3          (NDSEC=    3)

     (STX       STY       STZ       SCALE      ALF       THETA  INMODE  NODS  NPS  INTS)
   -.01524    .80000    .00056    .06100   2.12000   0.00000       0     1    2     3          (NDSEC=    4)

     (STX       STY       STZ       SCALE      ALF       THETA  INMODE  NODS  NPS  INTS)
   -.01525   1.00000   0.00000    .06100   0.00000   0.00000       0     3   10     3          (NDSEC=    5)

 (IDENT    MAKE)
      2       1                          (NPATCH=    2 )

                                    (NPC  INTC  KURV                NODS  NPS  INTS          AUTOMATIC TIP PATCH)
                                      3     3     0                   5    0    0

(END OF INPUT LIST FOR BASIC DATA AND PATCH GEOMETRY)

**************************************************

 CALCULATED BLADE ROTATION DATA

       (MT     TWISTO     DTHET    THET(1)      DWAKE       RTIP     RADIUS)
        3     2.6500     3.1000     4.3139      .0523      .9986     1.0000
```

BASIC PATCH DATA

| N | IDENT | KLASS | KJMP | NROW | NCOL | IPAN | LPAN |
|---|---|---|---|---|---|---|---|
| 1 | 1 | 1 | 1 | 10 | 15 | 1 | 150 |
| 2 | 2 | 1 | 1 | 3 | 5 | 151 | 165 |

GEOMIN TIME .305

INPUT DATA FOR 20 TABLES

PRINTOUT OF BASIC INPUT FOR DEFINED SECTION 1

ICOPY= 0 YOSEC = .14400

AERODYNAMIC TABLES FOR 0012

PRINTOUT OF BASIC INPUT FOR DEFINED SECTION 2

ICOPY= 1 YOSEC = 1.00000
ROTOR SOLIDITY(SOLID) = .03848

SURPAN DATA

SURPAN TIME 1.859

CONECT TIME 1.133

SURPHI TIME 23.661

INPUT LIST FOR BASIC WAKE GEOMETRY
**********

(VARIABLES ARE IDENTIFIED IN PARENTHESES FOR CONVENIENCE)

(IDENTW IFLEXW)
1 0 (NWAKE= 1 )

(KWPACH KWSIDE KWLINE KWPAN1 KWPAN2 INPUT)
1 2 0 1 10 2

(IDENTW IFLEXW)
1 1 (NWAKE= 2 )

(KWPACH KWSIDE KWLINE KWPAN1 KWPAN2 INPUT)
1 2 0 11 15 2

(END OF INPUT LIST FOR BASIC WAKE GEOMETRY)

**********

PRESCRIBED WAKE ITERATIONS 1

IGMX = 11

INITIAL WAKE PROPERTIES(COMPLETE WAKE INPUT)

PROPERTIES SEEN FROM TIP PATH PLANE

K1 = -.01149
K2 = -.04181
LAMBDA = .20466

K1(R=1) = -.07297
K2(R=1) = -.08955
K1(R=0) = 0.00000
K2(R=0) = -.03534

REARR(A) = .78000

| DPSIS1 | DPSIS2 | DPSIT1 | DPSIT2 | PSIB/ZPSIB | PSIF1/ZF1 | PSIF2/ZF2 |
|---|---|---|---|---|---|---|
| 30.00 | 30.00 | 30.00 | 30.00 | 180.00 | 479.99 | 519.99 |
| | | | | -.03610 | -.25501 | -.28420 |

PSIO = 180.00
PSIMxG = 30.00
RPSIB = .89576

INITIAL WAKE GEOMETRY(ROOT TO TIP)

NWAKE = 1
GEOMETRY SEEN FROM GENERAL COORDINATE SYSTEM

TRAILING FILAMENT 1

| XW | YW | ZW | RW | PSIW |
|---|---|---|---|---|
| .04452 | .14437 | -.00209 | .15108 | 17.14 |
| .07554 | .13084 | -.00224 | .15108 | 30.00 |
| .13084 | .07554 | -.00355 | .15108 | 60.00 |
| .15108 | .00000 | -.00436 | .15108 | 90.00 |
| .13084 | -.07553 | -.01516 | .15108 | 120.00 |
| .07554 | -.13083 | -.02045 | .15108 | 150.00 |
| .00001 | -.15108 | -.02676 | .15108 | 180.00 |
| -.07553 | -.13084 | -.05000 | .15108 | 210.00 |

OUTER TIP SHEET STARTS
NMRG = 1 PSIMRG = 30.00

TRAILING FILAMENT 13

| Xw | Yw | Zw | Rw | PSIw |
|---|---|---|---|---|
| .04434 | .91897 | .04505 | .92003 | 2.76 |
| .48816 | .84553 | .04471 | .97633 | 30.00 |
| .82617 | .47816 | .03961 | .95630 | 60.00 |
| .93830 | .00002 | .03352 | .93830 | 90.00 |
| .79860 | -.46103 | .02703 | .92212 | 120.00 |
| .45383 | -.78597 | .02193 | .90759 | 150.00 |
| .00005 | -.89453 | .01624 | .89453 | 180.00 |
| -.44135 | -.76455 | -.00565 | .88280 | 210.00 |
| -.75536 | -.43618 | -.02754 | .87226 | 240.00 |
| -.86278 | -.00007 | -.04943 | .86278 | 270.00 |
| -.73986 | .42707 | -.07132 | .85427 | 299.99 |
| -.42338 | .73316 | -.09321 | .84663 | 329.99 |
| -.00009 | .83976 | -.11511 | .83976 | 359.99 |
| .41671 | .72195 | -.13700 | .83358 | 389.99 |
| .71705 | .41411 | -.15889 | .82804 | 419.99 |
| .82305 | .00011 | -.18078 | .82305 | 449.99 |
| .70896 | -.40919 | -.20267 | .81857 | 479.99 |
| .40939 | -.70884 | -.22456 | .81857 | 509.99 |

TRAILING FILAMENT 14

| Xw | Yw | Zw | Rw | PSIw |
|---|---|---|---|---|
| .04432 | .93893 | .04627 | .93997 | 2.70 |
| .48816 | .84553 | .04471 | .97633 | 30.00 |

TRAILING FILAMENT 15

| XW | Yw | Zw | Rw | PSIW |
|---|---|---|---|---|
| .04430 | .95889 | .04749 | .95992 | 2.65 |
| .48816 | .84553 | .04471 | .97633 | 30.00 |

TRAILING FILAMENT 16

| XW | Yw | Zw | RW | PSIw |
|---|---|---|---|---|
| .04429 | .97886 | .04870 | .97986 | 2.59 |
| .48816 | .84553 | .04471 | .97633 | 30.00 |

TRAILING FILAMENT 17

| Xw | Yw | Zw | Rw | PSIw |
|---|---|---|---|---|
| .04427 | .99882 | .04992 | .99980 | 2.54 |
| .48816 | .84553 | .04471 | .97633 | 30.00 |

NUMBER OF WAKE SEGMENTS

| I | NWSG1 | NWSG2 |
|---|---|---|
| 1 | 8 | 8 |

CIRCULATION SOLUTION

| I | YBC | CIRC |
|---|---|---|
| 1 | .221517 | .003731 |
| 2 | .374328 | .005678 |
| 3 | .524144 | .006951 |
| 4 | .648991 | .007324 |
| 5 | .748868 | .007074 |
| 6 | .808795 | .006695 |
| 7 | .828770 | .006493 |
| 8 | .848745 | .006452 |
| 9 | .868721 | .006861 |
| 10 | .888696 | .007933 |
| 11 | .908672 | .009507 |
| 12 | .928647 | .008288 |
| 13 | .948623 | .007564 |
| 14 | .968598 | .006386 |
| 15 | .988573 | .004478 |

STEP 1 TIME 103.862

PRESSURE DISTRIBUTION ON FAI 1

COLUMN 1

| # | X | Y | Z | CDS | VX | VY | VZ | V | CP | X/C | CP* |
|---|---|---|---|---|---|---|---|---|---|---|---|
| 1 | .02371 | .22213 | .02414 | -.02171 | .22574 | -.02453 | -.02307 | .22862 | -.04376 | .73538 | -.21950E-02 |
| 2 | .00470 | .22174 | .01756 | -.02156 | .21647 | -.00412 | -.04357 | .22085 | .00975 | .30873 | .48009E-03 |
| 3 | -.01009 | .22171 | .01049 | -.02153 | .19759 | .00950 | -.06557 | .21076 | .40804 | .86547E-01 | .20100E-01 |
| 4 | -.01441 | .22159 | .00823 | -.02177 | .01183 | .01152 | -.01126 | .01998 | .99190 | .13913E-01 | .48912E-01 |
| 5 | -.01522 | .22153 | .00650 | -.02200 | -.02479 | .00295 | .19115 | .19278 | .24634 | .70917E-03 | .12147E-01 |
| 6 | -.01513 | .22150 | .01491 | -.02216 | .17472 | -.00172 | .38174 | .34885 | -1.46893 | .27613E-02 | -.72405E-01 |
| 7 | -.01396 | .22147 | .01554 | -.02246 | .37494 | .00602 | .15372 | .40537 | -2.33614 | .21854E-01 | -.11504 |
| 8 | -.00909 | .22145 | .01585 | -.02314 | .34381 | .01135 | -.03020 | .34400 | -1.45887 | .10331 | -.69210E-01 |
| 9 | .00455 | .22155 | .01403 | -.02424 | .28144 | .00504 | -.05646 | .28714 | -.67867 | .33043 | -.33334E-01 |
| 10 | .02936 | .22176 | .00736 | -.02549 | .24442 | -.01429 | -.07764 | .25867 | -.31422 | .74621 | -.15751E-01 |

SECTION CHORD XLE YLE ZLE
.0610 -.0154 .2215 .0145

CIRC CX CY CTS CTSCAM CLCAM CL CD CMX CMY CQS
.000731 .000345 -.000007 .000324 .000263 .552395 .690730 .094584 .000073 -.000000 .000010

COLUMN 2

| # | X | Y | Z | CDS | VX | VY | VZ | V | CP | X/C | CP* |
|---|---|---|---|---|---|---|---|---|---|---|---|
| 11 | .02870 | .37455 | .01248 | -.02135 | .38536 | -.03233 | -.02736 | .38762 | -.06292 | .73617 | -.86938E-02 |
| 12 | .00310 | .37470 | .01566 | -.02136 | .37345 | -.00615 | -.06418 | .37847 | -.02288 | .31031 | -.32120E-02 |
| 13 | -.01375 | .37457 | .01673 | -.02145 | .29190 | .00831 | -.13756 | .30185 | .35092 | .87769E-01 | .49259E-01 |
| 14 | -.01819 | .37450 | .02065 | -.02127 | .04155 | .00719 | -.03875 | .05756 | .97640 | .14491E-01 | .13708 |
| 15 | -.01551 | .37435 | .02169 | -.02165 | -.04458 | -.00548 | .29154 | .28512 | .42089 | .85877E-01 | .59083E-01 |
| 16 | -.01543 | .37431 | .02251 | -.02193 | .25168 | -.01455 | .48295 | .54957 | -1.15203 | .26117E-02 | -.16168 |
| 17 | -.01478 | .37426 | .02322 | -.02233 | .65041 | -.00327 | .26554 | .65652 | -2.67240 | .21275E-01 | -.29073 |
| 18 | -.00942 | .37426 | .02375 | -.02344 | .56767 | .00661 | .01512 | .56791 | -1.30118 | .10209 | -.16237 |
| 19 | .00621 | .37436 | .02218 | -.02527 | .47652 | .00190 | -.05128 | .47346 | -.64012 | .32885 | -.84721E-01 |
| 20 | .02945 | .37471 | .01622 | -.02736 | .41366 | -.01709 | -.11723 | .43031 | -.31078 | .74943 | -.43902E-01 |

SECTION CHORD XLE YLE ZLE
.0610 -.0154 .3743 .0222

CIRC CX CY CTS CTSCAM CLCAM CL CD CMX CMY CQS
.000678 .000307 -.000045 .000351 .000277 .497382 .625521 .075297 .009320 .000000 .000038

COLUMN 14

| K | X | Y | Z | DUB | VX | VY | VZ | V | CP | X/C | CP* |
|---|---|---|---|---|---|---|---|---|---|---|---|
| 131 | .02961 | .98859 | .04734 | -.00941 | 1.02666 | -.02047 | .04424 | 1.02782 | -.12438 | .73919 | -.11686 |
| 132 | .00267 | .98886 | .04727 | -.00837 | 1.04575 | .01084 | -.06132 | 1.04760 | -.16914 | .31635 | -.15877 |
| 133 | -.01067 | .98878 | .04884 | -.00711 | .92847 | .02781 | -.24127 | .95971 | .01872 | .92434E-01 | .17567E-01 |
| 134 | -.01555 | .98867 | .05043 | -.00712 | .93859 | .02674 | -.32940 | .94916 | .67867 | .16702E-01 | .63697 |
| 135 | -.01651 | .98861 | .05140 | -.00772 | -.04043 | -.00343 | .16944 | .17572 | .96710 | .14299E-02 | .90761 |
| 136 | -.01647 | .98859 | .05203 | -.00785 | .32466 | -.03737 | .79642 | .86086 | .21028 | .20406E-02 | .19734 |
| 137 | -.01543 | .98854 | .05296 | -.00952 | 1.11822 | -.03504 | .64860 | 1.29318 | -.78227 | .19065E-01 | -.73401 |
| 138 | -.01068 | .98849 | .05342 | -.01026 | 1.26867 | -.02536 | .17237 | 1.27859 | -.74269 | .97422E-01 | -.69671 |
| 139 | .00300 | .98851 | .05365 | -.01344 | 1.15373 | -.04541 | -.07209 | 1.15687 | -.42678 | .32281 | -.40033 |
| 140 | .02961 | .98872 | .05366 | -.01629 | 1.05205 | -.06493 | -.17868 | 1.07049 | -.22009 | .74241 | -.20672 |

SECTION

| CHORD | XLE | YLE | ZLE |
|---|---|---|---|
| .0610 | -.0156 | .9886 | .0517 |

| CIRC | CX | CY | CTS | CTSGAM | CLGAM | CL | CD | CMX | CMY | CQS |
|---|---|---|---|---|---|---|---|---|---|---|
| .006386 | .000247 | -.000133 | .002475 | .091969 | .216155 | .271690 | .027095 | .002404 | .000013 | .000239 |

COLUMN 15

| K | X | Y | Z | DUB | VX | VY | VZ | V | CP | X/C | CP* |
|---|---|---|---|---|---|---|---|---|---|---|---|
| 141 | .02960 | .98886 | .04855 | -.01021 | 1.04246 | .00714 | .05041 | 1.04370 | -.11309 | .73929 | -.11067 |
| 142 | .00265 | .98883 | .04834 | -.00877 | 1.06749 | .09367 | -.05423 | 1.07296 | -.17739 | .31655 | -.17345 |
| 143 | -.01049 | .98873 | .04985 | -.00745 | .98067 | .18339 | -.24324 | 1.02708 | -.07894 | .92589E-01 | -.77183E-01 |
| 144 | -.01561 | .98864 | .05145 | -.00724 | .92242 | .21050 | -.38058 | .67965 | .52724 | .16775E-01 | .51545 |
| 145 | -.01654 | .98857 | .05240 | -.00751 | -.01479 | .17666 | .06108 | .18751 | .96404 | .14489E-02 | .94243 |
| 146 | -.01650 | .98855 | .05302 | -.00776 | .28166 | .12651 | .70688 | .77137 | .39130 | .20216E-02 | .38251 |
| 147 | -.01547 | .98852 | .05386 | -.00830 | 1.05824 | .08944 | .62531 | 1.23244 | -.55402 | .18992E-01 | -.54150 |
| 148 | -.01070 | .98847 | .05443 | -.00979 | 1.23792 | .01461 | .17514 | 1.25034 | -.59986 | .97267E-01 | -.58617 |
| 149 | .00302 | .98849 | .05442 | -.01242 | 1.14033 | -.13064 | -.07158 | 1.15002 | -.35351 | .32261 | -.34542 |
| 150 | .02858 | .98865 | .05384 | -.01469 | 1.05024 | -.28252 | -.18581 | 1.10333 | -.24433 | .74231 | -.23903 |

SECTION

| CHORD | XLE | YLE | ZLE |
|---|---|---|---|
| .0610 | -.0155 | .9885 | .0527 |

| CIRC | CX | CY | CTS | CTSGAM | CLGAM | CL | CD | CMX | CMY | CQS |
|---|---|---|---|---|---|---|---|---|---|---|
| .004478 | .000264 | -.000112 | .002106 | .081409 | .148525 | .221955 | .028398 | .002088 | .000005 | .000267 |

PATCH 1

| CXP | CYP | CTP | CTPGAM | CMXP | CMYP | CQP |
|---|---|---|---|---|---|---|
| .000135 | -.000069 | .001313 | .091034 | .000918 | .000003 | .000094 |

PRESSURE DISTRIBUTION ON PATCH 2

| K | X | Y | Z | DUM | VX | VY | VZ | V | CP |
|---|---|---|---|---|---|---|---|---|---|
| 151 | .02554 | .99870 | .05187 | -.01067 | 1.02638 | -.00359 | .09612 | 1.03087 | -.06461 |
| 152 | .02345 | .99875 | .05077 | -.01060 | 1.01925 | -.00171 | .06016 | 1.02098 | -.04415 |
| 153 | .02342 | .99881 | .04969 | -.01074 | 1.01701 | -.00126 | .05151 | 1.01831 | -.03859 |
| 154 | .00294 | .99853 | .05435 | -.01047 | 1.02362 | -.00224 | .07029 | 1.02604 | -.05584 |
| 155 | .00282 | .99864 | .05216 | -.01035 | 1.02087 | -.00103 | .04719 | 1.02196 | -.04724 |
| 156 | .00270 | .99876 | .04998 | -.01025 | 1.01957 | -.00167 | .05940 | 1.02130 | -.04564 |
| 157 | -.01077 | .99850 | .05459 | -.01013 | 1.01979 | -.00003 | .02810 | 1.02017 | -.04377 |
| 158 | -.01046 | .99859 | .05240 | -.01007 | 1.01460 | -.00023 | .03170 | 1.01509 | -.03321 |
| 159 | -.01035 | .99867 | .05020 | -.01002 | 1.01615 | -.00138 | .05385 | 1.01758 | -.03810 |
| 160 | -.01551 | .99852 | .05395 | -.01002 | 1.01686 | .00147 | -.00053 | 1.01686 | -.03682 |
| 161 | -.01555 | .99857 | .05315 | -.01001 | .99898 | .00085 | .01079 | .99904 | -.00071 |
| 162 | -.01560 | .99861 | .05235 | -.01000 | 1.00726 | .00005 | .02622 | 1.00760 | -.01784 |
| 163 | -.01653 | .99853 | .05341 | -.01000 | 1.13328 | .00478 | -.06053 | 1.13490 | -.29140 |
| 164 | -.01654 | .99856 | .05320 | -.01001 | .99476 | .00246 | -.02001 | .99496 | .00747 |
| 165 | -.01655 | .99857 | .05300 | -.01001 | 1.01414 | .00074 | .01329 | 1.01423 | -.03132 |

| PATCH | Z | CXP | CYP | CTP | CTPGAM | CMXP | CMYP | CQP |
|---|---|---|---|---|---|---|---|---|
| | | -.000000 | .000000 | .000000 | 0.000000 | .000000 | -.000000 | -.000000 |

| TOTAL | CT | CTGAM | CMXB | CMYB | CQ |
|---|---|---|---|---|---|
| | .2620E-02 | .2069E-02 | .4179E-03 | .2788E-05 | .1879E-03 |

PROFILE LOADS BY TWO-DIMENSIONAL TABLES

| COL | Y | MACH | CL2D | CDD | CXD | CTSJ | CQSJ |
|---|---|---|---|---|---|---|---|
| 1 | .22152 | .12543 | .69077 | .01166 | .55525E-05 | 0. | .12300E-05 |
| 2 | .37433 | .21131 | .62552 | .01090 | .14825E-04 | 0. | .55495E-05 |
| 3 | .52414 | .29673 | .54754 | .00999 | .26643E-04 | 0. | .13963E-04 |
| 4 | .64899 | .36741 | .45738 | .00940 | .38449E-04 | 0. | .24953E-04 |
| 5 | .74867 | .42335 | .39188 | .00899 | .48928E-04 | 0. | .36633E-04 |
| 6 | .80879 | .45787 | .34366 | .00876 | .55650E-04 | 0. | .45010E-04 |
| 7 | .82877 | .46918 | .32504 | .00871 | .58089E-04 | 0. | .48143E-04 |
| 8 | .84575 | .48049 | .31364 | .00868 | .60694E-04 | 0. | .51514E-04 |
| 9 | .86372 | .49180 | .32517 | .00869 | .63705E-04 | 0. | .55342E-04 |
| 10 | .88870 | .50311 | .36609 | .00879 | .67416E-04 | 0. | .59913E-04 |
| 11 | .90867 | .51442 | .38417 | .00887 | .71975E-04 | 0. | .64584E-04 |
| 12 | .92865 | .52573 | .36755 | .00882 | .73816E-04 | 0. | .68549E-04 |
| 13 | .94862 | .53703 | .32375 | .00871 | .76109E-04 | 0. | .72199E-04 |
| 14 | .96860 | .54834 | .27170 | .00854 | .77772E-04 | 0. | .75330E-04 |
| 15 | .98857 | .55965 | .22196 | .00844 | .80068E-04 | 0. | .79153E-04 |

FINAL INTEGRATED PERFORMANCE

PROFILE THRUST COEFFICIENT TERM(CTJ) = 0.
PROFILE TORQUE COEFFICIENT(CQJ) = .43344E-04

INDUCED TORQUE PER TOTAL TORQUE = .813
PROFILE TORQUE PER TOTAL TORQUE = .187
HUB TORQUE PER TOTAL TORQUE = 0.000

FINAL THRUST COEFFICIENT = .26203E-02 THRUST COEFFICIENT/SOLIDITY = .66103E-01
TOTAL TORQUE COEFFICIENT = .23124E-03 TORQUE COEFFICIENT/SOLIDITY = .60102E-02

FIGURE OF MERIT = .410

ANALIZ TIME 2.607

TOTAL TIME 134.398

## LIST OF SYMBOLS

| | |
|---|---|
| B,C | Velocity potential influence coefficients for constant source and doublet distributions, respectively, on quadrilateral panels, Eq (5) |
| c | Airfoil chord |
| $C_p$ | Pressure coefficient |
| $C_L$ | Lift coefficient |
| $C_M$ | Moment coefficient |
| E | Quantity in Eq (5) |
| $\underline{i},\underline{j},\underline{k}$ | Orthogonal unit vector system defining the axes of the Cartesian coordinate system fixed relative to the blade, Figure 2 |
| N | Number of panels |
| n | Surface unit normal vector directed into the flow field |
| R | Position vector of a point relative to a point on the axis of rotation |
| S | Blade surface |
| s | Surface distance |
| $\underline{V}$ | Velocity |
| $\underline{v}$ | Perturbation velocity |
| W | Wake surface |
| x,y,z | Cartesian coordinates in the blade-fixed frame |
| $w_c$ | Normalized climb speed |
| $W_{climb}$ | Climb speed |
| $\underline{\omega}$ | Body rotation vector |
| $\Delta$ | Finite increment |
| $\mu$ | Doublet strength |

| | |
|---|---|
| $\Phi$ | Total velocity potential |
| $\phi$ | Perturbation velocity potential |
| $\sigma$ | Source strength |
| $\sigma_R, \underline{\sigma}_M$ | Source components due to unit pitch rotation and unit translation, respectively, Eq (7) |
| $\nabla$ | Gradient operator |

Subscripts

| | |
|---|---|
| J,K | Values on panels J, K, respectively |
| U,L | Upper, lower |
| W | Wake |
| $\infty$ | Reference onset condition |